SYNTHESIS AND CHARACTERIZATION OF STAR BLOCK COPOLYMERS FOR CONTROLLED DRUG DELIVERY

A Thesis Submitted to
the Graduate School of Engineering and Sciences of
İzmir Institute of Technology
in Partial Fulfillment of the Requirements for the Degree of

DOCTOR OF PHILOSOPHY

in Chemical Engineering

by
Gözde GENÇ ATİKLER

June 2010
İZMİR

We approve the thesis of **Gözde GENÇ ATİKLER**

Asst. Prof. Ayşegül BATIGÜN
Supervisor

Prof. Serdar ÖZÇELİK
Committee Member

Prof. Sacide ALSOY ALTINKAYA
Committee Member

Assoc. Prof. Mustafa DEMİR
Committee Member

Asst. Prof. Zehra ÖZÇELİK
Committee Member

9 June 2010

Prof. Mehmet POLAT
Head of the Department of
Chemical Engineering

Assoc. Prof. Talat YALÇIN
Dean of the Graduate School of
Engineering and Sciences

ACKNOWLEDGEMENTS

I would like to thank to my supervisor Ayşegül Batıgün for her support and guadiance. I thank very much to Prof. Sacide Alsoy Altınkaya and Prof. Serdar Özçelik, for their generous help and valuable critics. I am so much thankful to Assoc. Prof. Zehra Özçelik for her commendations and very kind interest. I have to express my deep gratitude to Assoc. Prof. Mustafa Demir for his encouraging attitude and to Prof. Muhsin Çiftçioğlu for his help and substantial recommendations. I need to express my gratitude to Prof. Devrim Balköse for her support and precious advices.

This research was financially supported by İYTE BAP (2006 İYTE 33) and all polymer samples used in this study were synthesized in Organic Chemistry Laboratory in İTÜ Chemistry Department with permission from Prof. Ümit Tunca and Prof. Gürkan Hızal for which I am very grateful. I would like to extend my special thanks to Prof. Ümit Tunca for his guadiance in polymer synthesis. I am thankful to Özcan Altıntaş, Eda Güngör and Aydan Dağ for their help and support in laboratory.

I thank very much to İYTE Materials Reserach Center staff, Evrim Yakut, Mine Bahçeci, Duygu Oğuz and Gökhan Erdoğan for they have always been so helpful and giving. I would like to thank to Dr. Hüseyin Özgener for his valuable advices and clues about chemical protocols. Sincere thanks to Özlem Çağlar Duvarcı for her favour in FTIR analysis, Burcu Alp for performing thermal analysis and Deniz Şimşek for his help in particle size analysis. I would also like to express my sincere thanks to my colleagues, Dane Rusçuklu, Diren Kaçar, Dilek Yalçın, Alihan Karakaya, Ali Bora Balta, Merve Şahin, İpek Erdoğan and Özge Tuncel for their help and company. I need to thank my friend Güler Narin for her support. Finally, thanks to my family for their understanding.

ABSTRACT

SYNTHESIS AND CHARACTERIZATION OF STAR BLOCK COPOLYMER FOR CONTROLLED DRUG DELIVERY

Amphiphilic multiarm block copolymers of hydrophobic poly(methyl methacrylate) core and hydrophilic poly(acrylic acid) corona has been synthesized, characterized and proposed for an anticancer drug that is 5 Florouracil (5FU). 3 arm, 4 arm and 6 arm PMMA-*b*-PtBA (poly(methyl methacrylate-*block*-poly(tertiary butyl acrylate)) copolymers with molecular weights from 18 kDa to 80 kDa were synthesized by Atomic Transfer Radical Polymerization and reacted into PMMA-*b*-PAA (poly(methyl methacrylate-*block*-poly(acrylic acid)) by hydrolysis of tBA chains. Optimum molecular weight and hydrophobic core ratio was determined by evaluation of critical micelle concentrations and maximum loading capacities with pyrene. Loading method was selected among simple equilibrium, solvent deposition, salting out and dialysis methods. Dialysis method yielded the highest loading contents of model drug indomethacin. Optimum loading conditions in terms of temperature, duration, pH and polymer concentration were determined with anticancer drug 5FU. 4 arm PMMA-*b*-PAA with molecular weight 18000 Da and hydrophobic core ratio 0.27 was proposed for controlled delivery of 5FU. Optimum loading conditions were determined as 15°C in acidic aqueous medium with pH 1.0-1.5 and loading interval as 4 hours. Minimum polymer concentration was estimated to be 2000 mg/L for an optimum loading. Drug loaded particles were characterized by FTIR, TGA, DTG and DSC. 5FU loaded PMMA-*b*-PAA samples with drug contents about 14-20 % were investigated by a continuous operation where a diffusion cell was employed to monitor release profiles. Controlled release of 5FU with zero order release kinetics for 18 days was provided by 4 arm PMMA-*b*-PAA. Biodegradation of loaded particles were monitored through particle size analysis by Dynamic Light Scattering and Atomic Force Microscopy.

ÖZET

KONTROLLÜ İLAÇ AKTARIMI İÇİN YILDIZ BLOK KOPOLİMER SENTEZİ VE KARAKTERİZE EDİLMESİ

Hidrofobik poli(metil metakrilat) merkez etrafında hidrofilik poli(akrilik asit) çeperden oluşan amfifilik yıldız blok kopolimerler sentezlendi ve kanser ilacı 5 Florourasil taşıyıcısı olarak kullanılmak üzere karakterize edildi. 18 kDa-80 kDa molekül ağırlığı aralığında 3-kollu, 4-kollu ve 6-kollu PMMA-*b*-PtBA (poli(metil metakrilat)-*blok*-poli(tersiyer bütil akrilat) kopolimerleri Atomik Transfer Radikal Polimerizasyon tekniğiyle sentezlendi ve tBA kollar hidroliz reaksiyonuyla akrilik asite dönüştürüldü. Kritik misel konsantrasyonları ve maksimum piren yüklenme kapasiteleri değerlendirilerek optimum molekül ağırlığı ve hidrofobik merkez oranı belirlendi. Model ilaç olarak kullanılan indometazinle yapılan deneylerde en yüksek yükleme miktarı diyaliz yöntemiyle elde edildi. Diyaliz yöntemiyle optimum yükleme koşullarının belirlenmesinde model ilaç olarak kanser ilacı 5-florourasil kullanıldı. 18 kDa molekül ağırlığı ve 0.25 hidrofobik merkez oranına sahip 4-kollu PMMA-*b*-PAA kopolimerin kontrollü 5FU salımı için optimum yükleme koşulları 15°C'de, 1.0-1.5 pH aralığında sulu çözelti içinde, yükleme süresi 4 saat ve minimum polimer konsantrasyonu 2 g/L olmak üzere belirlendi. İlaç yüklü polimer numuneleri FTIR, TGA, DTG ve DSC ile karakterize edildi. 5FU yüklenme miktarları 14-20% olan PMMA-*b*-PAA numuneler difüzyon hücresine yerleştirildi ve salınan ilaç miktarları UV-spektroskopi yöntemiyle belirlendi. 4-kollu PMMA-*b*-PAA kopolimeriyle 18 gün süresince kontrollü salım sağlandı. İlaç yüklü polimerlerin biyolojik parçalanma özellikleri Dinamik Işık Saçılımı ve Atomik Güç Mikroskopi yöntemleriyle belirlenen parçacık büyüklükleri bazında incelendi.

TABLE OF CONTENTS

LIST OF FIGURES

LIST OF TABLES

LIST OF SYMBOLS AND ABBREVIATIONS

A	Area of diffusion (cm^2)
C_d	Concentration of drug in donor compartment (mg/ml)
C_o	Original drug concentration in formulation (mg/ml)
C_r	Concentration of drug in receptor compartment (mg/ml)
D	Diffusivity (cm^2/min)
F	Flowrate (ml/min)
f_c	Hydrophobic core ratio
J	Mass flux
η	Viscosity (cP)
k	Constant of release kinetics
k_B	Boltzmann constant
K	Partition coefficient
K_{ATRP}	Rate constant of atomic transfer radical polymerization reaction
K_a	Rate constant of activation
K_d	Rate constant of deactivation
K_p	Rate constant of propagation
κ	Constant ($=AP/V_r$)
M	Amount of drug released at infinity (mg)
M_t	Amount of drug released at time t (mg)
MW	Molecular weight (Da)
n	Degree of power law release kinetics
n_p	Number of moles of product
n_r	Number of moles of reactant
P	Permeability (cm/min)
q	Amount of substance transferred (mg)
r_h	Hydrodynamic radius (nm)
r_p	Radius of spherical particle
R_p	Rate of polymerization reaction
T	Temperature (°C)
t	Time (min)
V_r	Receptor volume (ml)

w_p	Weight of product (g)
w_r	Weight of reactant (g)
x	Distance

AA	Acetic Acid
AFM	Atomic Force Microscopy
ATRP	Atomic Transfer Radical Polymerization
CMC	Critical Micelle Concentration
diPENTA	Dipentaerythritol
DLC	Drug Loading Content (or Drug Loading Capacity)
DLE	Drug Loading Efficiency
DLS	Dynamic Light Scattering
DMAP	Dimethylaminopyridine
DMF	Dimethylformamide
DMSO	Dimethylsulfoxide
DSC	Differential Scanning Calorimetry
DTG	Differential Thermal Gravimetry
FTIR	Fourier Transform Infrared Spectroscopy
GPC	Gel Permeation Chromatography
MMA	Methyl Methacrylate
MPEG	Methoxy Poly(Ethylene Glycol)
MWCO	Molecular Weight Cut-Off
NMR	Nuclear Magnetic Resonance
OEG	Oligo Ethylene Glycol
OSM	Oligo Sulfamethazine
PAA	Poly(Acrylic Acid)
PAMAM	Polyamidoamine
PBS	Phosphate Buffer Solution
PCL	Poly(*1*-Caprolactone)
PDMAEMA	Poly(2-(N,N-Dimethylamino)Ethyl Methacrylate)
PDLLA	Poly(D,L-Lactide)
PEG	Poly(Ethylene Glycol)
PENTA	Pentaerythritol
PEO	Poly(Ethylene Oxide)

PHPMA	Poly(N-(2-Hydroxypropyl)Methacrylamide)
PI	Polydispersity Index
PLA	Poly(Lactic Acid)
PLGA	Poly(Lactic-*co*-Glycolic Acid)
PLLA	Poly(L-Lactide)
PMDETA	N,N,N',N",N"-Pentamethyl Diethylenetriamine
PMMA	Poly(Methyl Methacrylate)
PNIPAAm	poly(*N*-Isopropylacrylamide)
PTMC	Poly(Thrimethylene Carbonate)
PVP	Poly(Vinyl Pyrolidone)
PtBA	Poly(*tert*- Butyl Acrylate)
SANS	Small Angle Neutron Scattering
SAXS	Small Angle X-Ray Scattering
tBA	*tert*- Butyl Acrylate
TEA	Triethylamine
TFA	Trifluoro acetic acid
TGA	Thermal Gravimetric Analysis
THB	1,3,5-Trihydroxibenzene
THF	Tetrahydrofuran

CHAPTER 1

INTRODUCTION

Water soluble amphiphilic polymer particles are good candidates for drug delivery with their thermodynamic and kinetic stabilities, high drug loading capacities and low critical micelle concentrations. Their structures with hydrophobic cores and hydrophilic coronas provide beneficial properties such as elimination of additional surfactants in drug formulations, protection of drug from premature degradation and opportunities for controlled and targeted delivery (Leroux and Ranger, 2002; Nishiyama and Kataoka, 2006).

One of the best candidates for delivery of hydrophobic drugs is star polymers which are branched polymer chains around a multifunctional core. The number of the active sites of the core molecule of a unimolecular polymeric carrier determines the number of arms. They may be classified as dendrimers, symmetrical star block copolymers and miktoarm block copolymers where each arm is another type of polymer chain (Deng et al., 2007; Tunca et al., 2002). Synthesis of miktoarm star polymers requires sophisticated initiators whose active sites show different reactivities with different monomer species.

Dendrimers are the most famous star shaped polymers introduced by Tomalia's and Freche's studies in 1980's. Polyamidoamine (PAMAM) is the most widely studied dendrimer for biomedical applications and is reported to be stable, biodegradable and nontoxic under certain conditions (Svenson and Tomalia, 2005; Patri et al., 2005; Tomalia et al., 2006). Dendritic structures including all star shaped polymers can be synthesized by two techniques as shown in Figure 1.1. These may be explained as achieving the synthesis around a core and repeating the procedure for addition of branches several times (divergent method) or, simply producing the branched chains and attaching them around an initiator which has various active sites (convergent method).

PAMAM is produced by divergent synthesis while dentritic structures of block copolymers of polyethyleneoxide (PEO), mostly studied by Fréchet and coworkers (Tomalia and Fréchet, 2005; Grayson and Fréchet, 2001, Gillies and Fréchet, 2004), are

synthesized by convergent methods. But the synthesis of dendrimers are hard to control in either cases and the reaction yields are low. Hence star block copolymers constitute a good alternative with the possibility of using controlled polymerization techniques.

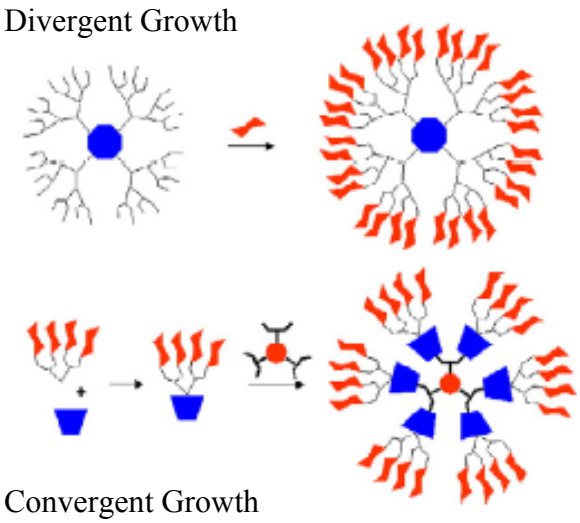

Figure 1.1. Schematic presentation of divergent and convergent synthesis (Source: Tomalia et al., 2006).

Star block copolymers are the most versatile type of dendritic structures with the numerous possibilities of synthesis, modifications and applications. They can be sorted according to number of arms and distribution of polymers that constitutes the star shaped polymer as summarized in Figure 1.2 (Haddleton et al., 1997; Ganguly, 2002; Kilian, 2004; Yin et al., 2005; Chu et al., 2004; Ishizu and Uchida, 1999). Amphiphilic structure is often produced by block copolymers constituting hydrophilic and hydrophobic polymer blocks in numerous shapes, built by both convergent and divergent techniques Such block copolymers have recently drawn significant attention with their perfect solubilizing properties (Kilian, 2004). Their potential in drug delivery area has also been widely studied, especially in gene delivery, and delivery of chemotherapeutic agents (Gaucher et al., 2005; Kakizawa and Kataoka, 2002).

Figure 1.2. Schematic representation of simple AB graft, A*n*B*n*, and (AB)*n* star-block copolymers. (Source: Ishuzu and Uchida, 1999)

Star block copolymers form polymeric micelles where interior spaces of polymeric structure constitute a reservoir for the drug. Hydrophobic cores and hydrophilic coronas are particularly favoured to solubilize hydrophobic drugs. The substance can be stocked in the particles by hydrophobic-hydrophobic interactions, diffusion or conjugation (Marion et al., 1999; Chytil et al., 2006). Star block copolymers have also been proposed as good candidates for smart drug delivery systems like pH sensitive, thermosensitive or targeted drug delivery. Generally polyethylene glycols, polylactides and block copolymers of poly ethylene oxides have been used for drug delivery studies for they are approved biodegradable and biocompatible polymers. Polystyrene has also been widely investigated for core-and-shell type unimolecular polymer structures. In the last decade, acrylic block copolymers have gained attention for their extremely low critical micelle concentrations, amphiphilic properties and relative ease of controlled polymerization techniques.

ATRP (Atom Transfer Radical Polymerization) is a beneficial controlled polymerization technique for it allows shorter reaction times at high reaction temperatures and yields acceptable polydispersities (Krishnan and Srinivasan, 2004). Block copolymers synthesized by controlled polymerization techniques can be designed as linear, branched or star shaped unimolecular structures. The linear block copolymers may act as surfactants in aqueous media and produce polymeric micelles with low

critical micelle concentrations (Gaucher et al., 2005). The critical micelle concentrations of star block copolymers are even lower. Block copolymer systems, linear or star shaped, have been widely studied for their loading capacities with various hydrophobic drugs and have shown versatile characteristics in terms of drug loading, drug release performance, critical micelle concentrations and cytotoxicity. Each parameter has been claimed to depend on molecular weight, arm length, composition and concentration of the polymer, drug type, dosage and preparation method. Therefore, polymer architecture is quite important when the material is to be used as a drug carrier for controlled delivery. Whether they are used for oral, intravenous or transdermal drug delivery, drug loading capacity, release kinetics, particle stability and compatibility are all related with polymer architecture as well as molecular weight and type of polymer (Qiu and Bae, 2006).

Controlled and sustained delivery profiles are not only desired to provide constant plasma levels of the drug after administration. With polymeric particles that are capable of sustained and/or controlled drug delivery, enhanced permeability and retention characteristics of cancerous tumors can be expected to serve for the wellbeing of the patient. This expectancy can be explained by increased drug levels in tumors by passive diffusion. Polymeric micelles have been reported to show prolonged circulation times after intravenous administration and minimum accumulation in liver. Besides drug distribution is reported to be higher in tumors due to perivascular accumulation of macromolecules in tumor tissues with reduced drug levels in general (Sahoo and Labhasetwar, 2003).

Especially for amphiphilic systems, properties of the core material such as hydrophobicity and size of the core are known to be important parameters that determine the performance of polymer in specific applications. It has been reported that hydrophobic core block-length determines stability and loading performance as well as release kinetics. Drug loading performance of the polymer synthesized is expected to increase with increasing molecular weight of hydrophobic core. On the other hand, high molecular weight PMMA cores were not desired for they don't produce biodegradable polymeric materials. Therefore an ideal polymeric micelle for drug delivery purposes must comprise a PMMA core at a molecular weight of oligomer level where PMMA core has to have 10-100 repeating units (Allen et al., 1999) and the resulting polymer should not be greater than 50000 Da in molecular weight (Bontha et al., 2006; Nishiyama and Kataoka, 2006).

In our study main purpose is to synthesize biocompatible and biodegradable amphiphilic nanoparticles that can be effectively loaded by an anticancer drug and tend to accumulate in solid tumors by avoiding reticuloendothelial system. For this reason polymeric micelles with particles sizes less than 100 nm, made of hydrophobic PMMA core and hydrophilic PAA shell have been synthesized and characterized. Considering all the approaches and requirements summarized above, an ideal carrier was tried to be selected among various star block copolymers (# arm PMMA-*b*-PAA) with different number of arms, molecular weights and hydrophobic core ratios. The star block copolymers PMMA-*b*-PAA were synthesized by atomic transfer radical polymerization (ATRP) technique through a two-stage reaction and hydrolysis. The polymers synthesized were investigated in terms of their critical micelle concentrations, maximum loading capacities and drug loading efficiencies. 4 arm PMMA-*b*-PAA with molecular weight about 20 kDa and hydrophobic core ratio of 0.25 is proposed as an ideal drug carrier for parenteral administration and controlled delivery of a widely used anticancer drug, 5 Fluorouracyl.

CHAPTER 2

LITERATURE REVIEW

2.1. Atomic Transfer Radical Polymerization

Star polymers have drawn attention as one of the most promising materials for biomedical applications. They can be tailored for specific purposes providing many opportunities in synthesis (selection of initiators, monomers, catalysts, reaction media, etc.) through the use of controlled polymerization techniques.

The controlled polymerization methods used for the synthesis of block copolymers from vinyl monomers can be listed as ROP (Ring Opening Polymerization), SFRP (Stable Free Radical Polymerization) and ATRP (Atomic Transfer Radical Polymerization) can be employed in various combinations (Tunca et al., 2002; Celik et al., 2003; Erdoğan et al., 2004) ATRP is a beneficial controlled polymerization technique for it allows shorter reaction times at high reaction temperatures and yields acceptable polydispersities (Krishnan and Srinivasan, 2004; Brar and Saini, 2007). Since the initiation is fast and termination is negligible for controlled polymerization techniques, ratio of dead chains are as small as 10% compared to conventional radical polymerization. Another important advantage is possibility of elimination of catalysts used in controlled polymerization while initiator residues inevitably remain in final polymer in radical polymerization (Braunecker and Matyjaszewski, 2007).

Major advantage of ATRP among radical polymerization techniques is availability of reagents which are procurable commercial chemicals such as alkyl halides, transition metals and various ligands. Another important advantage ATRP provides is the precise control over polymerization reaction. Zhao claims that ATRP reaction has almost linear kinetics which paves the way for high reaction yields (Zhao et al, 2001). Polymerization rate mainly depends on initiator concentration and ratio of activator to deactivator concentration as in Equation 2.1.

$$R_p = -\frac{d[M]}{dt} = K_p[M][R\bullet] = K_p[M]K_{ATRP}[RX]\left(\frac{L_m Met^{+n}}{L_m Met^{+(n+1)}}\right) \quad (2.1)$$

R_p is the rate of polymerization, K_p is the propagation constant, [M] is the monomer concentration, and [R·] is the concentrtation of organic radicals generated from alkyl halide initiator (RX). K_{ATRP} is the ratio of activation constant to deactivation constant (=K_a/K_d). L_mMet^{+n} is a transition metal complex that cleaves the alkyl halogen bond of RX and genertes the organic radical species besides the metal halide complex having a higher oxidation state notated as $L_mMet^{+(n+1)}X$. The organic radicals (R·) may either propogate or terminate after they are generated but termination at this stage is generally negligible for ATRP reactions (Braunecker and Matyjaszewski, 2007)..

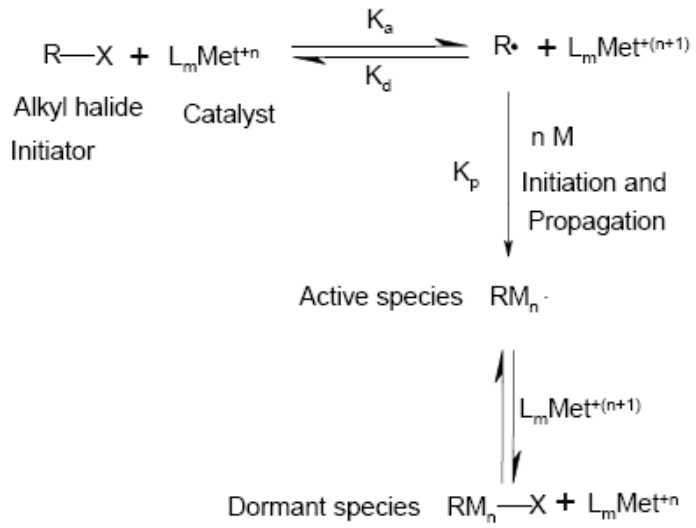

Figure 2.1 Schematic presentation of atom transfer radical polymerization where K_a is rate constant of activation, K_d is rate constant of deactivation and K_p is the rate constant of propagation (Source: Ibrahim, 2006).

Both kinetics and yield of ATRP reactions can be controlled by two major factors; considerably high rate of initiation and persistent radical effect which means continuous activity of catalyst through reaction. For a successful ATRP reaction, termination of the living polymers must be kept at a minimum level. Termination occurs as an undesired reaction between the radical species (RM_n·) which appear as active species in Figure 2.1. The number of radical species is kept low as the reaction equilibrium favors the deactivated (dormant species) side and at low concentration of

radical species a minimum termination occurs. Hence, the kinetic behavior of the reaction mechanism is vitally important to produce a polymer with controlled molecular weight and polydispersity. A fast initiation and rapid reversible deactivation is necessary for uniform growth of polymer chains and narrow molecular weight distributions. An equilibrium between propagating radicals (or active species) and dormant species can be provided by selection of appropriate catalyst and ligand that minimizes termination. Therefore it is a critical issue to create an efficient ligand and catalyst system for a specific polymer. (Coessens et al., 2001; Ibrahim, 2006)

ATRP of vinyl monomers require three components: an organo-halide type initiator, a catalyst which is salt of a transition metal in lower oxidation state and a ligand which is generally an amine compound. ATRP reactions can be mediated by various metals such as Ti (Group 4), Mo (Group 6), Re (Group 7), Fe, Ru, Os (Group 8), Rh, Co (Group 9), Ni, Pd (Group 10) and Cu (Group 11) which is the most efficient. Generally used ligands are nitrogen based compounds which can be listed as bidentate bipyridine, pyridine imine, tridentate diethylenetriamine, tetradentate tris[2-aminoethyl] amine, tetraazacyclotetradecane, etc. (Malinowska et al., 2005; Braunecker and Matyjaszewski, 2007). The homogeneity and distribution of reactants is another important issue and can be acquired by the ligand. 2,2 bipyridine derivatives or linear amines are used as ligands to increase the solubility of the catalyst and accelerate copper mediated ATRP reactions. PMDETA (N,N,N',N",N"-pentamethyl diethylenetriamine) as a ligand was also reported to prove the living character of the polymerization and as the most suitable ligand for ATRP of all functional acrylates and methacrylates. Type of solvent used as reaction media is effective on solubility of the catalyst (Yin et al., 2005; Ibrahim, 2006).

ATRP reaction can be used for the both convergent and divergent synthesis of star block copolymers. Several molecules with various numbers of active sites can be used to initiate reaction. AB and ABC types of block copolymers of a group of monomers involving styrene, vinyl pyridine, acrylates and methacrylates can be produced by ATRP reactions starting from bromo-macromolecules. (Sun et al., 2005)

Active sites generally constitute brominated or chlorinated endgroups. Phenolic ester based initiators or tetra-, hexa-, octa- functional initiators based on calyx[n]arene cores have been proposed for activation in order to be used in ATRP reactions. Multisulfonyl chlorides and brominated D-glucose molecules have also been offered. Chlorinated siloxane, brominated phosphazene molecules may well provide multiarm

initiators for ATRP. Finally, multifunctional initiators brominated by bromoisobutyryl bromide have successfully been used as initiators for ATRP yielding low polydispersities. Divinyl benzene is the most widely used initiator in convergent approach where polymerized arms are connected to each other to form a unimolecular starlike molecule by a difunctional linker which constitutes the very center of the molecule.

ATRP is a robust technique for functional methacrylates. Acrylic acid is an exceptional acrylic monomer that is not easily polymerized by ATRP, because carboxyl groups of acrylic acid interacts with the catalyst. Use of a precursor like tertiary butyl acrylate is preferred for synthesis of poly(acrylic acid). In that case PtBA is synthesized through ATRP, at 60-90°C by using CuBr as catalyst in the presence of a ligand which may be PMDETA or a specific bipyridine. About 25(v)% solvent would better be added to help dissociation of catalyst. PtBA can then be reacted to poly(acrylic acid) (Coessens et al., 2001).

2.2. Biodegradable Polymers Used for Drug Delivery

Smart drug carriers are one of the most attractive research subjects of our era since medicine and medical technologies has been developing so fast parallel to increasing demand of quality in healthcare. One of the most problematic therapies are protein administration and cancer chemotherapy which require controlled doses intravenously applied. Most neoplastic anticancer drugs are hydrophobic and require use of a dissolving agent such as surfactants or specific buffer compositions to be applied.

Especially in chemotherapy, the greatest problems may be counted as short half-life of chemotherapeutic agent, side effects and toxicity besides drug resistance (Manocha and Margaritis, 2008). Because of those problems cancer therapy requires high doses which increases undesired side effects tremendously. Hence, development of controlled drug delivery systems have been a challenge for several decades. Unfortunately an optimized drug delivery system has not been settled yet and so many researches with biodegradable, biocompatible materials such as chitosan, poly(ethylene glycol), poly lactides, polyamidoamine and poly(ethyleneoxide) dendrimers has been going on. In order to obtain an enhanced solubility and controlled delivery of the drug,

commercial liposomes are coupled with anticancer drugs but their use is not a responsive solution due to their poor stability and possible toxicity over critical doses (Qui and Bae, 2006).

Polymeric nanoparticles and especially block copolymers are proposed for their low critical micelle concentrations. A low CMC provides a better stability and solubilization of hydrophobic drugs in aqueous media with very low polymer concentrations when compared to liposomes and conventional surfactants (Rösler et al., 2001; Allen et al., 1999; Tao and Uhrich, 2006; Jones et al., 2008). Theoretical studies on micelle formation of block copolymers focus on CMC since it indicates a measure on aggregation number or number of chains that form a micelle structure. Conventional characterization of block copolymer micelles are known as X-ray scattering, neutron scattering and light scattering techniques. Structure of polymeric micelles can be determined by SAXS (small angle x-ray scattering) of SANS (small angle neutron scattering). Turbidity can be employed for polymers with high molecular weights. Sedimentation and viscometric studies can also be useful for caharacterization of micelle forming polymeric structures. (Gast, 1997)

Micelle formation performance of polymeric micelles are generally estimated by combination of light scattering and determination of CMC by fluorescence spectroscopy. TEM might be used to confirm structures of micelles in addition to those two techniques. Dynamic Light Scattering (DLS) is a very common method to determine hydrodynamic radius of small particles. DLS correlates intensity fluctuations with the scattered light and z-average diffusion coefficient of the scatterers and calculates hydrodynamic from Stokes-Einstein equation given as Equation 2.2. (Candau and Otterwill, 1998).

$$r_h = \frac{k_B T}{6\pi\eta D} \tag{2.2}$$

where k_B is Boltzmann constant, T is temperature, η is solvent viscosity and D is z-average diffusion coefficient.

Fluorescence methods can be used to determine loading capacities besides CMC or CAC by using a fluorophore instead of drug (Zhang et al., 2007). The major problem that emerges with polymeric micelles is optimization of loading conditions to maximize

drug loading efficiencies, because although polymeric micelles have been reported to have very high loading capacities (Leroux and Ranger, 2002) block copolymers of biodegradable polymers generally exhibit low drug loading performances.

Loading a polymeric nanoparticle with a chemically active drug can be possible by both chemical conjugation and physical adsorption/absorption. Physical adsorption has advantages over conjugation for the sake of simplicity of release mechanism, and less sensitivity to changing medium conditions. In this case loading is provided by drug-hydrophobic core interaction which also determines the release characteristics based on diffusion. Both loading and release performances are affected by solvent used as medium, concentration and duration of operation (Qui and Bae, 2006).

As the criteria for evaluating performance of a polymeric drug carrier, properties such as critical micelle concentration, maximum loading capacity, stability and biodegradability has to be considered besides drug release characteristics of the material. The method of loading has been a critical issue which affects all these properties of the loaded particles. According to that, the efficiency is directly dependent on the physical and chemical structure of the polymeric carrier, the drug or selected medium for loading. Several loading methods can be listed as simple equilibrium, co-precipitation, dialysis, solvent deposition and salting-out methods (Gaucher et al., 2005; Lukyanov and Torchilin, 2004; Allen et al., 1999).

Direct solution or simple equilibrium method is recommended for highly soluble amphiphilic copolymers. For acrylic star block copolymers, neutralization and heating treatment may be necessary for solubilizing the polymer in aqueous medium (Burguiere et al., 2003). Hardly soluble block copolymers can be micellized by dialysis method by use of a water miscible solvent or oil in water emulsion (solvent deposition) methods. But these methods require a very careful selection of the solvent for it significantly affects the yield of drug loading. Table 2.1 summarizes studies on drug loading performances of several biodegradable homopolymers and block copolymers, comparing drug loading capacities (as % drug contents) according to loading methods employed. Drug loading capacities are generally expressed in terms of drug loading contents (% DLC) and drug loading efficiencies (% DLE) whose definitions are given in Equations 2.3 and 2.4. m_{drug} the is amount of drug loaded by carrier particle and $m_{particle}$ is the total weight of drug loaded particle in Equation 2.3. In Equation 2.4, $(m_{drug})_{actual}$ is amount of drug that was actually loaded and $(m_{drug})_{theoretical}$ is the amount of drug initially introduced to be loaded by the drug carrier.

Table 2.1. Literature survey for drug loading performances of various biocompatible homopolymers or block copolymers.

Polymer (MW)	**Drug**	**Loading Method**	**DLC %**	**Reference**
PEG dendrimers (>3500)	Indomethacin	Coprecipitation	11	Liu et al., 2000
PCL-PHPMA (25000-35000)	Indomethacin	Dialysis	5-12	Lele and Leroux 2002
PEG (5000, 17000)	Indomethacin Ketoprofen Piroxicam	Coprecipitation	0.7 0.4 1.7	Djordjevic et al., 2003
PLA-PEG (6000-60000)	5-FU Paclitaxel	Dialysis	0.1-2.7	Jie et al., 2005
PEG-*b*-PTMC (20000-70000)	Dexamethasone	Single Emulsion Salting Out	2-14 12-16	Zhang et al., 2006
PLA/PLGA (16000, 100000, 200000)	Doclataxel	Solvent deposition method	<1	Musumeci et al., 2006
PCL-PEO (10000-30000)	at-Retionic acid	Coprecipitation in water	0.2-0.9	Quaglia et al., 2006
PHPMA (15000-35000)	Doxorubicin	Conjugation	4-7	Chytil et al., 2006
PEG-PDLLA-OSM (3000-4000)	Paclitaxel	Solid dispersion pH induced micellization	6.4 7.6	Shim et al., 2006
PEO-*b*-PMA (25000)	Cysplatin	Single Emulsion (incubation at 37ºC)	22	Bontha et al., 2006
PLLA-*b*-PDMAEMA (20000-200000)	Chlorambucil	Film casting	5	Yuan et al., 2007
PNIPAAm-PMMA (80000)	Prednison acetate	Dialysis	11	Wei et al., 2007
MPEG-PCL (18600-30500)	Docetaxel	Nanoprecipitation	19.4	Zheng et al., 2009

$$\%DLC = \frac{m_{drug}}{m_{particle}} \times 100 \tag{2.3}$$

$$\%DLE = \frac{\left(m_{drug}\right)_{actual}}{\left(m_{drug}\right)_{theoretical}} \times 100 \tag{2.4}$$

The drugs used as model drugs are anticancer and anti-inflammatory drugs with hydrophobic character which require aid to be dissolved in aqueous media for administration. A suitable carrier is expected to have a good solubilizing performance for administration as well as keeping plasma levels of drug after administration. Therefore designing smart biodegradable polymeric particles with high loading capacities and good stabilities for controlled delivery of specific drugs is a huge research area where so many approaches are proposed but very few materials could have been commercialized to be used for drug delivery.

Water soluble amphiphilic polymer particles with hydrophobic cores and hydrophilic branches allow solubilization of hydrophobic drugs in aqueous media with no addition of other chemicals such as surfactants. A number of biodegradable, biocompatible polymeric micelles with sustained delivery characteristics have been proposed for both parenteral and transdermal delivery of various drugs, especially the ones that cannot be administered by oral route. Dendritic materials like PAMAM (polyamidoamine) dendrimers (Svenson and Tomalia, 2005; Cheng and Xu, 2008; Asthana et al., 2005; Aulenta et al., 2003) and commercial Eudragit suspensions (methyl methacrylate and methyl methacrylic acid copolymers) (Castelli et al., 2003; Eerikäinen et al., 2004) have been studied in terms of encapsulation and controlled release performance of anti-inflammatory drugs. Polycaprolactam, poly lactic acid, polyvinyl pyrolidone and polyethylene glycol have been the most famous biodegradable polymers proposed for drug delivery (Breitenbach et al., 2000; Kang and Leroux, 2004; Yang et al., 2007; Bartolozzi et al., 2007). But biodegradable polylactide nanospheres were generally reported to indicate relatively low loading capacities (less than 5w%) (Klose et al., 2008; Kang et al.,2008; Castelli et al., 1997) and a burst effect due to relatively high loading of drug (Musumeci et al., 2006). Star shaped PEG micelles which were commonly loaded by co-precipitation method also yielded low loading capacities with anti-inflammatory drugs (Djordevic et al., 2003).

Frechet proposes pH sensitive poly ethylene oxide block copolymers as drug carriers for cancer therapy because tumors have slightly more acidic media compared to normal metabolism (Gillies and Frechet, 2004). Diblock copolymers of *t*-butyl methacrylate and 2-(diethylamino)ethyl methacrylate were also reported to show pH sensitivity (Mao et al., 2005). Doxorubicin loaded poly(ethylene oxide):poly(b-benzyl L-aspartate) micelles were reported to have thermosensitivity properties, besides small diameters and a low critical micelle concentrations (Marion et al., 1999).

Nondegradable *N*-(2-Hydroxypropyl)methacrylamide copolymers and biodegradable poly(ethyleneglycol) multiblock copolymers were designed as water-soluble carriers of anticancer drug doxorubicin and the drug release of the conjugates was observed to be faster under mildly acidic conditions (Chytil et al., 2006; Ulbrich et al., 2003). Some commercial polymeric micelles (Pluronic and polyethylene glycol–distearoylphosphatidyl ethanolamine) were tried for the solubilization of several poorly water-soluble anticancer drugs and it was reported that, polymeric micelles were highly stable up to particle size of 100 nm and the loading capacities changed according to polymer and drug type (Sezgin et al., 2006).

Poly (trimethylene carbonate)–poly(ethylene glycol)–poly(trimethylene carbonate) nanoparticles were studied for the controlled release of methotrexate (a, hydrophobic, anticancer drug) but the loading capacities were relatively low (Zhang and Zhuo, 2005a).

Nanospheres prepared by solvent displacement method using polylactic acids (PLA) at different molecular weight and polylactic-co-glycolic acid (PLGA) were studied for their drug loading and drug release performances with the drug doclataxel. Poly(d,l-lactide-*co*-glycolide) was studied for a controlled release of another anti-cancer drug, paclitaxel (Kang et al., 2004). The biodegradable nanospheres also showed relatively low loading capacity, and a burst effect prior to sustained release profiles (Musumeci et al., 2006).

Effect of crosslinking was investigated on block ionomer complexes of poly (ethylene oxide)-*b*-poly(methacrylic acid) copolymers which constituted hydrophilic nanospheres of core-shell morphology. It was reported that crosslinked polymethacrylate cores exhibited pH dependent swelling behavior and cisplatin, a potent chemotherapeutic agent, was incorporated into the ionic core of the micelles with remarkably high efficiency (22% w/w). The drug-loaded micelles were stable in aqueous dispersions exhibiting no aggregation or precipitation for a prolonged period of time. Slow release of platinum complexes was observed in sustained manner from the cisplatin-loaded cross-linked micelles (Bontha et al., 2006). An overview of the studies suggest that loading capacities of block copolymers with acrylic blocks are much higher than conventional biodegradable polymers. PEG carriers grafted or copolymerized with block or branched polymers involving phenolic or acrylic groups exhibited improved loading and solubilizing capacities exceeding 10w% (Sant et al., 2005; Liu et al., 2000). PCL (Lele and Leroux, 2002; SanMiguel et al., 2008), PVP (Sairam et al., 2007), and

PEO (Bontha et al., 2006) polymers showed superior drug loading performances when compared to other polymeric carriers when copolymerized with acrylic polymers.

The selection of acrylic star block copolymers as anticancer drug carriers also depend on their reported advantages over many of other biomaterials. They have extremely low critical micelle concentrations, can be designed and synthesized in a controlled manner with low polydispersities and can be modified for specific purposes. Poly (methyl methacrylate)-block poly(t-butyl acrylate) copolymers yield stable amphiphilic polymeric nanoparticles with very high stability in aqueous media. Their ease of precisely controlled molecular weights, number of arms and hydrophobic core ratios is an opportunity for optimization of those for physical drug loading for a specific drug. It has been reported that hydrophobic core block-length determines stability and loading performance as well as release kinetics. Hence, drug loading performance is expected to increase with increasing molecular weight of hydrophobic core. On the other hand, high molecular weight PMMA cores were not desired for the difficulty of biodegradation as molecular weight increases. Hence an ideal polymeric micelle for drug delivery purposes must consist of a PMMA core at a molecular weight of oligomer level where PMMA core has to have maximum 10-100 repeating units (Allen et al. 1999) and the resulting polymer should not be greater than 50000 Da in molecular weight (Nishiyama and Katakoa 2006, Bontha et al. 2006). An ideal drug carrier should have a size less than 200 nm (preferably 10-100 nm) and should remain in bloodstream for long time for a successful biodistribution. But it should not accumulate within the liver, kidneys or lungs. This accumulation phenomenon called as "glomerular excretion" can be avoided by water-soluble polymeric carriers (with 42-50 kDa molecular weights) despite their elongated durations in blood circulation system. On the contrary, they tend to accumulate in tumors (Nishiyama and Kataoka, 2006).

Poly methyl methacrylate is known as a non-degradable biocompatible polymer widely used as joints for bone repairing and in dental applications. It has also been reported as a drug release agent and has been listed among biocompatible core materials to form amphiphilic block copolymers to serve as drug carriers (Brannon-Peppas, 1997; Ning et al., 2002). Poly methyl methacrylate grafted chitosan particles were reported to be nontoxic and blood-compatible (Radhakumary et al., 2005). A four arm star copolymer of poly acrylic acid arms with pentaerythritol core was investigated as a dental filler and was found that cytotoxicity depended on molecular weight and dose (Xie et al., 2006).

Poly (acrylic acid) is the most suitable and common hydrophilic acrylic polymer used in medicine and food chemistry. PtBA completely hydrolyses to produce poly acrylic acid which is an approved food and drug ingredient and a conventional controlled drug delivery agent (Burguiere et al., 2003; Brannon Peppas, 1997). Polymeric micelle produced from a PMMA core and PAA shell synthesized by hydrolysis of PMMA-*b*-PtBA has been reported to have acceptable solubilizing performance of silver particles (Ishizu et al., 2005). In fact, many studies are available on synthesis and characterization of acrylic block copolymers by controlled polymerization techniques but studies that focus on solubilization performance are rather few (Narrainen et al., 2002; Even et al., 2003; Limer et al., 2006).

2.3. Delivery of Anticancer Drugs with Biodegradable Particles

Cancer as one of the major issues in medicine still occupies a great deal of research in hope of improving chemotherapy and radiotherapy. Therapeutic difficulties of these applications mainly originate from the nature of disease that has the ability to modify its surrounding for its growing and proliferation. Drug resistance and lack of selectively toxic anticancer agents are other issues that make cancer treatment difficult and risky. Drug resistance or chemotherapy resistance means the low uptake of drug by solid tumors which require either increasing doses or enhancing diffusion through cancerous tissues. Increased doses cause detrimental side effects which may sometimes be fatal. Therefore invention of smart drug carriers or targeting mechanisms constitutes an extremely important part of cancer research. For designing a system that aims a chemotherapy with increased influence on tumors or/and cancer cells and minimized contact with healthy cells, it has to be considered how cancer grows.

Cancer starts in mutated single cells which replicate at higher rates than normal cells. Cancerous cells occupy most nutrients and oxygen in their environment and replace normal cells by growing faster than them. The growth continues until tumor reaches to its diffusion limited maximal size which claims a steady state. At this state, the nutrients and oxygen occupied by cancerous cells at the surface cannot diffuse through solid tumor and reach to the core where cell death begins. At this maximal size which is about 2 mm^3 number of proliferated cells is about the same as the ones that die due to lack of nutrients. For further growing, cancerous tissue organizes vascularization

which provides more nutrients and oxygen by formation of new vessels. This phenomena is called as angiogenesis. Next and most dangerous activity of cancerous cells is transportation through blood or nymph vessels and cause formation of new tumors as shown in Figure 2.2. Different approaches for site specific chemotherapy have been proposed to prevent formation and proliferation of cancerous cells for different stages of tumor formation. (Brannon-Peppas and Blanchette, 2004; Manocha and Margaritis, 2008) They may be listed as follows:

1. Avoiding reticuloendothelial system: Reticuloendothelial system is defense mechanism of metabolism for the clearance of alien particles and microorganisms from the body. Alienated particles are filtered through liver, spleens and lungs and are sequestered by macrophages. If a particle designed for specific drug delivery purpose have the size, morphology and surface characteristics that avoid being eliminated by the reticuloendothelial system, it may remain in circulatory system until it degrades and rather accumulates in solid tumors. These particles should have a particle size less than 100 nm and hydrophilic surface.

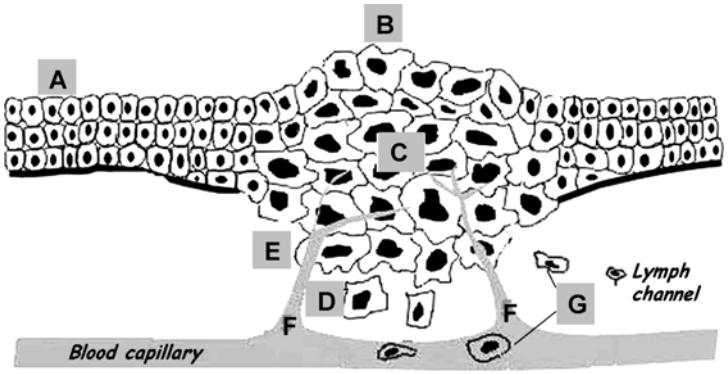

Figure 2.2. Stages in tumor development: (A) healthy cells—nutrient rich, normal replication rate; (B) peripheral cancerous tissues bathe in nutrients, higher replication rate, gradient decrease in nutrient supply from periphery to core; (C) necrotic core—very low to no nutrient supply, interstitial pressure decreases from core to periphery; (D) tumor reaches diffusion-limited maximum size (2 mm^3), cells break off from primary tumor; (E) cancer cells invades into local tissues; (F) angiogenesis; and (G) metastasis via blood and lymph vessels. (Manocha and Margaritis, 2008)

2. Enhanced permeability and retention: Ensembled cancerous cells have been observed to have enhanced permeability due to vascularization around the tumor formation. Although it allows overfeeding of cancerous tissues, in classical

chemotherapy this is thought to be the reason for the effectiveness of toxic drugs on cancerous tissues rather than healthy cells although it may not work for every case. Retention is another property observed in solid tumors due to poor lymphatic drainage.

3. Tumor specific targeting: Since cancer cells need overfeeding, particular antigens within their medium are overexpressed. Folic acid is the most famous protein observed at extended amounts in tumors. Folate receptors are expected to tend to cancer cells which allow tumor targeting.

4. Prodrugs: Prodrugs are complexes that have been designed to activate only after reaching tumors. For this purpose specific linkers and ligands are used. Toxic drug is conjugated by a linker that is usually broken by peptidase or acidic medium that are peculiar to environments of cancerous cells. But the mechanism may not work properly in any case for *in vivo* conditions may vary from person to person and are hard to predetermine.

5. Targeting through angiogenesis: Instead of overexpressed antigens, some angiogenesis stimulating molecules can be targeted to get into tumors. The molecules that have this capability are vascular endothelial growth factor, basic fibroplast growth factor, platelet-derived growth factor, and some metalloproteinases which indicate suspicious vascularization. To prevent angiogenesis and in turn avoid feeding of cancerous cells can be possible by limiting endothelial proliferation, introducing angiogenesis inhibitors, avoiding angiogenesis stimulatory factors. Both are possible to prevent angiogenesis or use angiogenesis as a selective route to deliver toxic drugs to cancerous sites.

5FU is a hydrophobic neoplastic anticancer drug which is widely used in breast, colon, pancreas and eye cancer (Pascu et al., 2003). To prevent side effects, decrease drug resistance, provide elongated influence in circulatory system and a controlled delivery, various nanocarriers were investigated in terms of 5FU loading and release performance as listed in Table 2.2. With poly(lactide-*co*-glycolide) 3.8 % drug content could be achieved (McCarron and Hall, 2008). Entrapment of 5FU by crosslinking during loading was studied with acrylic copolymers but loading with adsorption/absorption yielded better drug loading efficiency which depended on drug concentration (Babu et al., 2006).

One way of minimizing toxic side effects of 5FU was proposed as preparation of polymer-5FU conjugates. Sulfated polysaccharides have been proposed for 5FU conjugation although the release properties were not desirable for cancer therapy.

Table 2.2 Drug Loading Contents (DLC) and Drug Loading Efficiencies (DLE) of several biomaterials loaded with anti-cancer drug 5-FU.

Material	MW (kDa)	Loading Method	DLE* %	DLC* %	Reference
PAMAM dendrimer	5-20	Conjugation	-	<1	Zhuo et al, 1998
PVP hydrogel network	10-18	Conjugation	-	<1	Liu & Rimmer, 2002
PLGA microsphere	40-75	Solvent Evaporation	50	<1	Gupte & Ciftci, 2004
PLA-*b*-PEG nanoparticles	8-60	Solvent Evaporation	10-50	<2	Jie et al, 2005
PDTC-*b*-PEG-*b*-PDTC	74-13	Dialysis	17-7	4-2	Zhang & Zhuo, 2005b
PLA fibers	100-200	Wet Spinning	75-90	10	Gao et al, 2007
Chitosan/PAsp nanoparticles	18/5	Absorption	10-35	10-28	Zheng et al, 2007
Chitosan	55-550	Crosslinking	28-66	-	Yang & Hon, 2009
Chitosan/PEG microparticles	300	Phase Inversion	70	<1	Lin & Fu, 2009
Porphyran LMW Porphyran	250 5	Conjugation	80 60	4-7 18	Zhang et al, 2010

* DLC and DLE are defined by Equations 2.3 and 2.4.

The conjugates showed fast initial releases reaching almost equilibrium within the first 10 hours with relatively higher rates of release in basic media while it is known that the medium is slightly acidic in cancerous regions (Zhang et al., 2009). Zhuo et al achieved controlled release profiles over seven days of periods by dendrimer conjugates of 5FU (Zhuo et al., 1999). Another succesfull attempt is 5FU conjugates with poly(N-vinyl pyrrolidone) derivatives which provide quite slow release profiles (Liu and Rimmer, 2002). The main disadvantage in this application is that minute amounts of drug can be introduced by conjugation due to great difference in molecular weights of drug and conjugated polymer.

Polyorganophosphazene microparticles were loaded with indomethacin and 5FU by solvent evaporation technique yielding very high loading contents up to 50%. But the microparticles delivered loaded drug very fast (Gudasi et al., 2006).

Chitosan is another biomaterial proposed for controlled 5FU delivery (Yang et al., 2009). Some studies with hydroxyapetite and chitosan yield insignificant 5FU loading contents less then 1% although they have been proposed as controlled delivery agents (Dodova et al., 2009; Santos et al., 2009). Lin et al. studied crosslinking of chitosan / polyethylene glycol microparticles to provide controlled release of 5FU and Jain improved release profiles with incorporation of hyaluronic acid in chitosan particles. But drug loading capacities were still poor and 50% of the loaded drug was released in the first 12 hours (Lin and Fu, 2009; Jain and Jain, 2008). Zheng et al. attained high loading drug contents (20-30%) by using hydrophilic particles of chitosan and polyaspartic acid salt and they could obtain controlled release from particles through glutaraldehyde crosslinking (Zheng et al., 2007).

Acrylamide methyl methacrylate copolymers of core and shell type were also loaded to yield high 5FU contents (5-15%) by *in situ* polymerization of monomers. The release rates were proposed to depend on degree of crosslinking via N,N'-methylene bisacrylamide and 5FU contents of loaded microparticles (Babu et al., 2006). 5FU loaded nanoparticles (30 nm) of poly(γ-benzyl-L-glutamate) (PBLG) as and poly(ethylene glycol) (PEG) exhibited very high loading capacity about 27% by dialysis method. But 40% of loaded content was released in two hours (Li et al., 2008).

5FU loading to PLGA particles is commonly achieved by precipitation/solvent evaporation techniques. Main problem reported about drug delivery performance of PLGA is the burst effect which means sudden release of loaded drug due to fast degradation (Gupte and Ciftci, 2004). Poly(L-lactic acid) microfibres were loaded with 5FU achieving high loading capacities (10%) by wet-spinning method but burst effect remains as a challenging problem (Gao et al., 2007).

CHAPTER 3

THEORY

3.3. Theoretical Models for Drug Release

Practical use of controlled drug release systems require well-defined kinetic behavior that provides administration of a specific drug at an optimum level through release process. Tailored materials proposed for drug delivery are investigated in terms of capacity and length of release in the search of accomplishing a controlled release behavior. Controlled release of drugs from nanoparticles that were administered into circulatory system is required to provide safe and efficient plasma levels of the drug.

Controlled release systems by using biodegradable particles can be categorized as reservoir systems, matrix systems, chemically controlled systems and swelling particles. Although it is difficult to make certain distinctions between release profiles of those systems, each system exhibits characteristic release properties in parallel to physical and structural conditions they occupy.

Reservoir and matrix systems are commonly expected to be diffusion derived systems. An ideal reservoir system can be defined as a sorce of drug, covered with a permeable membrane that provides a constant release. This ideal case can be expressed by zero order release kinetics. Another ideal case is bioerodible particles that disintegrate with a constant rate and converge to first order release kinetics. On the other hand, when the only release mechanism is diffusion through a membrane Fick's diffusion equation (Equation 3.1) applies (Langer and Peppas, 1981; Crank, 1975).

$$J = -D\frac{dc_i}{dx} = -DK\frac{dc}{dx} \tag{3.1}$$

where J is flux of active ingredient, D is diffusivity of the active ingredient in the rate controlling membrane, and dc_i/dx is the concentration gradient of the substance in the membrane. Equation 3.1 can be written substituting concentration gradients between

solutions on the two sides of the membrane with introduction of K, ratio of concentration in the membrane to the concentration in the solution named as partition coefficient. KD can also be expressed as permeability of the membrane, P.

Fickian diffusion through a rate controlling membrane is the most general form of release mechanism in reservoir type drug release systems. Fickian diffusion through spherical particles is commonly expressed as in Equation 3.2, by transient diffusion equation which is used to find diffusion coefficient through polymeric particles:

$$\frac{\partial q}{\partial t} = \frac{D}{r^2}\frac{\partial}{\partial r}\left(r^2 \frac{\partial q}{\partial r}\right) \tag{3.2}$$

Equation 3.2 shows the change in amount of substance released from spherical particles, where q represents amount of substance transferred through particle, r is distance from the center of the sphere and D is diffusion coefficient. This equation assumes constant diffusion coefficient and the case is valid at low concentrations considering the following initial and boundary conditions (Crank, 1975; Klose et al. 2008) :

$$\begin{gathered} \text{at } t = 0,\ q = M \\ \text{for } t > 0 \text{ and at } R = R_p,\ q = M_t \\ \text{for } t > 0,\ \left(\frac{\partial q}{\partial r}\right)_{r=0} = 0 \end{gathered} \tag{3.3}$$

Integration of Equation 3.2 with the boundary conditions given by Equation 3.3 ends in Equation 3.4 for spherical particles and that can be simplified as in Equation 3.5 by reducing the series to the first term (n=1). Equation 3.6 is a further simplified form to be used for calculation of diffusivity from initial slope of M_t/M versus $t^{1/2}$ graph.

$$\frac{M_t}{M} = 1 - \frac{6}{\pi^2}\sum_{n=1}^{\infty}\frac{1}{n^2}\exp\left(-\frac{n^2\pi^2 Dt}{r_p^2}\right) \tag{3.4}$$

$$\frac{M_t}{M} = 1 - \frac{6}{\pi^2} \exp\left(- \frac{\pi^2 Dt}{r_p^2} \right) \tag{3.5}$$

$$\frac{M_t}{M} = 4\left(\frac{Dt}{\pi r_p^2} \right)^{1/2} \tag{3.6}$$

However, release kinetics observed in most of the systems that depend on diffusion are preferably modeled by zero order or first order kinetics. Zero order kinetics considers release systems where release rate remains constant and is independent of the instantaneous drug content of the reservoir. First order release kinetics generally indicate proportionality of release rate to drug content of reservoir. These ideal and extreme conditions can be expressed by the simple mathematical equations given by Equations 3.7-3.9. But it shoul be reminded that most of the actual drug release system, a correspondence with theoretical models can merely be obtained in the first one third interval of total release period. (Ritger and Peppas, 1987; Ho and Sirkar, 1992; Heng et al. 2001; Prabakaran et al. 2003).

Zero Order ;

$$M_o - M_t = k_o t \tag{3.7}$$

First Order;

$$\frac{M_t(t)}{M} = kt \tag{3.8}$$

Fickian Diffusion model;

$$\frac{M_t(t)}{M} = kt^{0.5} \tag{3.9}$$

Ritger-Peppas model;

$$\frac{M_t(t)}{M} = kt^n \tag{3.10}$$

Ritger and Peppas stated by Equation 3.10 provides a far more general definition of release system with any value of n, covering $t^{-1/2}$ release systems. Value of n determined by Ritger-Peppas model virtually shows the diffusion characteristics of the system. For the cases where n=0.5, cartesian system of mass transfer is said to be Fickian and the transfer is completely diffusion driven. When the diffusion occurs through spherical particles n is expected to be 0.43 to be considered Fickian. An n value between 0.5 and 1 indicates anomalous behavior which may be explained by existance of a release profile driven by both diffusion and another release mechanism. Any deviation from predetermined power of theoretical kinetic model can be caused by other physical aspects of the system like swelling, relaxation or erosion of the particles (Lowman and Peppas, 1999).

3.2. Description of the System

Drug release profile of loaded PMMA-*b*-PAA nanoparticles were estimated by a continuous release process which took place in a diffusion cell that is schematically shown in Figure 3.1. Loaded particles were placed in donor compartment and released amount of drug that passed through a semipermeable membrane was continuously monitored from the stream passing through receptor compartment.

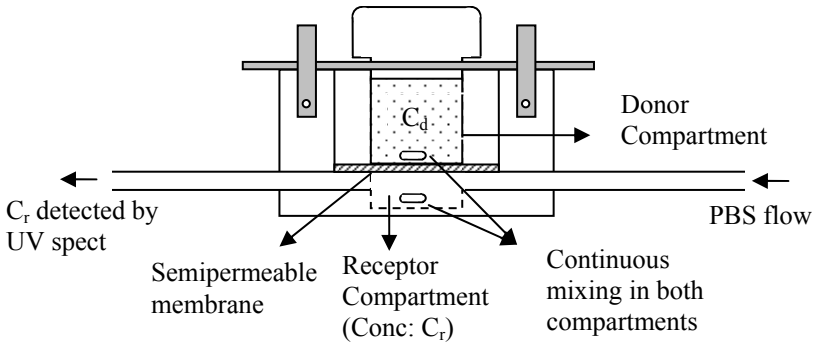

Figure 3.1. Schematic representation of the diffusion cell where drug release occurs.

Since both compartments are well mixed, the mass transfer resistance is assumed to be the resistance of membrane that separated the two compartments. Therefore overall mass transfer coefficient occurs to be the permeation of the membrane and Equation 3.13 which is derived from Equation 3.1 is used to determine drug concentration in donor compartment starting from drug concentration measured from receptor compartment.

$$\frac{d\mathrm{M}}{dt} = AP(C_d - C_r) \tag{3.13}$$

$$M = C_r V_r \tag{3.14}$$

where M is amount of drug that is transferred by diffusion through membrane and defined as in Equation 3.14, C_d is concentration of drug in donor compartment, C_r is concentration of drug in receptor compartment, V_r is volume of receptor compartment, A is area of diffusion and P is permeability (Lowman and Peppas, 1999).

$$\frac{d(C_r V_r)}{dt} = AP(C_d - C_r) \tag{3.15}$$

For the volume of receptor (V_r) is constant;

$$\frac{dC_r}{dt} = \frac{AP}{V_r}(C_d - C_r) \tag{3.16}$$

Substituting C_r= Y(t) and C_d= X(t) :

$$\frac{dY(t)}{dt} = \frac{AP}{V_r}(X(t) - Y(t)) \tag{3.17}$$

$$\frac{dY(t)}{dt} + \frac{AP}{V_r}Y(t) = \frac{AP}{V_r}X(t) \tag{3.18}$$

In Equation 3.18, both concentration functions in donor and receptor compartments are time dependent. Y(t), namely drug concentration in receptor compartment can be experimentally determined and is to be dependent on drug concentration in donor compartment. Therefore a mathematical expression that represents drug release profile from polymeric nanoparticles is required for an ultimate analysis of drug release behavior of drug loaded particles. It can be managed by analytial solution of Equation 3.18 assuming $X(t)=k_n t^n$, expecting that drug release from particles will be explained by one of the well-known mechanisms which can be summarized as zero order kinetics (n=0) or Fickian diffusion (n=0.5) or first order kinetics (n=1).

Solution of the first order linear differential equation given by Equation 3.18 is as follows:

$$\frac{dY(t)}{dt}e^{\frac{AP}{V_r}t} + \frac{AP}{V_r}e^{\frac{AP}{V_r}t}Y(t) = \frac{AP}{V_r}e^{\frac{AP}{V_r}t}X(t) \tag{3.19}$$

$$\frac{d}{dt}\left(Y(t)e^{\frac{AP}{V_r}t}\right) = \frac{AP}{V_r}e^{\frac{AP}{V_r}t}X(t) \tag{3.20}$$

$$\frac{d}{dt}\left(Y(t)e^{\frac{AP}{V_r}t} \right) = \frac{AP}{V_r} e^{\frac{AP}{V_r}t} (k_n t^n) \tag{3.21}$$

$$\int d\left(Y(t)e^{\frac{AP}{V_r}t} \right) = \frac{AP}{V_r} \int e^{\frac{AP}{V_r}t} (k_n t^n) dt \tag{3.22}$$

$$Y(t)e^{\frac{AP}{V_r}t} + C_0 = \frac{AP}{V_r} \int e^{\frac{AP}{V_r}t} (k_n t^n) dt \tag{3.23}$$

Integrating Equation 3.23 by using "integration by parts": $\int udv = uv - \int vdu$,

$u = t^n$, $du = nt^{n-1}dt$, $v = \frac{e^{\kappa t}}{\kappa}$, $dv = e^{\kappa t}dt$ (where $\kappa = \frac{AP}{V_r}$)

$$Y(t)e^{\kappa t} = \kappa k_n \left[\frac{t^n e^{\kappa t}}{\kappa} - \frac{n}{\kappa} \int e^{\kappa t} t^{n-1} dt \right] + C_1 \tag{3.24}$$

$$Y(t)e^{\kappa t} = k_n t^n e^{\kappa t} - k_n n \int e^{\kappa t} t^{n-1} dt + C_1 \tag{3.25}$$

$u = t^{n-1}$, $du = (n-1)t^{n-2}dt$, $v = \frac{e^{\kappa t}}{\kappa}$, $dv = e^{\kappa t}dt$

$$Y(t)e^{\kappa t} = k_n t^n e^{\kappa t} - k_n n \left[\frac{t^{n-1} e^{\kappa t}}{\kappa} - \frac{n-1}{\kappa} \int e^{\kappa t} t^{n-2} dt \right] + C_2 \tag{3.26}$$

$u = t^{n-2}$, $du = (n-2)t^{n-3}dt$, $v = \frac{e^{\kappa t}}{\kappa}$, $dv = e^{\kappa t}dt$

$$Y(t)e^{\kappa t} = k_n t^n e^{\kappa t} - k_n n \frac{t^{n-1}}{\kappa} e^{\kappa t} + \frac{k_n n(n-1)}{\kappa} \left[\frac{t^{n-2} e^{\kappa t}}{\kappa} - \frac{n-2}{\kappa} \int e^{\kappa t} t^{n-3} dt \right] + C_3 \tag{3.27}$$

$$Y(t) = k_n t^n - k_n n \frac{t^{n-1}}{\kappa} + k_n n(n-1)\frac{t^{n-2}}{\kappa^2} - k_n n(n-1)(n-2)\frac{t^{n-3}}{\kappa^3} + ... - k_n n! \frac{t^0}{\kappa^n} + \frac{C_n}{e^{\kappa t}} \quad (3.28)$$

Equation 3.28 is verified by analytical solution of integration in the form $\int e^A x^m dx$ where A is defined as bx provided that b is a constant (Tuma, 1987).

Converting concentration of drug in receptor compartment which is a function of time given in Equation 3.27 to amount of released drug shown in Equation 3.28, it will be possible to compare theoretical amount of released drug with experimental data that represented the amount of drug released from polymer particles within donor compartment, permeated to receptor compartment through membrane and measured continuously by UV-spectrophotometry. Once again, concentration variation of drug in receptor compartment is denoted by Y(t), and in donor compartment by X(t). M_t represents the cumulative amount of drug continuously released from the system and determined by summation of instantaneous amounts at certain time intervals determined by UV-spectrophotometry. F is volumetric flow rate of buffer solution passing through receptor compartment.

$$M_t(t) = \int Y(t) F dt \quad (3.29)$$

$$M_t(t) = k_n \frac{t^{n+1}}{n+1} F - k_n \frac{t^n}{\kappa} F + k_n n \frac{t^{n-1}}{\kappa^2} F - k_n n(n-1)\frac{t^{n-2}}{\kappa^3} F + ... + C_n e^{-\kappa t} + C \quad (3.30)$$

Equation 3.29 is an alternating series which converges and can be reduced to the first five terms as in Equation 3.30.

$$\begin{aligned} M_t(t) = k_n \frac{t^{n+1}}{n+1} F - k_n \frac{t^n}{\kappa} F + k_n n \frac{t^{n-1}}{\kappa^2} F - k_n n(n-1)\frac{t^{n-2}}{\kappa^3} F \\ + k_n n(n-1)(n-2)\frac{t^{n-3}}{\kappa^4} F + C_n e^{-\kappa t} + C \end{aligned} \quad (3.31)$$

where C_n and C are integral constants.

3.3. Permeation through Membrane

In order to define the system schematically described in Figure 3.1 by a mathematical model, permeability of the membrane that separates two compartments of the diffusion cell has to be known. Permeability is estimated by performing an experiment where a known concentration of drug solution not loaded to any carrier has been placed in donor compartment, passed through the membrane and monitored versus time.

Assumptions related to this experiment performed in the diffusion cell are:

- Initial drug concentration is constant.
- Solutions in both compartments are homogeneous.
- Permeation is unidirectional in normal direction to the membrane.
- Perfect sink conditions are provided.

Then Equation 3.16 can be reconsidered for these conditions where C_d is constant and known. Integrating Equation 3.16 for boundary conditions that are $C_r=0$ at $t=0$, and $C_r=C_r(t)$ at $t=t$:

$$\int \frac{dC_r}{(C_d - C_r)} = \int \frac{AP}{V_r} dt \tag{3.32}$$

$$-\ln(C_d - C_r)\Big|_0^t = \frac{AP}{V_r} t \tag{3.33}$$

$$-\left[\ln(C_d - C_r) - \ln(C_d)\right] = \frac{AP}{V_r} t \tag{3.34}$$

$$-\frac{V_r}{A}\left[\ln\frac{C_d - C_r}{C_d}\right] = Pt \tag{3.35}$$

$$-\frac{V_r}{A}\ln\left[1 - \frac{C_r}{C_d}\right] = Pt \tag{3.36}$$

CHAPTER 4

MATERIALS AND METHODS

4.1. Materials

Pentaerythritol (PENTA) (Aldrich, 98%) and dipentaerythritol (diPENTA) (Charmor, 96%) was dried at 180 ºC for 3 hours and cooled under nitrogen. 1,3,5-trihydroxybenzene was dried at 110 ºC and cooled under nitrogen. 2-bromoisobutyryl bromide (Fluka, 97%), triethylamine (TEA) (Riedel-de-Haen, 99%) and 4-dimethylaminopyridine (DMAP) (Fluka, 99%) were used as received. Tertiary butyl acrylate (tBA) (Aldrich, 99%) and methyl methacrylate (MMA) (Aldrich, 99%) were passed through basic alumina columns for removal of stabilizers. N,N,N',N",N"-pentamethyl diethylenetriamine (PMDETA) (Aldrich, 99%) was distilled over NaOH before use. Tetrahydrofuran (THF) (J.T. Baker, 99.8%) was dried and distilled over $LiAlH_4$. The other solvents, namely ethanol, methanol, n-hexane, diethyl ether and dichloromethane were purified by conventional procedures. CuBr (Aldrich, 99.999%) and anisole (Aldrich, 99%) was used without further purification. Other solvents such as dimethyl formamid, dichloromethane, ethanol and methanol were at reagent grade. Trifluoroacetic acid (TFAA) (Aldrich, 99%) was used for hydrolysis. Pyrene (Fluka, 99%) was employed as the fluorescent probe. Indomethacin (Fluka, 99%) and 5 Fluorouracil (5FU) (Aldrich, 99%) were used as model drugs. Standard PBS (phosphate buffer solution) at pH value 7.4 was prepared by dissolving 8 g NaCl, 0.2 g KCl, 1.44 g Na_2HPO_4 and 0.24 g KH_2PO_4 in 1 L deionized water.

4.2. Synthesis of Initiators

Brominated 1,3,5-trihydroxybenzene so called 1,3,5-(2-bromo-2-methyl propionate) benzene was synthesized from 1.73 gr 1,3,5-trihydroxybenzene in THF (tetrahydrofuran). 1 gr DMAP (dimethyl amino pyridine) was dissolved in 130 ml THF, and 1,3,5-trihydroxybenzene was added. 6.7 ml TEA (triethyleneamine) was dissolved

in 30 ml THF and added under nitrogen. Then 6 ml 2-BIB (2-bromoisobutyryl bromide) was added dropwise at 0˚C in 20 minutes. Afterwards addition of reactants, reaction vessel was stirred at room temperature overnight. The product was filtered, THF was evaporated, the powder was dissolved in Cl_2CH_2, washed with water twice, washed with 5% sodium bicarbonate solution to remove unreacted 2-bromoisobutyryl bromide, Cl_2CH_2 phase was seperated, dried over $MgSO_4$, and finally vacuum dried. For further purification brominated 1,3,5-trihydroxybenzene is dissolved in 150 ml Cl_2CH_2, washed with 50 ml 1% NaOH solution and water, dried over $MgSO_4$, then vacuum dried, dissolved in diethyl acetate and recrystallized in 20% ethyl acetate-80% hexane solution.

Brominated pentaerythritol so called pentaerythritol tetrakis (2-bromoisobutyrate) was synthesized from 1.09 gr pentaerythritol in THF. 1 gr DMAP was dissolved in 130 ml THF, and pentaerythritol was added. 6.7 ml TEA was dissolved in 30 ml THF and added under nitrogen. Then 6 ml 2-BIB was added dropwise at 0˚C. The reaction vessel was warmed up to room temperature and stirred under nitrogen overnight. The product was filtered, THF was evaporated, the powder was dissolved in Cl_2CH_2, washed with water twice, washed with 5w% sodium bicarbonate aqueous solution to remove unreacted 2-bromoisobutyryl bromide. Cl_2CH_2 phase was separated and dried over $MgSO_4$ and finally vacuum dried. For further purification, the initiator was dissolved in Cl_2CH_2, washed with 1w% NaOH solution and deionized water, dried over $MgSO_4$, vacuum dried and recrystallized in diethyl ether.

Brominated dipentaerythritol so called di-pentaerythritol hexakis (2-bromoisobutyrate) was synthesized from 1.35 gr pentaerythritol in THF as described above. For further purification brominated pentaerythritol is dissolved in Cl_2CH_2, washed with 1% NaOH solution and water, dried over $MgSO_4$, vacuum dried and recrystallized in diethyl ether.

4.3. Synthesis of Macroinitiators

Multiarm PMMA macroinitiators were synthesized from 10 ml of methyl methacrylate. Monomer was diluted with anisole at 1:1 volumetric ratio. For the polymerization reaction, 78.1 μL ligand (PMDETA) and 0.037 gr catalyst (CuCl) was introduced. Initial molar ratio of monomer/initiator was 250 for each arm. The reactants

were purified from oxygen by degassing through three freeze-thaw cycles. Freezing and thawing process was performed on a vacuum line schematically shown in Figure 4.1. Then reactants eliminated from dissolved O_2 and moisture were reacted for 10-12 minutes at 70 ºC as shown in Figure 4.2. The product was passed through neutral activated alumina column, vacuum dried, diluted in tetrahydrofuran and precipitated in hexane for purification.

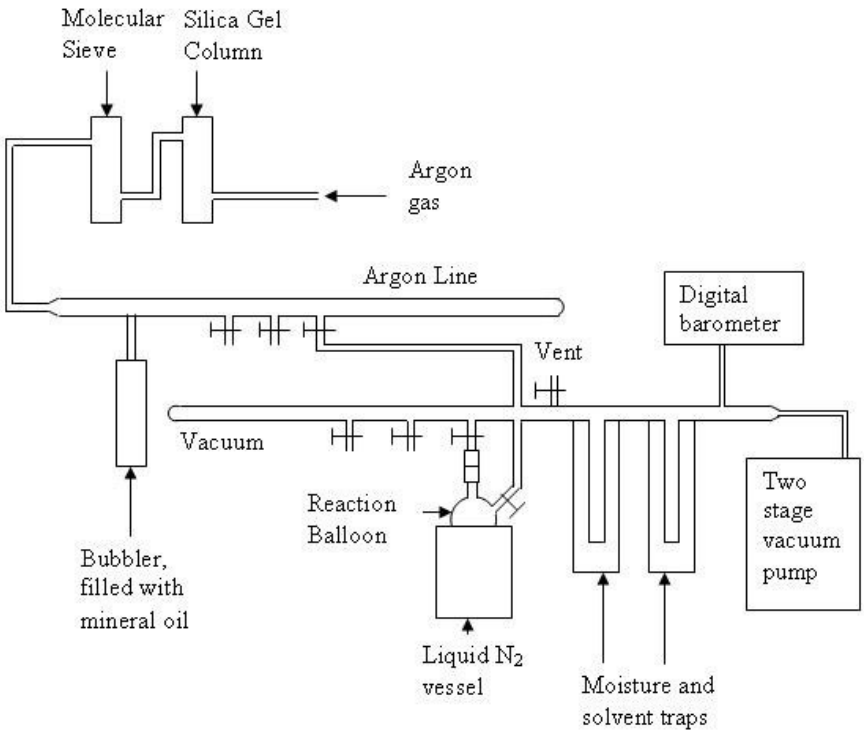

Figure 4.1. Experimental set up for degassing the reactants prior to ATRP reaction

4.4. Synthesis of Multiarm PMMA-*b*-PAA Copolymers

For polymerization of tBA to synthesize PMMA-*b*-PtBA from PMMA macroinitiator, 7 ml of tBA was used as monomer and diluted with anisole at 1:1 volumetric ratio. 196 µL ligand (PMDETA) and 0.015 gr catalyst (CuBr) was introduced. Initial molar ratio of monomer/initiator was 600 for each arm. The reactants were degassed through three freeze-thaw cycles then reacted for 4-12 hours at 90 ºC. The product was passed through neutral activated alumina column, vacuum dried, diluted in tetrahydrofuran and precipitated in methanol-water mixture to eliminate residual monomer.

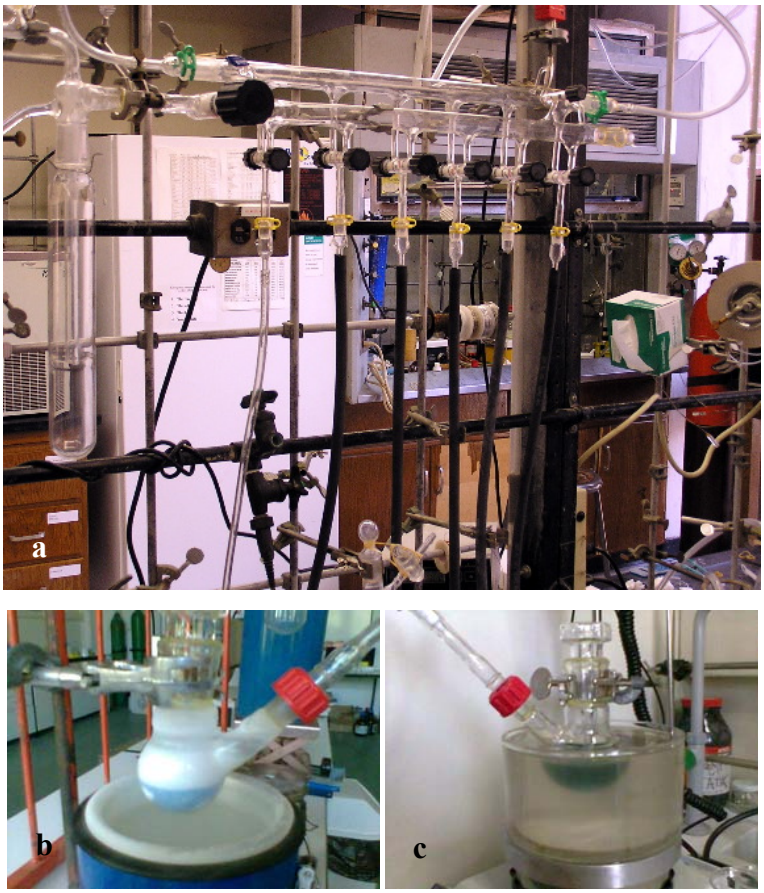

Figure 4.2. Fotographs of experimental setup for ATRP synthesis of star block copolymers (a) vacuum line for degassing, (b) freeze-thaw process and (c) reaction carried in oil-bath.

The polymer sample was dissolved in dichloromethane, dried over Na_2SO_4, filtered and vacuum dried. PMMA-*b*-PtBA samples were hydrolized with trifluoroacetic acid. The polymer synthesized was dissolved in 10 ml distilled dichloromethane and 2 ml of trifluoroacetic acid was added. Reaction was completed by 24 hours of stirring at room temperature.

4.5. Characterization

Molecular weights of the star block copolymer were determined by Gel Permeation Chromatography (GPC). GPC analysis were achieved with an Agilent model 1100 instrument equipped with a pump, refractive-index, UV detectors and four Waters Styragel columns (HR 5E, HR 4E, HR 3, and HR 2). THF was the eluent stream passing with a flow rate of 0.3 mL/min at 30 °C. Toluene was used as an internal

standard. The molecular weights of the polymers were calculated on the basis of linear PMMA standards (Polymer Laboratories).

Chemical structures of the initiator (pentaerythritol tetrakis (2-bromoisobutyrate)), macroinitiator (PMMA) and the star block copolymer (PMMA-*b*-PtBA) were determined by Bruker NMR spectrometer (250 MHz for ^{1}H-NMR). ^{1}H-NMR and ^{13}C-NMR analysis of hydrolyzed copolymer was achieved by Varian 400-MR spectrometer. The efficiency of the hydrolysis reaction was confirmed by Fourier Transform Infrared Spectroscopy.

Loaded particles were characterized by Differential Scanning Calorimetry (DSC-50 Shimadzu), Thermal Gravimetric Analysis and Differential Thermal Gravimetry (Seteram Labsys) in addition to Fourier Transform Infrared Spectrophotometry (Shimadzu FTIR 8400 S).

4.6. Maximum Loading Capacity

Pyrene stock solutions and polymer solutions with constant concentrations were prepared. Each sample of 4 ml included 20 µL ethanol. Pyrene aliquots were taken into test tubes at twelve different dozes which vary between $2.5x10^{-7}$ M and $30x10^{-7}$ M. After vacuum drying for 4 h at 25 °C, polymer solutions at determined polymer concentration were transferred into pyrene containing tubes and were kept at 4 °C, dark medium for 16 hours being stirred. Then 750 µL samples were centrifuged with 1500 rpm for 10 minutes. Centrifuged samples were scanned in fluorescent spectrophotometer to determine maximum capacity of pyrene loading. Fluorescent measurements were performed at Varioskan Flash microplate reader. Emission spectra in 360-450 nm interal were recorded with excitation at 330 nm wavelength and intensities at 393 nm were recorded versus increasing pyrene concentrations.

Experiment is performed at two diferent polymer concentrations which were 200 mg/L and 500 mg/L. Change in intensity of pyrene loaded polymer samples with increasing pyrene concentrations were compared to blank pyrene solutions that took the same treatment as the pyrene loaded polymer solution samples. Blank solutions contained the same pyrene concentrations of the polymer solutions.

4.7. Critical Micelle Concentration

Pyrene was dissolved in chloroform and diluted to $2x10^{-5}$ mg/ml. 10 μL aliquots were taken into test tubes which were dried under vacuum for 4 hours at 25°C. 20 mg polymer sample was dissolved in 1 ml alcohol to obtain a stock solution. Then aliquots taken from stock solutions were diluted to 5 ml to obtain different polymer concentrations from 0.015 mg/L to 1500 mg/L. Then 5 ml polymer solutions were transferred into pyrene containing test tubes. Each tube had a pyrene concentration of $2x10^{-7}$ M. The tubes were kept at 4 °C for 16 hours being stirred at a dark medium. 750 μL samples were drawn for fluorescence measurements. The samples were centrifuged at 1500 rpm for 10 min before fluorescence measurements. Fluorescence measurements were performed at Varioskan Flash microplate reader. Excitation spectra were obtained in 300-360 nm interval keeping the emission wavelength at 393 nm. Bandwidth was kept 5 nm and stepsize was 3 nm during all scans. Critical micelle concentration was determined from emmision intensity ratios of the excitation bands at 336 nm and 333 nm (I_{336}/I_{333}) versus polymer concentration on logarithmic scale. CMC determined from shifts in excitation spectra was verified by I_1/I_3 ratio changes in emmission spectra and also by UV-spectroscopy at 266 nm.

4.8. Drug Loading

Drug loading was achieved by several methods for comparison. The methods applied to load multiarm star block copolymer samples with the model drugs indomethacin and 5-FU were performed as follows:

1. Simple equilibrium method: The polymer and drug were simply added into buffer saline solution under agitation and filtered.
2. Co-precipitation: The drug and the polymer were dissolved in appropriate solvents. Polymer and drug solutions were mixed and kept for 30-60 min. (The solution may be dispersed by ultrasonic treatment.) Then the homogeneous solution was added into suitable nonsolvent (that was generally a nonpolar solvent like hexane, diethyl ether or a mixture of the two) drop by drop under agitation. The polymer precipitate is filtered and vacuum dried.

3. Dialysis: The polymer and drug are dissolved in appropriate solvents and kept for 30-60 minutes. (The solution may be dispersed by ultrasonic treatment.) Then 5 ml of water is added drop wise into the solution, and poured into dialysis bag. The polymer+drug solution is dialyzed against 2 L of water for 24 hours and the medium is freshened in 12 hours. The ingredients after 24 hours is freeze-dried for determination of drug loading efficiency.

4. Solvent deposition method (Coacervation): The polymer and drug are dissolved in appropriate solvents. The organic phase is poured into water phase (water or PBS). Solvent is evaporated under vacuum or polymer is micellized in water medium and drug is separately dissolved in solvent. Then the drug solution is poured into micelle and solvent is evaporated under vacuum. Then the solution is centrifuged (or filtered) several times to remove precipitates.

5. Salting-out method: The polymer and drug are dissolved in appropriate solvents. Then the solvent is evaporated. The film formed is hydrated in buffer solution, and the micelle is formed with intensive shaking. Excess drug precipitates and is removed by filtration.

Drug loading conditions were optimized in terms of type of medium, temperature, loading interval and polymer concentration. For the selection of loading medium, 20 mg polymer samples was introduced to equal amount of drug in water, ethanol, 1% acetic acid, dimethyl sulfoxide and dimethyl formamide. In each experiment polymer sample was dissolved in 0.25 ml ethanol then diluted to specific concentration with solvent of interest in which 20 mg of drug was previously dissolved. All loading experiments were performed at room temperature for 2 hours. After loading, loaded sample was washed off excess drug by dialysis method and freze dried. Drug content of each sample was determined from spectrophotometric analysis of dialysis media. Dialysis was performed in 100 ml portions of distilled water and medium was refreshed at every one hour period. Concentrations of 100 ml dialysis media was followed until ultimate purification of loaded polymer samples from excess drug which took 12-18 hours depending on type of solvent.

After selection of medium, optimum temperature of loading medium and duration of loading was determined through trials performed at three temperatures, 25°C, 15ºC and 5ºC. Polymer samples of 10 mg were dissolved in 0.25 ml ethanol, mixed with equal amount of drug dissolved in selected loading medium in water bath kept at specific temperature. Drug content of samples were monitored versus time and

loading intervals to reach equilibrium besides drug loading efficiencies were determined.

In order to determine effect of polymer and initial drug concentration on loading performance 20 mg polymer samples were dissolved in 0.5 ml of ethanol and 20 mg drug portions were dissolved in 1.5 ml 1 % HCl. Polymer solutions were diluted with distilled water to have concentrations of 500 mg/L, 2000 mg/L or 3500 mg/L. After addition of drug into polymer solutions, loading was achieved at 15 °C under stirring in 4 hours. The solutions were transferred into dialysis tubes which were placed in 1 L of water. The dialysis media were refreshed at 5^{th} and 12^{th} hours. Further dialysis in 100 ml of water for 1 hour was employed for checking by UV-spectroscopy to understand whether samples were completely washed off excess drug or not. The drug content of the samples were estimated by subtracting the amount of excess drug washed out by dialysis from the initial content.

Quantities of excess drug were determined by measuring absorbance of certain volume of dialysis media by UV-Vis Spectrophotometry (Perkin Elmer) at 266 nm for 5FU.

4.9. Drug Release

Drug release profiles were obtained by a continuous process which involved a diffusion cell as in Figure 4.3 and a flow cell attached to a UV-Vis Spectrophotometer. 5 mg of drug loaded polymer sample was dissolved in 1 ml PBS within donor compartment of diffusion cell which was kept at 37 Cº through experiment. Fresh buffer was passed through the diffusion cell with a 0.025 ml/min flowrate by using a syrince pump. The donor and acceptor compartments of the diffusion cell were separated by cellulosic membrane with 12000-14000 MWCO. UV-absorbance data of the dowstream passing through the diffusion cell and then a flow cell placed within spectrophotometer were simultaneously recorded with respect to time. Absorbance data was converted to concentration values of the drug by using Beer's law. Calibration curve of 5FU in PBS was used to determine released amount of drug by multiplying instantaneous concentration (mg/ml) data collected at 1 minute intervals by volumetric flowrate (ml/min).

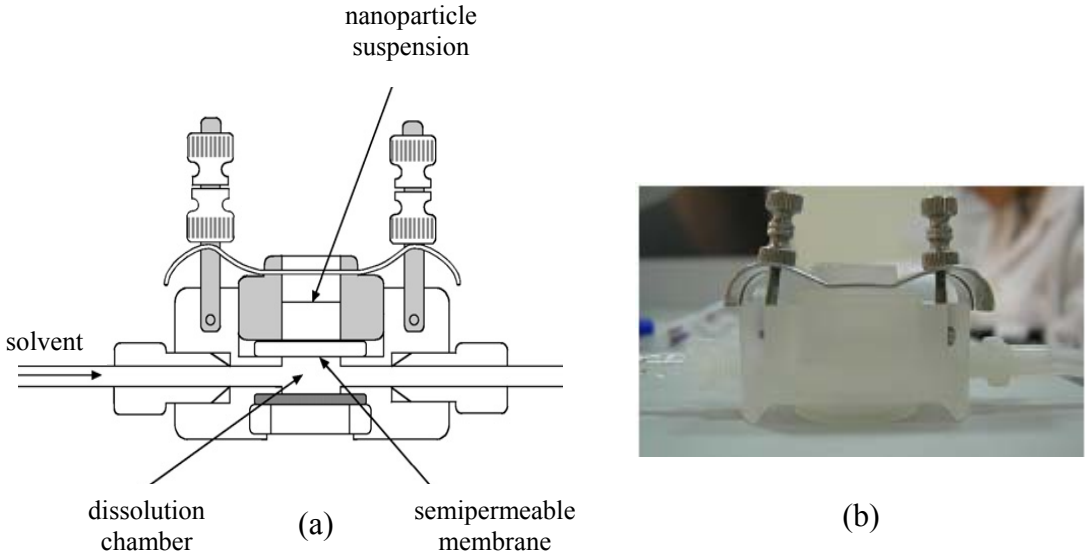

Figure 4.3. (a) Flow-through dissolution apparatus used to measure free drug flux arising from a nanoparticulate suspension held separated from a dissolution chamber by a semi-permeable membrane (Source: McCarron and Hall, 2008). (b) Photograph of the diffusion cell used in drug release studies.

4.10. Biodegradation

Particle size analysis by dynamic light scattering was achieved by Zetasizer (3000 HSA, Malvern). Polymer samples were prepared by dissolving polymer in limited amount of alcohol then diluting to 2 mg/ml with PBS. Each sample was filtered through 0.2 µm teflon membrane prior to measurement (n=4). Biodegradion of polymer samples at different polymer concentrations (1,2,4,6 and 8 mg/ml) were also investigated. Loading ability of biodegraded polymer samples were detected by UV-spectrophotometer after they were loaded with pyrene as described in section 4.6.

The results were also compared to particle size analysis of AFM micrographs (Digital Instruments MMAFM-2/1700EXL). Freeze dried polymer samples were dissolved in deionized water at a concentration of 5 mg/L and kept in thermoshaker at 37ºC for degradation. 5 ml samples taken daily were filtered through 0.45 µm teflon membrane and dripped on glass supports. Each sample was immediately frozen at -20ºC, freeze dried (Telstar, Cryodos) for 48 hours and kept at dessicator for dehumidification for 24 hours. AFM images were obtained by tapping mode.

CHAPTER 5

RESULTS AND DISCUSSION

5.1. Synthesis of Initiators

Initiators with three, four and six brominated active sites were synthesized in tetrahydrofuran and under N_2 as described by Jankova et al. (Jankova et al., 2005; Even et al., 2003). Starting materials were 1,3,5-trihdiroxybenzene with three –OH groups, pentaerythritol with four –OH groups and dipentaerythritol with six –OH groups. Bromination of –OH groups was achieved by reacting with 2-bromoisobutyryl bromide by using a ligand. Triethyleneamine (TEA) was used as ligand for bromination of 1,3,5-trihdiroxybenzene while dimethylaminopyridine (DMAP) was used for bromination of pentaerythritol and dipentaerythritol. All reactions were carried in tetrahydrofuran (THF) and all reactants were completely dried before reaction. The reactions shown in Figures 5.1, 5.2 and 5.3 were carried under nitrogen and the system was carefully prevented from oxygen and moisture in order to produce extremely pure brominated products. Reaction conversions were simply calculated from molar conversion of starting material as shown by Equation 5.1 where n is number of moles, MW is molecular weight and w is weight of reactants and products, and given in Table 5.1.

$$Conversion(\%) = \frac{n_p}{n_r} \times 100 = \frac{w_p / MW_p}{w_r / MW_r} \times 100 \qquad (5.1)$$

Table 5.1. Conversions of bromination reactions of starting materials to synthesize initiator molecules with 3, 4 and 6 brominated active sites.

Reactant	MW (Da)	$W_{reactant}$ (gr)	Product	MW (Da)	$W_{product}$ (gr)	Conversion (%)
THB	162	1.73	THB-Br	499	5.04	94.5
PENTA	136	1.09	PENTA-Br	572	3.50	76.3
diPENTA	254	1.35	diPENTA-Br	956	3.42	67.3

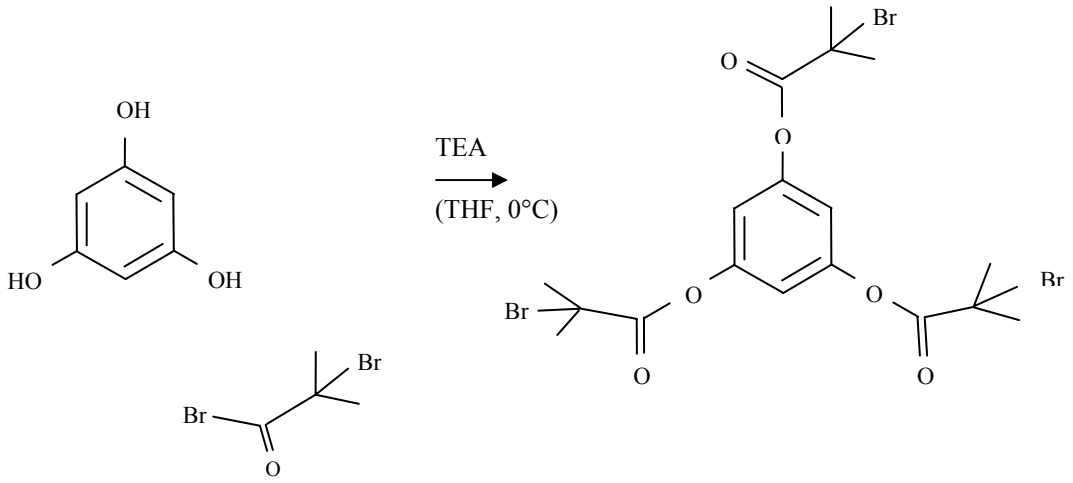

Figure 5.1. Schematic presentation of bromination reaction of 1,3,5-trihydroxybenzene to synthesize 1,3,5- (2-bromo-2-methyl propionate) benzene

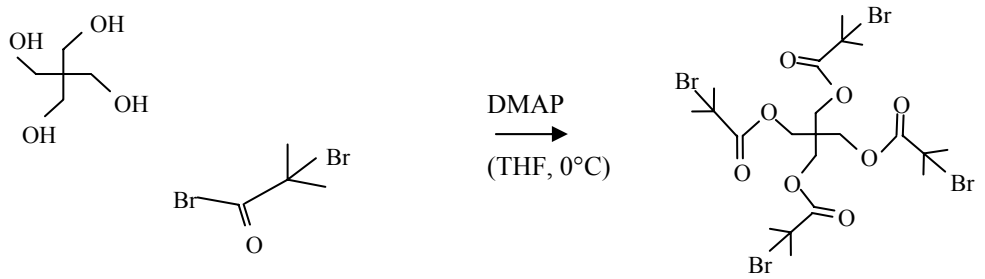

Figure 5.2. Schematic presentation of bromination reaction of pentaerythritol to synthesize pentaerythritol tetrakis (2-bromoisobutyrate).

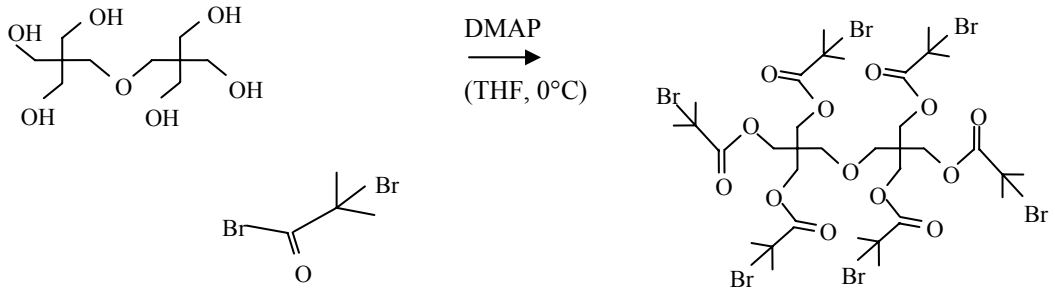

Figure 5.3. Schematic presentation of bromination reaction of di-pentaerythritol to synthesize di-pentaerythritol hexakis (2-bromoisobutyrate)

Bromo-initiators, namely 1,3,5- (2-bromo-2-methyl propionate) benzene with three active sites, pentaerythritol tetrakis (2-bromoisobutyrate) with four active sites and dipentaerythritol hexakis (2-bromoisobutyrate) were compared with starting materials by thermal analysis. The change in thermal behavior of materials as shown in Figures 5.4-5.6 confirmed that bromination reactions were completed.

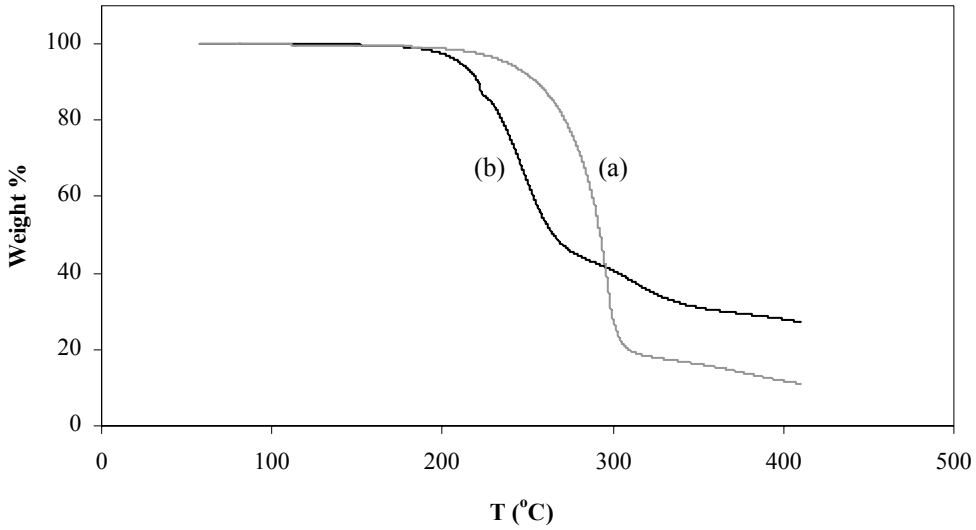

Figure 5.4. TGA overlay of (a) unreacted 1,3,5-trihydroxybenzene and (b) 1,3,5- (2-bromo-2-methyl propionate) benzene.

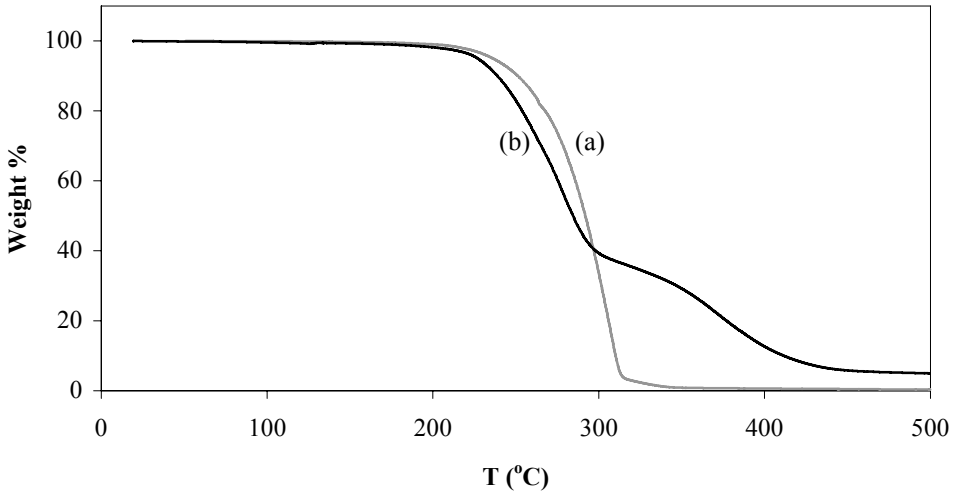

Figure 5.5. TGA overlay of (a) unreacted pentaerythritol and (b) synthesized pentaerythritol tetrakis (2-bromoisobutyrate).

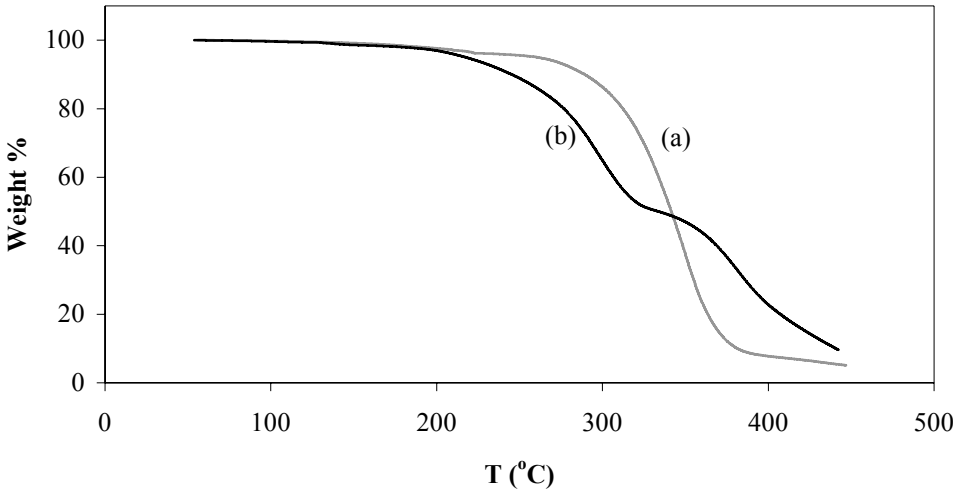

Figure 5.6. TGA overlay of (a) unreacted di-pentaerythritol and (b) synthesized di-pentaerythritol hexakis (2-bromoisobutyrate).

^{1}H-NMR spectra of each sample was evaluated to determine purity of the products. Purity of the initiators were determined by comparing the specific peak areas obtained from ^{1}H-NMR spectrum to the stoichiometric ratios of types of hydrogen groups observed in molecular structure.

Brominated and purified 1,3,5-trihydroxybenzene has two types of hydrogen groups, one belonging to the benzene ring and the other to the methyl groups of added isopropyl bromide arms, which were notated as **a** and **b** respectively in Figure 5.7. As can be calculated from the molecular structure, the ratio of these two types of hydrogen atoms are 3/18 (=1/6) in number for the molecule has three CH and six CH_3 groups. The characteristic peak of CH appears at 2.04-2.06 ppm interval and has a peak area of 58.381 while signals of the 2-bromopropanoate groups [$COO(CH_3)_2Br$] are 6.95-6.97 ppm with a total peak area of 7.912. The ratio of the integrals (areas) of the peaks was determined as 1/7.37 which corresponds to a 82% purity.

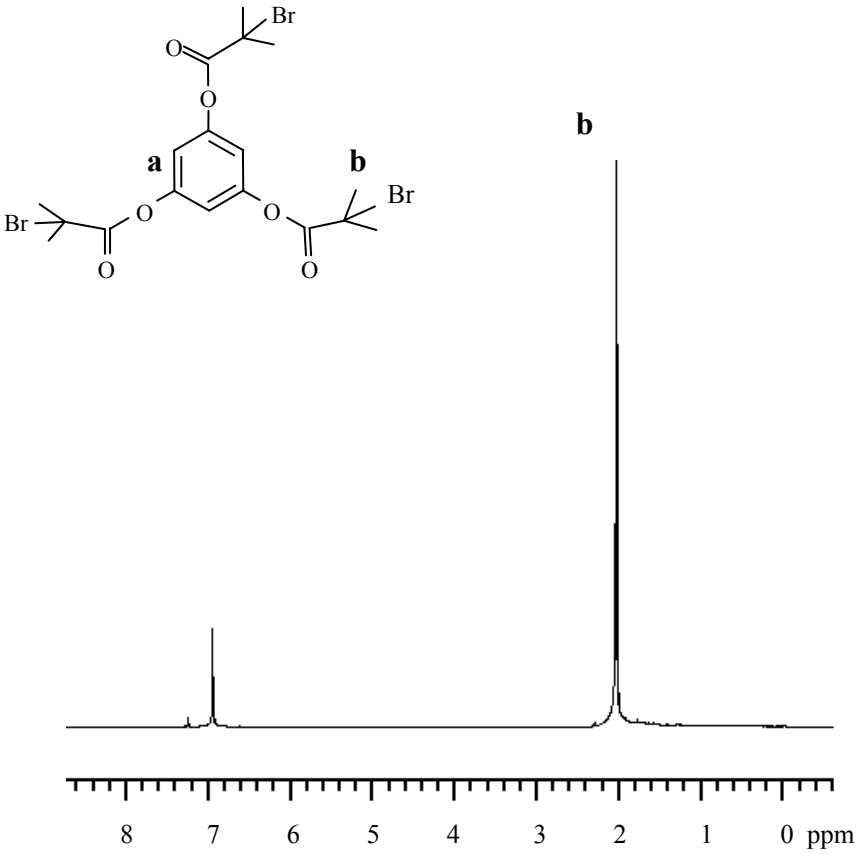

Figure 5.7. ^{1}H-NMR spectrum of 1,3,5- (2-bromo-2-methyl propionate) benzene.

H-NMR spectrum of brominated pentaerythritol provided two peaks that belong to $C(CH_2)_4$ and bromopropanoate groups 4[COOC(C*H*3)$_2$Br] at 4.31 and 1.92 ppm with peak areas of 7.912 and 32.793 respectively (Figure 5.8). Comparing the ratio of the peak areas to the stoichiometric H ratio (8/24) it was determined that 99% purity was obtained after purification although the purity of the synthesized material had been determined as 64.7% before purification.

Brominated dipentaerythritol, on the other hand, could be purified to 100% purity according to the signals that appear as follows: 2[C(C*H*2)$_3$] at 4.28 ppm, O(C*H*2)$_2$ at 3,58 and 6[COOC(C*H*3)Br] at 1.92 ppm with the peak areas of 13.688, 4.57 and 41.645 (Figure 5.9).

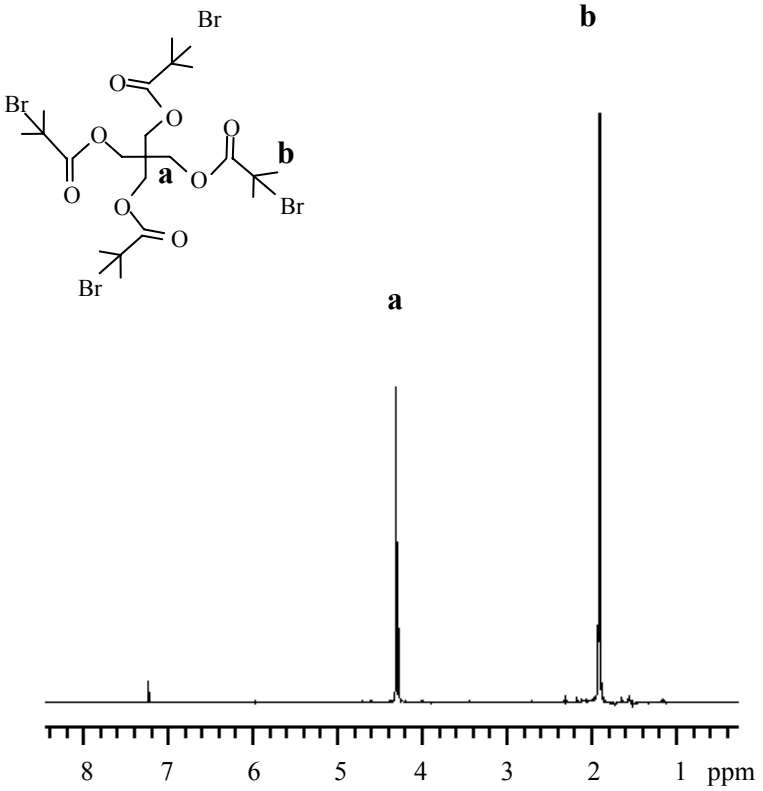

Figure 5.8. ^{1}H-NMR spectrum of pentaerythritol tetrakis (2-bromoisobutyrate).

5.2. Synthesis of PMMA-*b*-PAA Polymers

Synthesis of PMMA-*b*-PAA block copolymers constitutes of two stage ATRP reaction to produce PMMA-*b*-PtBA copolymer and hydrolysis of PMMA-*b*-PtBA to react tertiary butyl acrylate groups into acrylic acid. ATRP synthesis of 3 arm, 4 arm and 6 arm PMMA initiators is the first stage of the polymerization reaction and are shown in Figures 5.10-5.12.

For the ATRP synthesis of PMMA macroinitiators from the bromo-initiators synthesized and purified previously, CuCl was used as catalyst in stoichiometric ratio. PMDETA was used in 10% excess to increase solubility of catalyst and provide persistent radical effect of the catalyst.

Dilution of monomer with an appropriate solvent that was anisole was employed to keep concentration of active species as high as possible throughout reaction. This was also expected to minimize termination reactions via coupling of active species. A third advanage of addition of a strong solvent was further solubilization of catalyst as well.

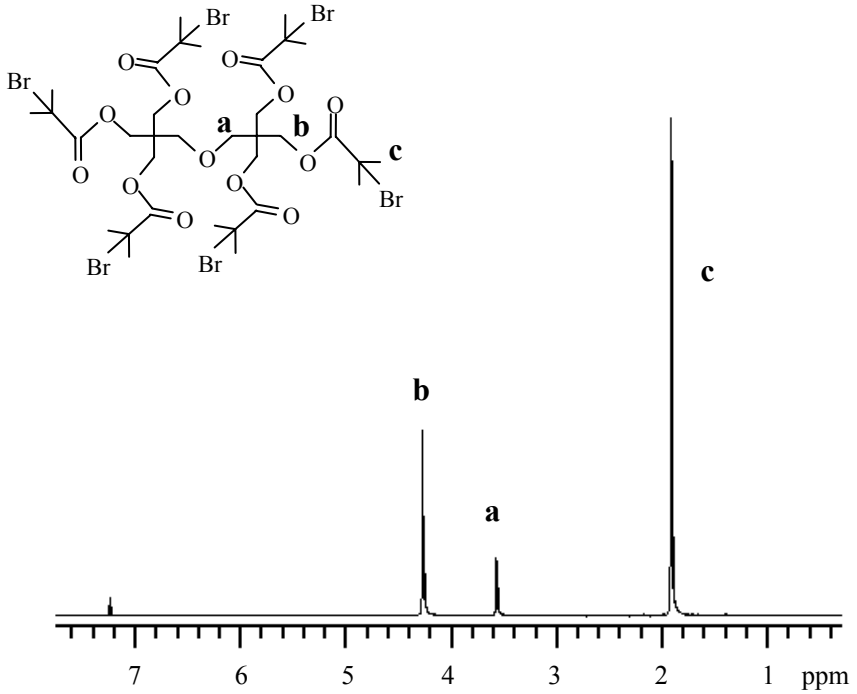

Figure 5.9. ^{1}H-NMR spectrum of di-pentaerythritol hexakis (2-bromoisobutyrate).

Amount of monomer, methyl methacrylate (MMA) to be reacted was determined as a result of trials achieved by various M/I_o (monomer to initiator molar ratio) values between 100 and 250. Since CuCl is a very effective catalyst when combined with MMA, reaction is quite fast still depending on initial monomer ratio as shown by Equation 2.1. When M/I_o ratio was as high as 250, ATRP reaction at 60°C yielded macroinitiators having desired molecular weights (<5000 Da) within 10-12 minutes. High rate of reaction provided a very low polydispersity, on the other hand reaction conversions were as low as 3-5% (Table 5.2). Although the conversions were too low to propose they can be improved and still provide acceptible polydispersities by an optimization study of reaction conditions (temperature, time, M/I_o ratio) to obtain reaction conversions. In this study low conversions were tolerated since minimum molecular weight distribution of the macroinitiator was extremely important at this stage of synthesis in order to prevent side reactions at the second stage of synthesis.

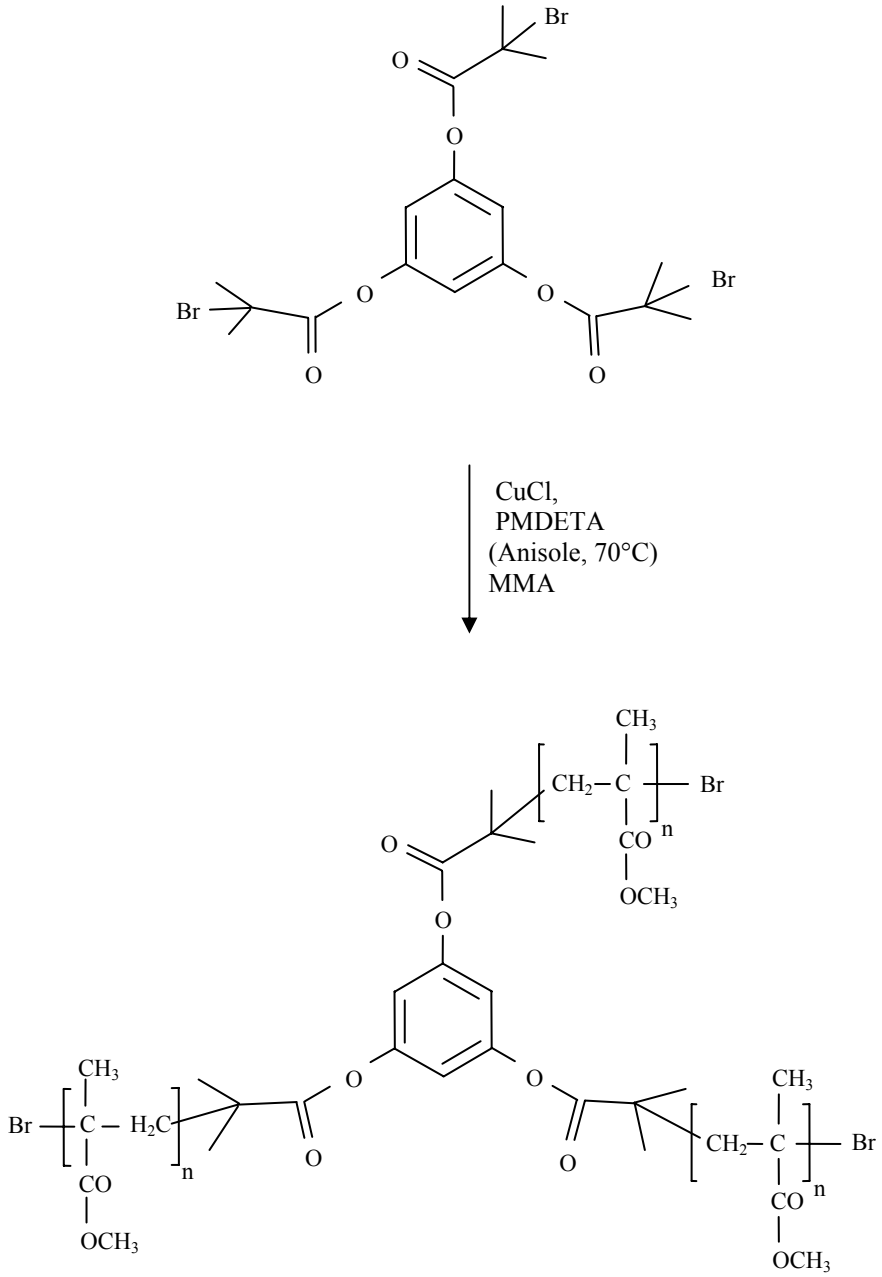

Figure 5.10. ATRP synthesis of 3 arm PMMA from 1,3,5- (2-bromo-2-methyl propionate) benzene.

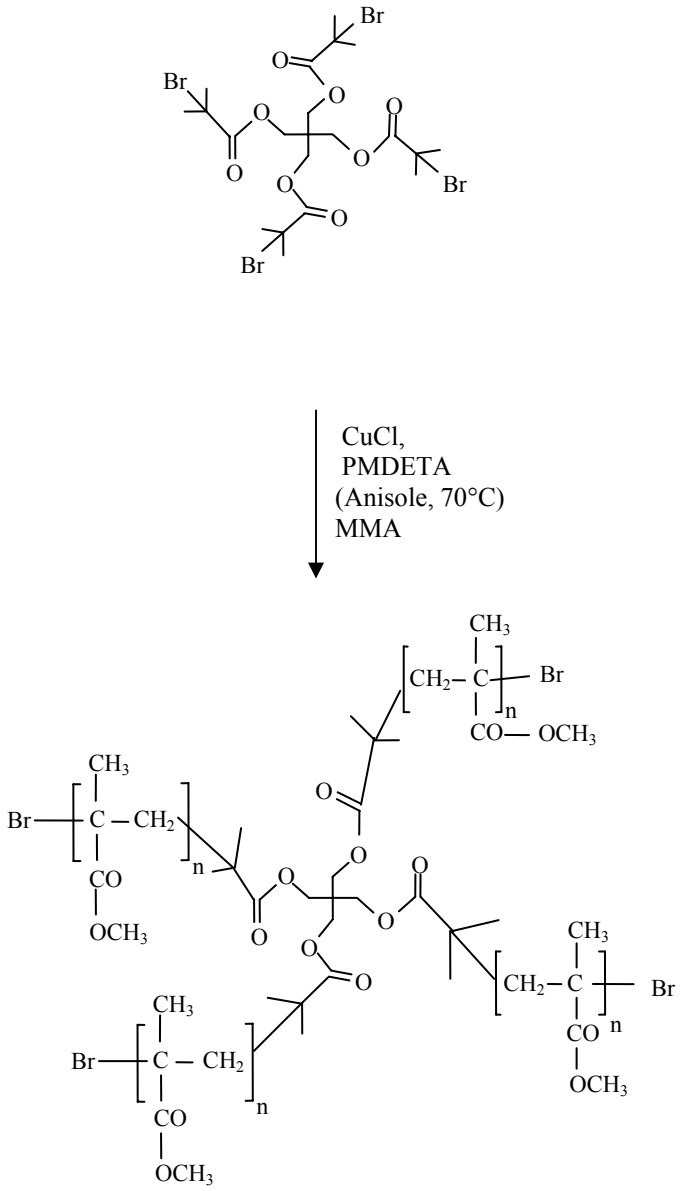

Figure 5.11. ATRP synthesis of 4 arm PMMA from pentaerythritol tetrakis (2-bromoisobutyrate).

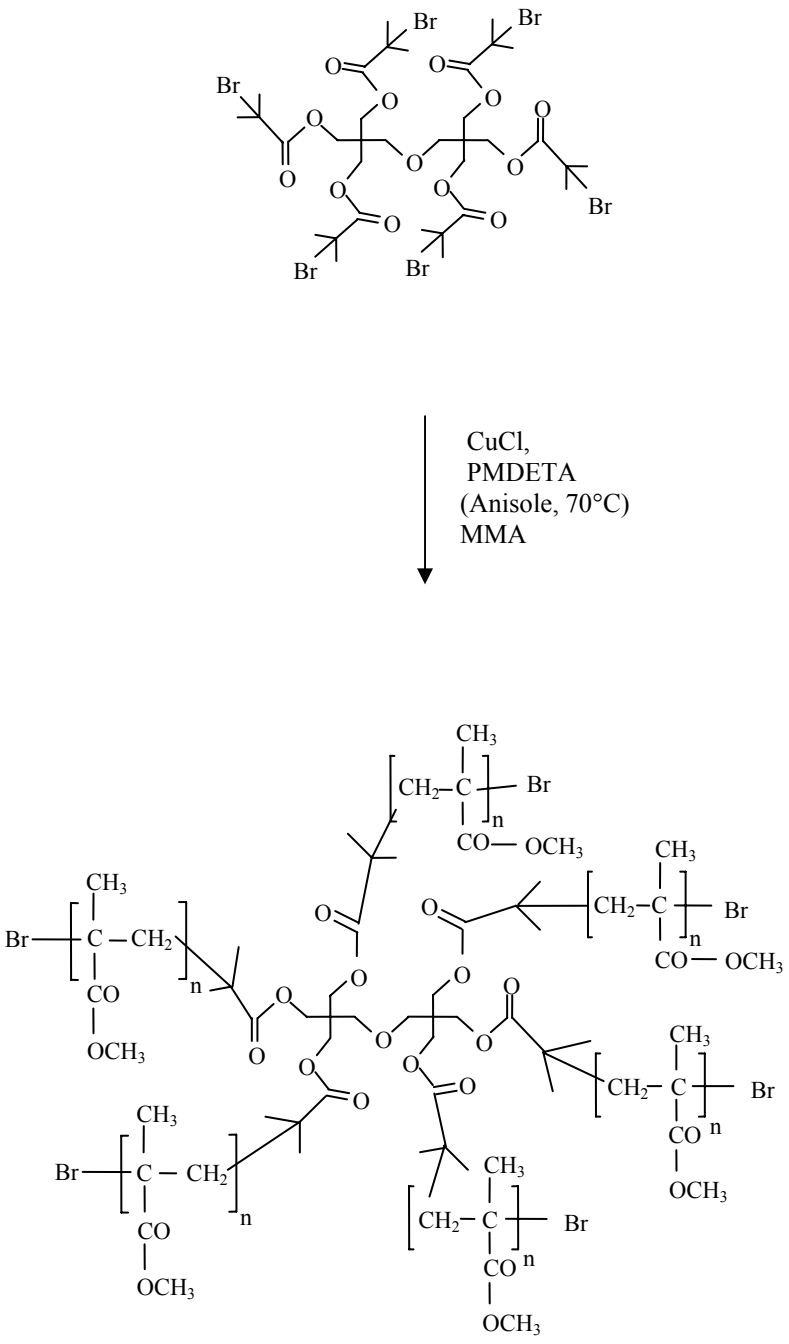

Figure 5.12. ATRP synthesis of 6 arm PMMA from di-pentaerythritol hexakis (2-promoisobutyrate).

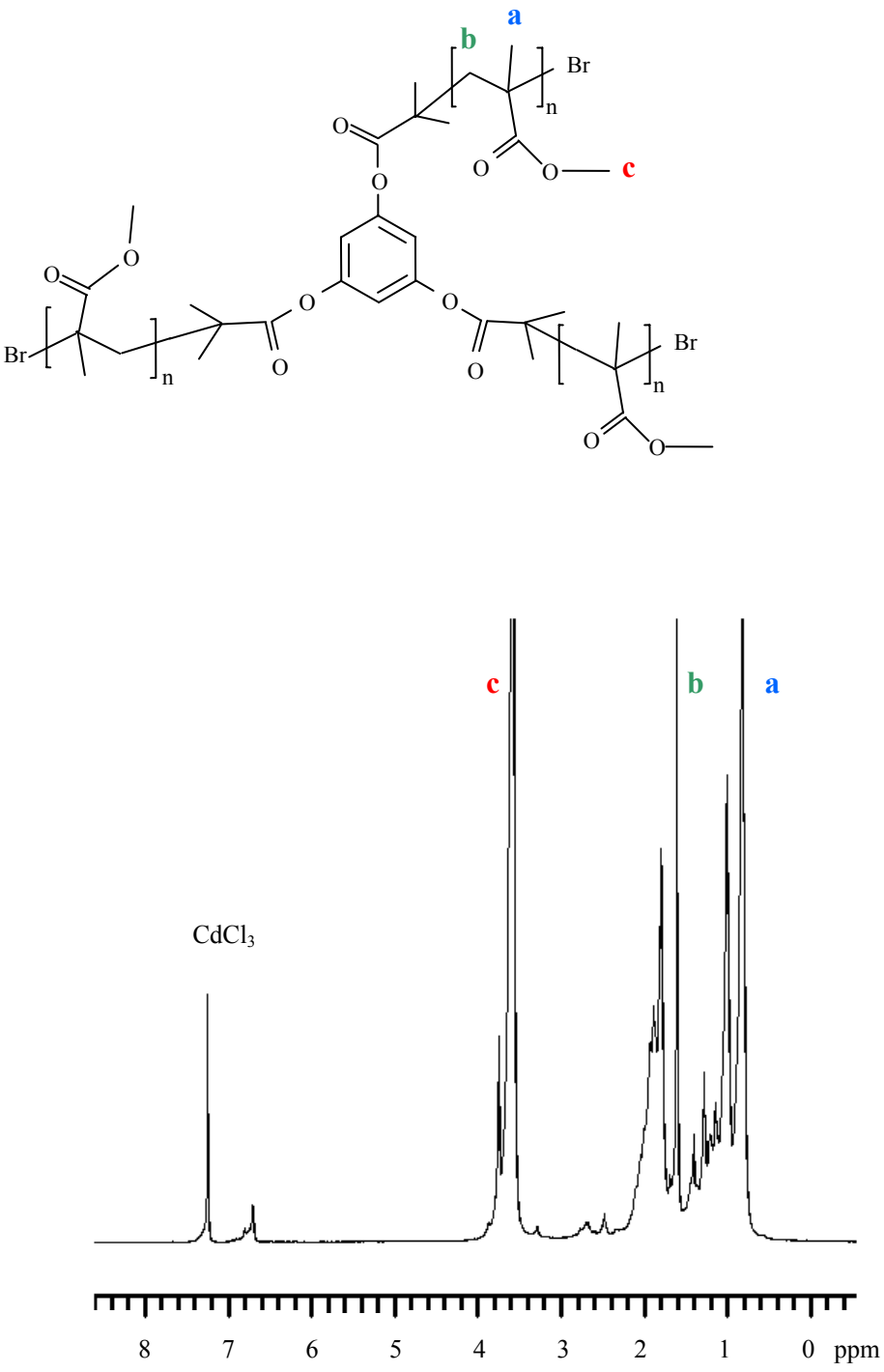

Figure 5.13. ^{1}H-NMR spectrum of 3 arm PMMA.

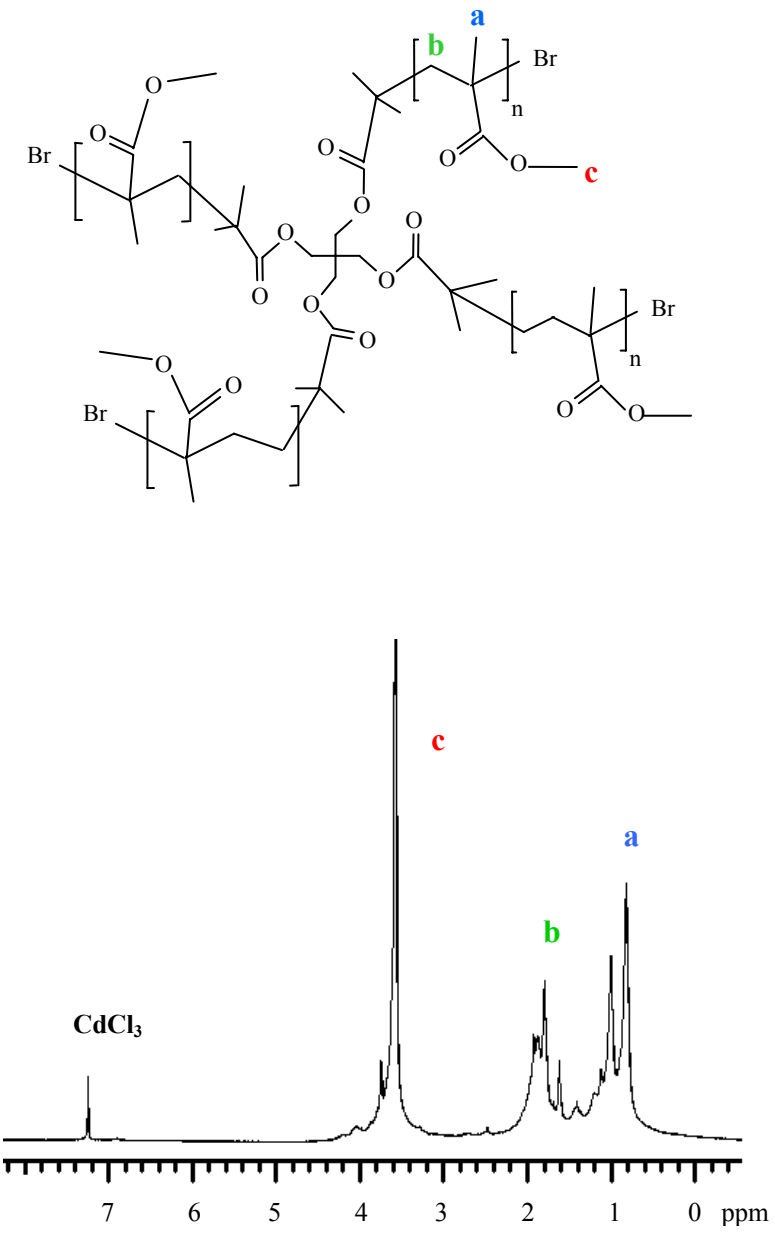

Figure 5.14. ^{1}H-NMR spectrum of 4 arm PMMA.

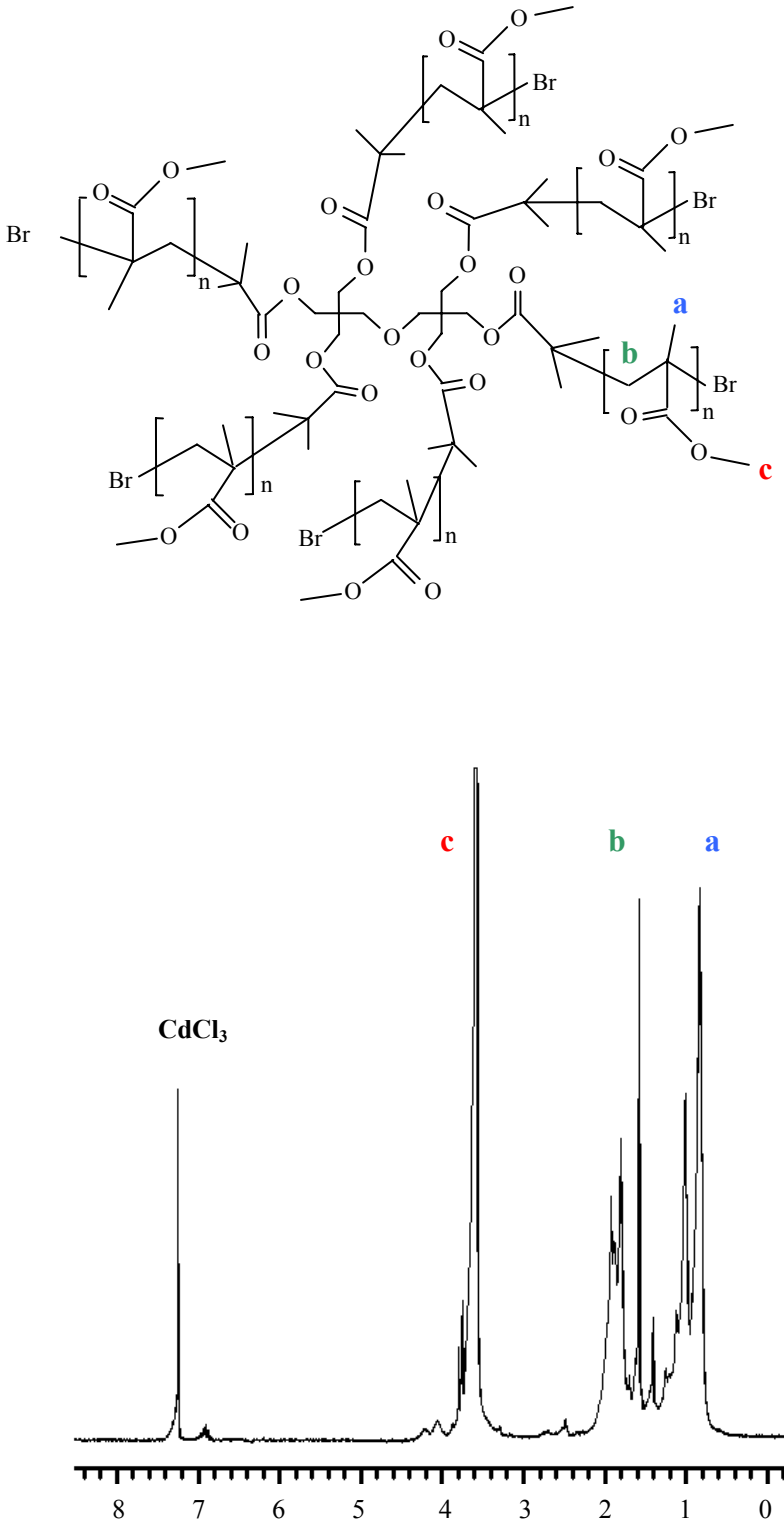

Figure 5.15. ^{1}H-NMR spectrum of 6 arm PMMA.

The chemical structure of each macroinitiator synthesized was analized by ^{1}H-NMR and given by Figures 5.13-5.15. ^{1}H -NMR spectrum of PMMA is δ: 0.8–1.0 ppm (3H, CH_3), 1.7 ppm (2H, CH_2), 3.6 ppm (3H, $COOCH_3$), 7.25 ppm (H, $CHCl_3$). (Malinowska et al., 2005; Ishizu et al., 2005; Nurmi et al., 2007). CH_2 peak labelled with letter 'b' in Figures 5.13-5.15 depicts a number of shifts within the range 1.35-2.3 ppm probably due to molecular interactions between chains. Areas of related peaks of H groups belonging to PMMA have been consistent with molecular structures.

Molecular weights of PMMA and PMMA-*b*-PtBA copolymers were determined by Gel Permeation Chromotography (Figures 5.16-5.18). For performing the second stages of polymerization reactions that are presented schematically by Figures 5.19-5.21 experimental molecular weight of PMMA initiator was used to determine quantity of PMMA initiator to be reacted with certain volume of tBA. Stoichiometric ratio of monomer to initiator (M/I_1) determines rate of reaction (as mentioned in Chapter 3), final molecular weight of copolymer and also polydispersity. The reaction conditions and conversions are tabulated in Table 5.2 for the samples of 3 arm, 4 arm and 6 arm PMMA-*b*-PAA polymers having molecular weights as follows; 3 arm PMMA(MW: 5600 Da)-*b*-PtBA (MW: 22000 Da), 4 arm PMMA(MW: 4700 Da)-*b*-PtBA (MW:27000 Da), 6 arm PMMA(MW: 8100 Da)-*b*-PtBA (MW:77000 Da, 45000 Da and 18000 Da).

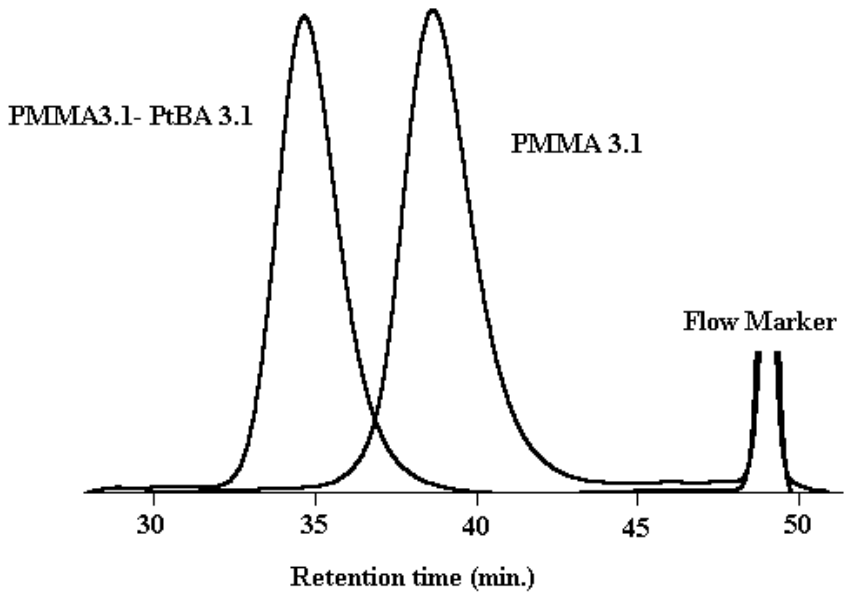

Figure 5.16. GPC profiles of 3 arm PMMA macroinitiator and the 3 arm star PMMA-*b*-PtBA copolymer having molecular weights of 5600 Da and 22000Da.

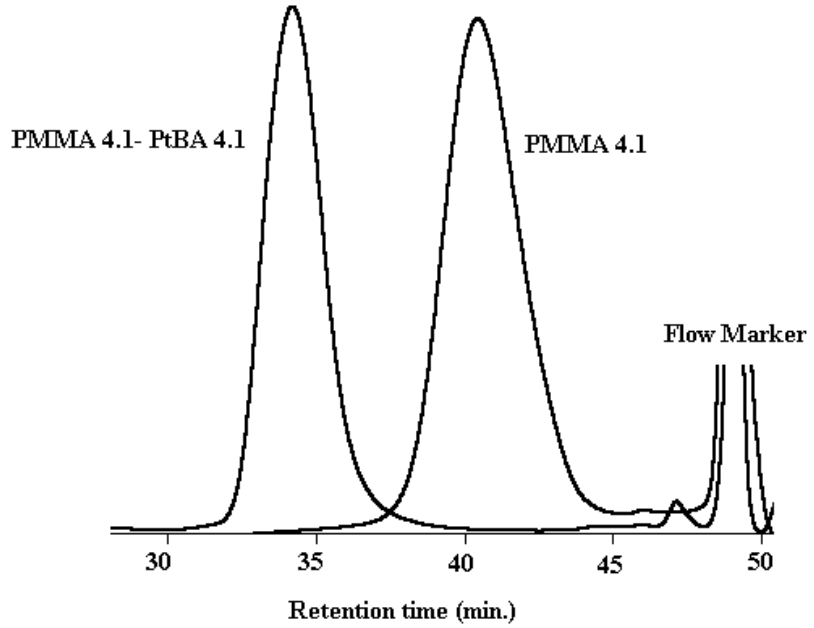

Figure 5.17. GPC profiles of 4 arm PMMA macroinitiator and the 3 arm star PMMA-*b*-PtBA copolymer having molecular weights of 4700 Da and 27000 Da.

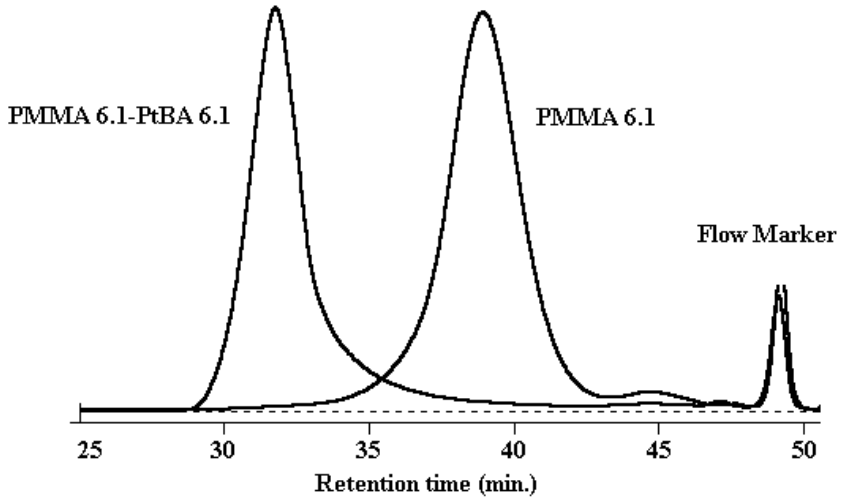

Figure 5.18. GPC profiles of 6 arm PMMA macroinitiator and the 3 arm star PMMA-*b*-PtBA copolymer having molecular weights of 8000 Da and 77000 Da.

Table 5.2. Reaction conditions and conversions of PMMA-*b*-PAA synthesis by 2 stage ATRP polymerization and hydrolysis reactions.

	PMMA-*b*-PtBA 3.1	**PMMA-*b*-PtBA 4.1**	**PMMA-*b*-PtBA 6.1**
Initiator (Io)	1,3,5- (2-bromo-2-methyl propionate) benzene	Pentaerythritol tetrakis (2-Bromoisobutyrate)	Dipentaerythritol hexakis (2-Bromoisobutyrate)
Monomer	MMA (10 ml)	MMA (10 ml)	MMA (10 ml)
Mo/Io	750	1000	1500
Solvent	Anisole (1:1 V_m/V_s)	Anisole (1:1 V_m/V_s)*	Anisole (1:1 V_m/V_s)
Catalyst	CuCl (3x Io)	CuCl (4x Io)	CuCl (6x Io)
Ligand	PMDETA (3x Io)	PMDETA (4x Io)	PMDETA (6x Io)
Reaction T (ºC)	60	60	60
Reaction time (min)	12	12	12
MW (Da)	5600	4700	8100 Da
PI	1.09	1.14	1.15
Weight of product (gr)	0.25	0.34	0.32
C_p (%)	2.0	2.9	2.6

Initiator (I_1)	3- arm PMMA-Br (MW 5600 Da)	4 arm PMMA-Br (MW 4700)	6- arm PMMA-Br (MW 8100)
Monomer	4 ml tBA	4 ml tBA	5 ml tBA
Solvent	Anisole (1:1 V_m/V_s)	Anisole (1:1 V_m/V_s)	Anisole (1:1 V_m/V_s)
Mo/I_1	1500	2500	3000
Catalyst	CuBr (3.3x I_1)	CuBr (4.4x I_1)	CuBr (6.6x I_1)
Ligand	PMDETA (33x I_1)	PMDETA (44x I_1)	PMDETA (66x I_1)
Reaction T (ºC)	90ºC	90ºC	90ºC
Reaction time (h)	5	6	17
MW (Da)	22000	27000	77000
PI	1.22	1.16	1.83
Weight of product (gr)	0.44	0.44	0.78
Weight of product after hydrolysis (gr)	0.22	0.25	0.41
C_p (%)	10.0	11.0	24.0
C_h (%)	62.0	80.0	84.0

$$C_p\% = \frac{w_p - w_i}{w_m} \times 100 \tag{5.1}$$

$$C_h\% = \frac{n_{AA}}{n_{tBA}} = \frac{\frac{w_{PMMA-b-PAA} - w_{PMMA}}{MW_{AA}}}{\frac{w_{PMMA-b-PtBA} - w_{PMMA}}{MW_{tBA}}} \times 100 \tag{5.2}$$

where C_p is molar conversion of polymerization, C_h is molar conversion of hydrolysis reaction, w_p is net weight of polymer synthesized, w_i is weight of initiator used and w_m is the initial weight of monomer incorporated in Equation 5.1. In Equation 5.2., n_{AA} is number of moles of acrylic acid produced and n_{tBA} is number of moles of tBA that reacted with TFAA during the hydrolysis reaction.

Chemical structure of the synthesized PMMA-*b*-PtBA block copolymers were investigated by ^{1}H-NMR. ^{1}H-NMR spectrum of PMMA-*b*-PtBA is δ: 1.4 ppm (9H, $COOC(CH_3)_3$), 1.7 ppm (2H, CH_2 of PMMA and PtBA), 2.4 ppm (H, CH of PtBA), 3.6 ppm (3H, $COOCH_3$ of PMMA), 6.9 ppm (9H, $COOC(CH_3)_3$ of tBA), 7.25 ppm (s; H, $CHCl_3$) (Malinowska et al., 2005; Ishizu et al., 2005; Nurmi et al., 2007). CH_2 It was observed that residual tBA monomer remained besides specific peaks of PMMA and PtBA blocks in ^{1}H-NMR spectra of copolymers given by Figures 5.22-5.24.

Multiarm PMMA-*b*-PAA molecules were produced by hydrolysis reaction (Figure 5.25). The residual monomer observed in ^{1}H-NMR analysis of PMMA-*b*-PtBA was eliminated during hydrolysis reaction since the polymer was reacted with trifluoroacetic acid in dichloromethane. Amphiphilic PMMA-*b*-PAA copolymer produces a solid precipitate which separates from reaction medium. ^{1}H and ^{13}C-NMR analysis showed that monomer residue was eliminated through hydrolysis reaction (Figure 5.26).

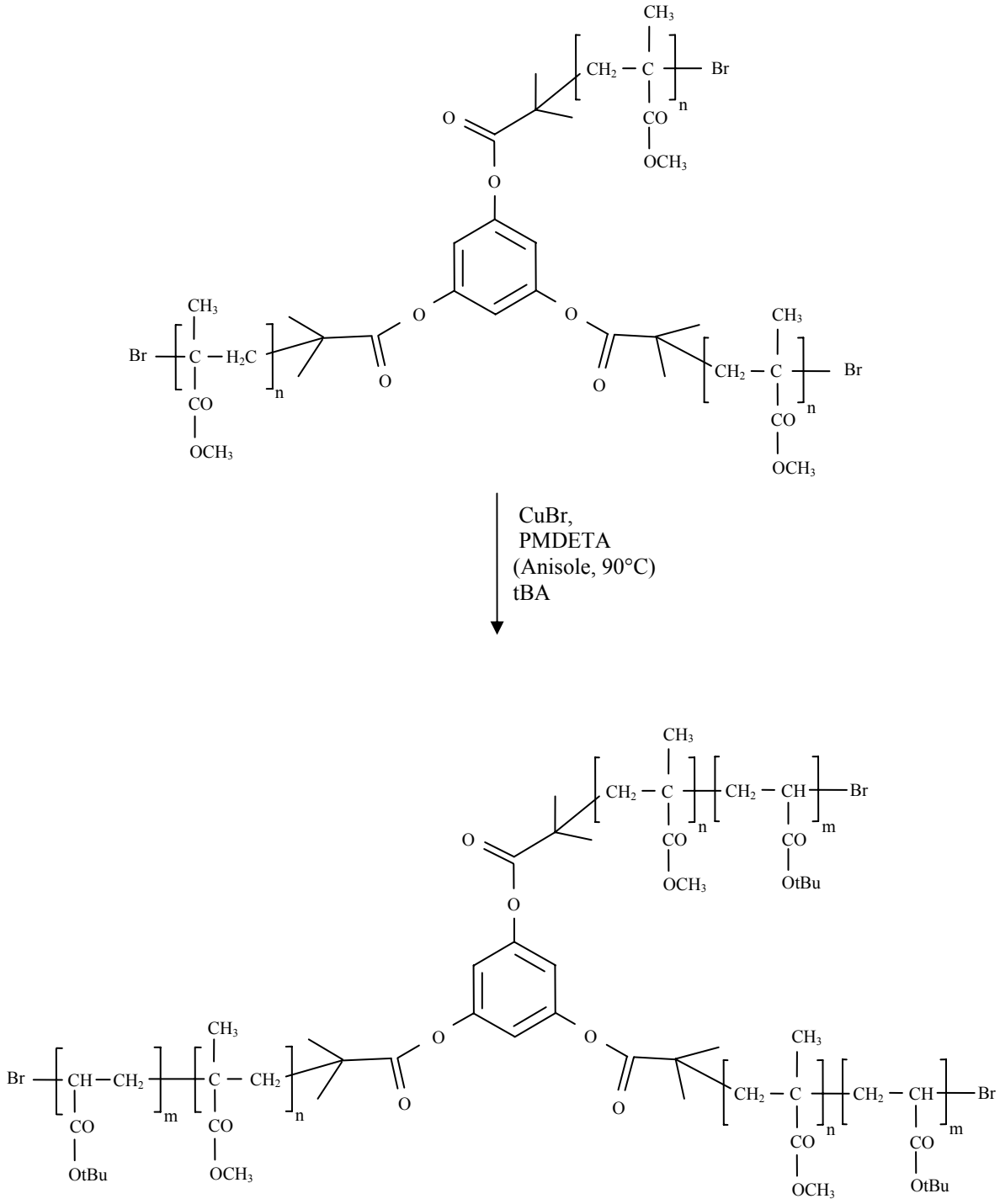

Figure 5.19. ATRP synthesis of 3 arm PMMA-*b*-PtBA from 3 arm PMMA macroinitiator.

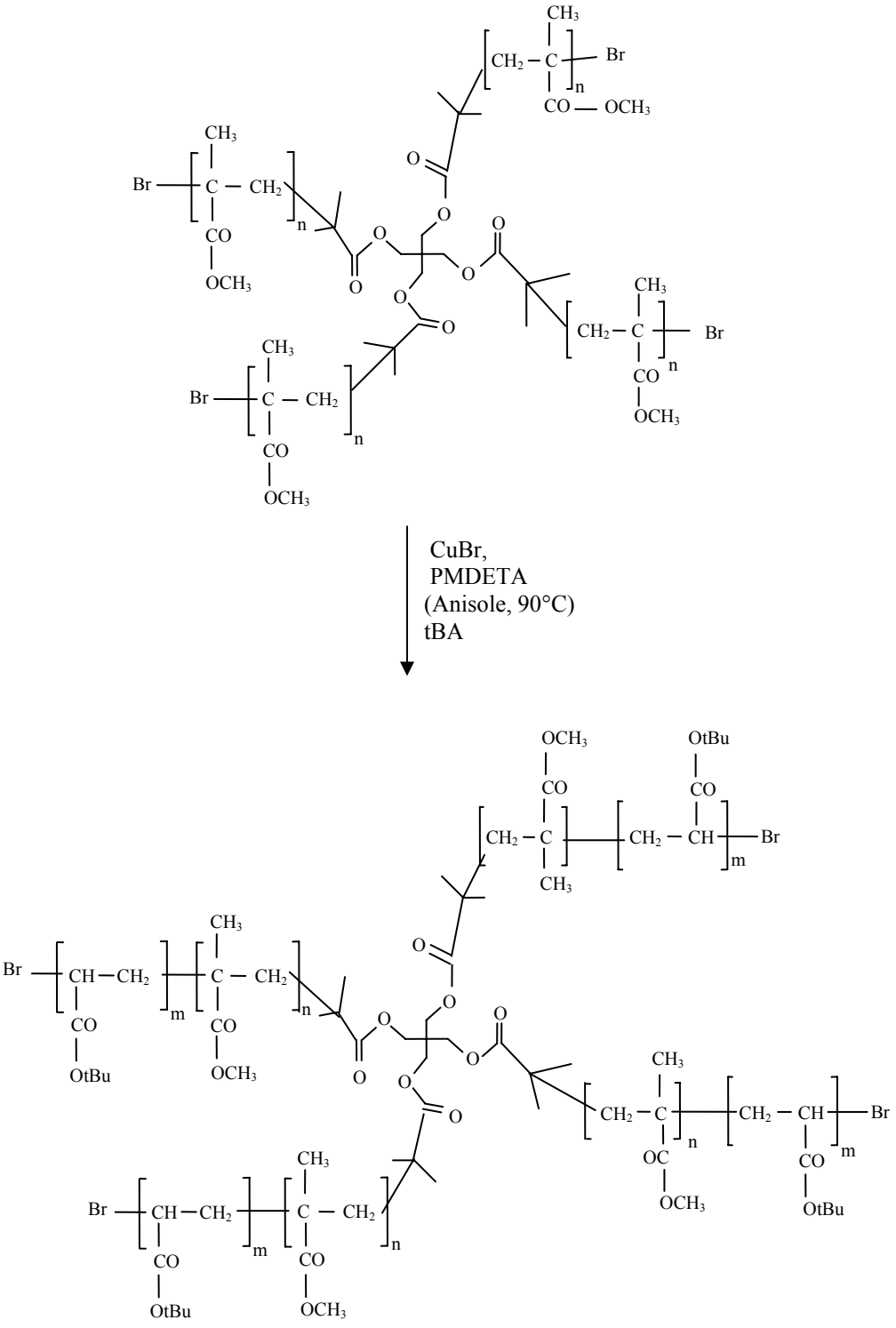

Figure 5.20. ATRP synthesis of 4 arm PMMA-*b*-PtBA from 4 arm PMMA macroinitiator.

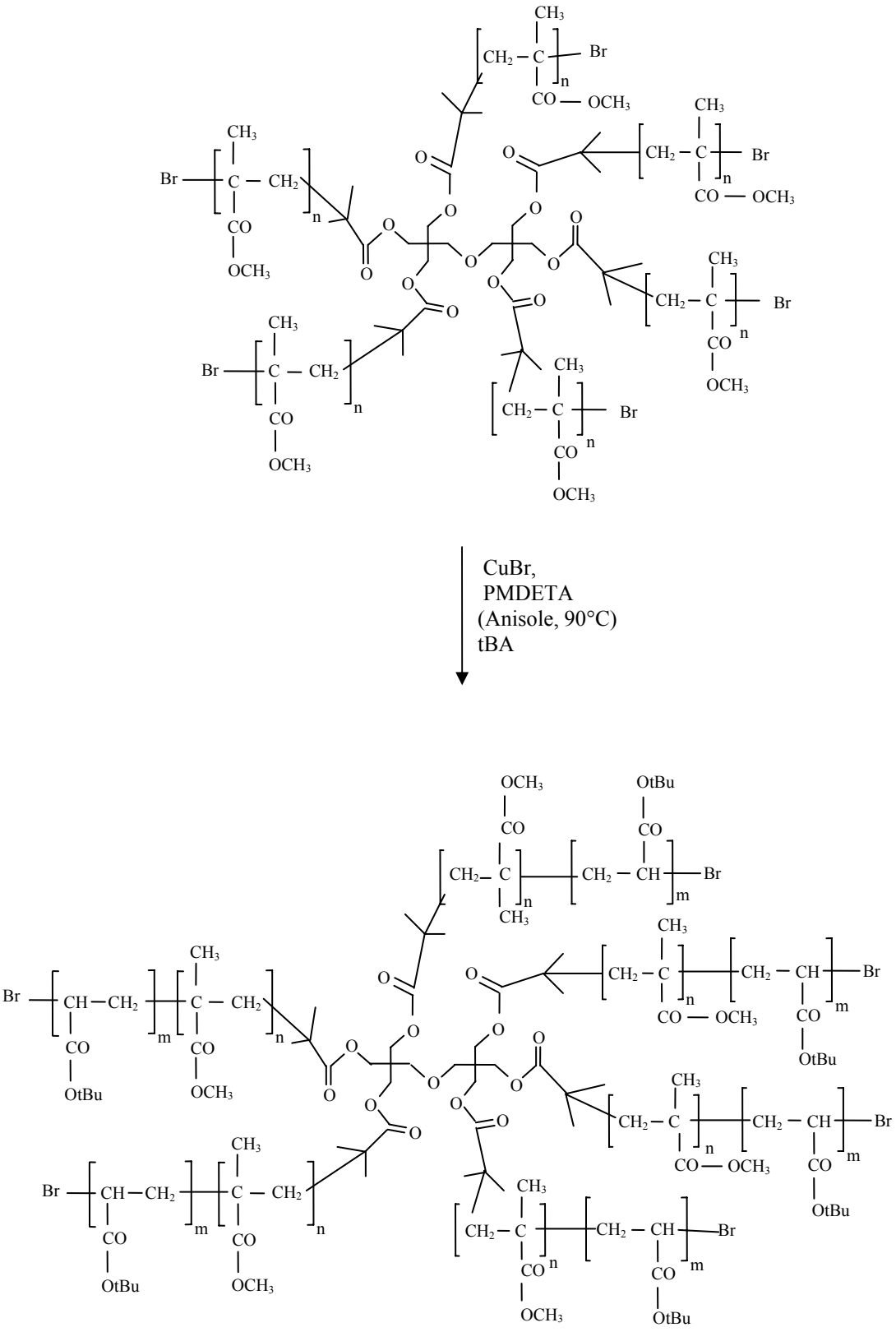

Figure 5.21. ATRP synthesis of 6 arm PMMA-*b*-PtBA from 6 arm PMMA macroinitiator.

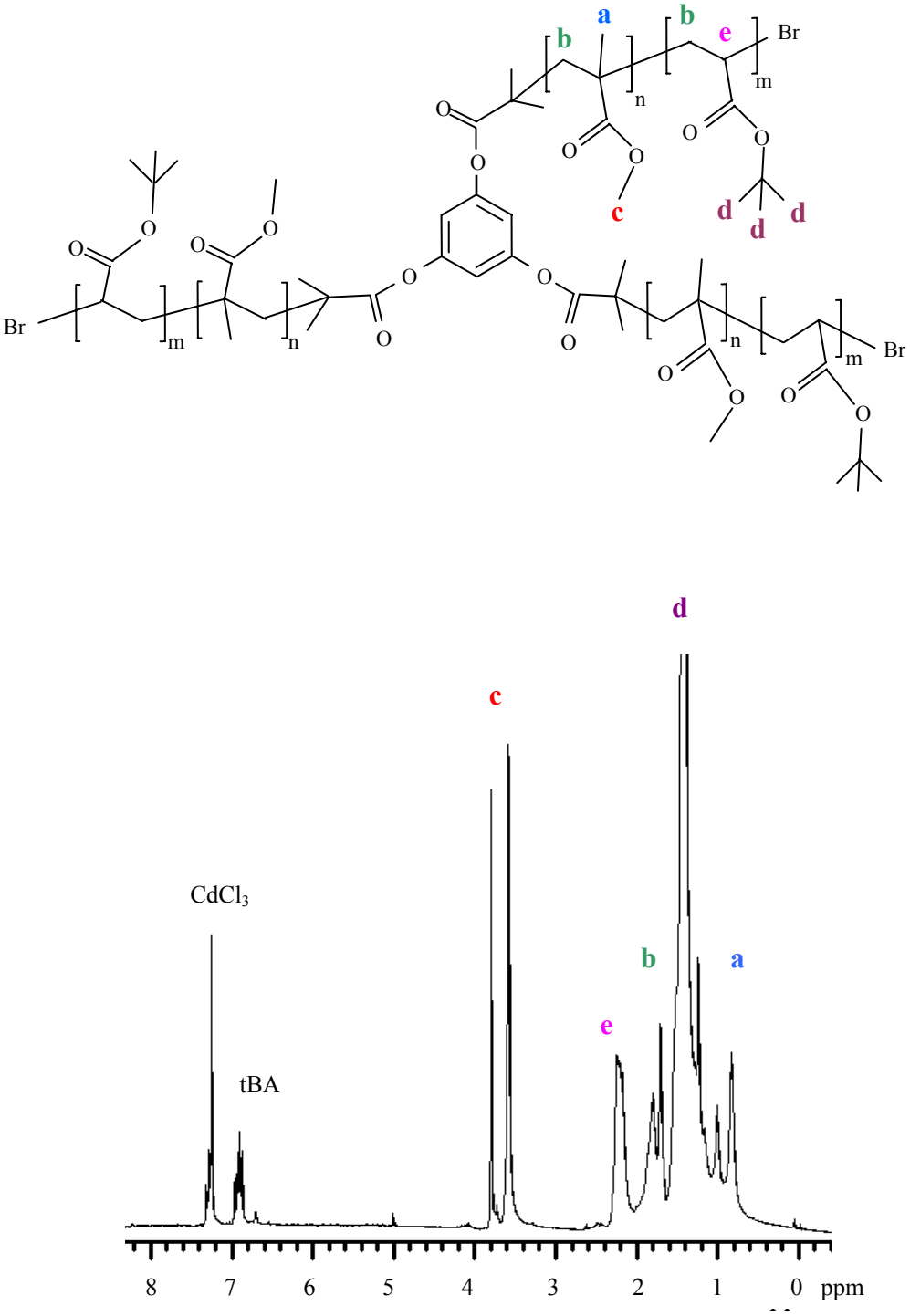

Figure 5.22. ^{1}H-NMR spectrum of 3 arm PMMA-*b*-PtBA.

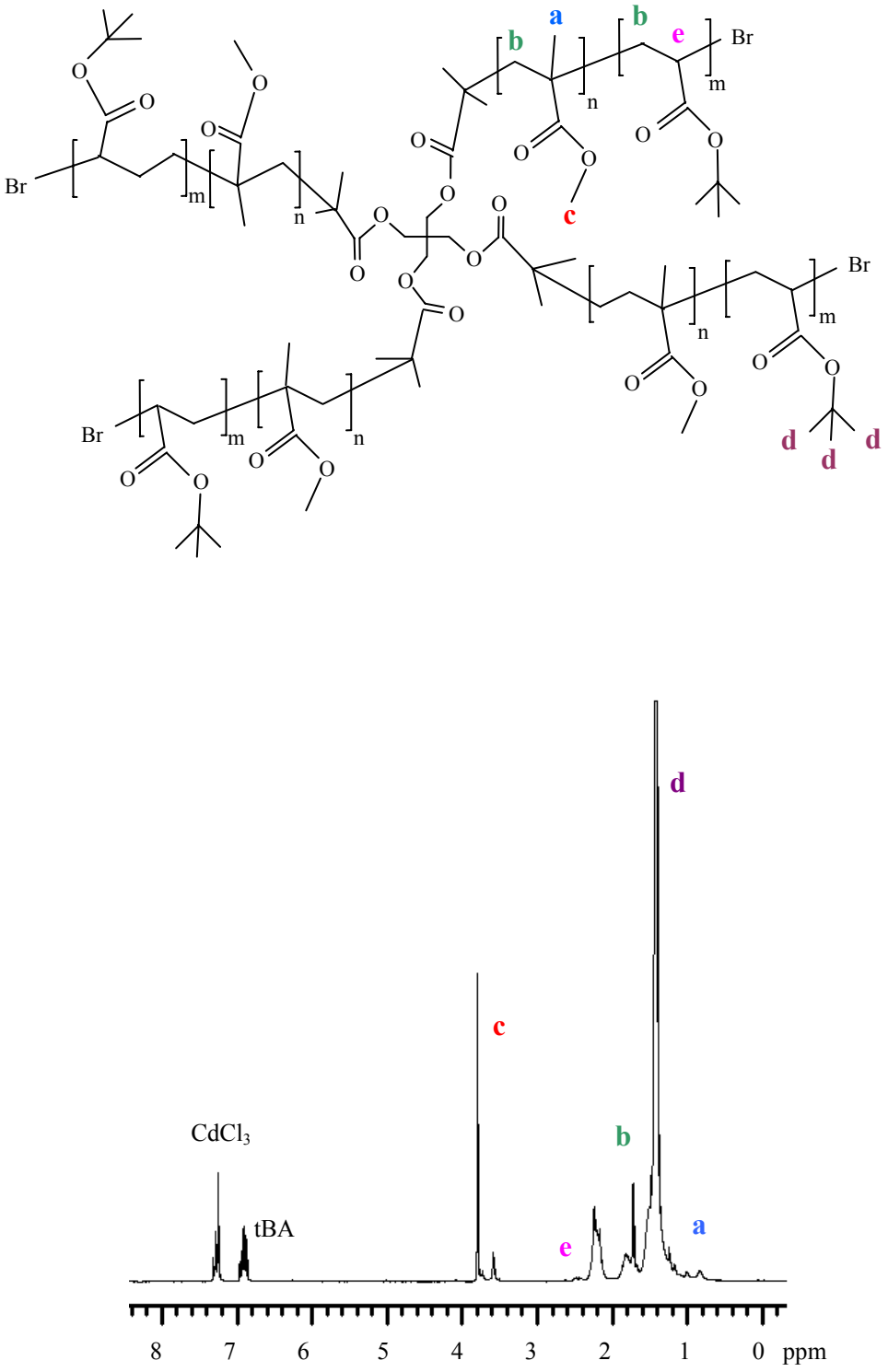

Figure 5.23. ^{1}H-NMR spectrum of 4 arm PMMA-*b*-PtBA.

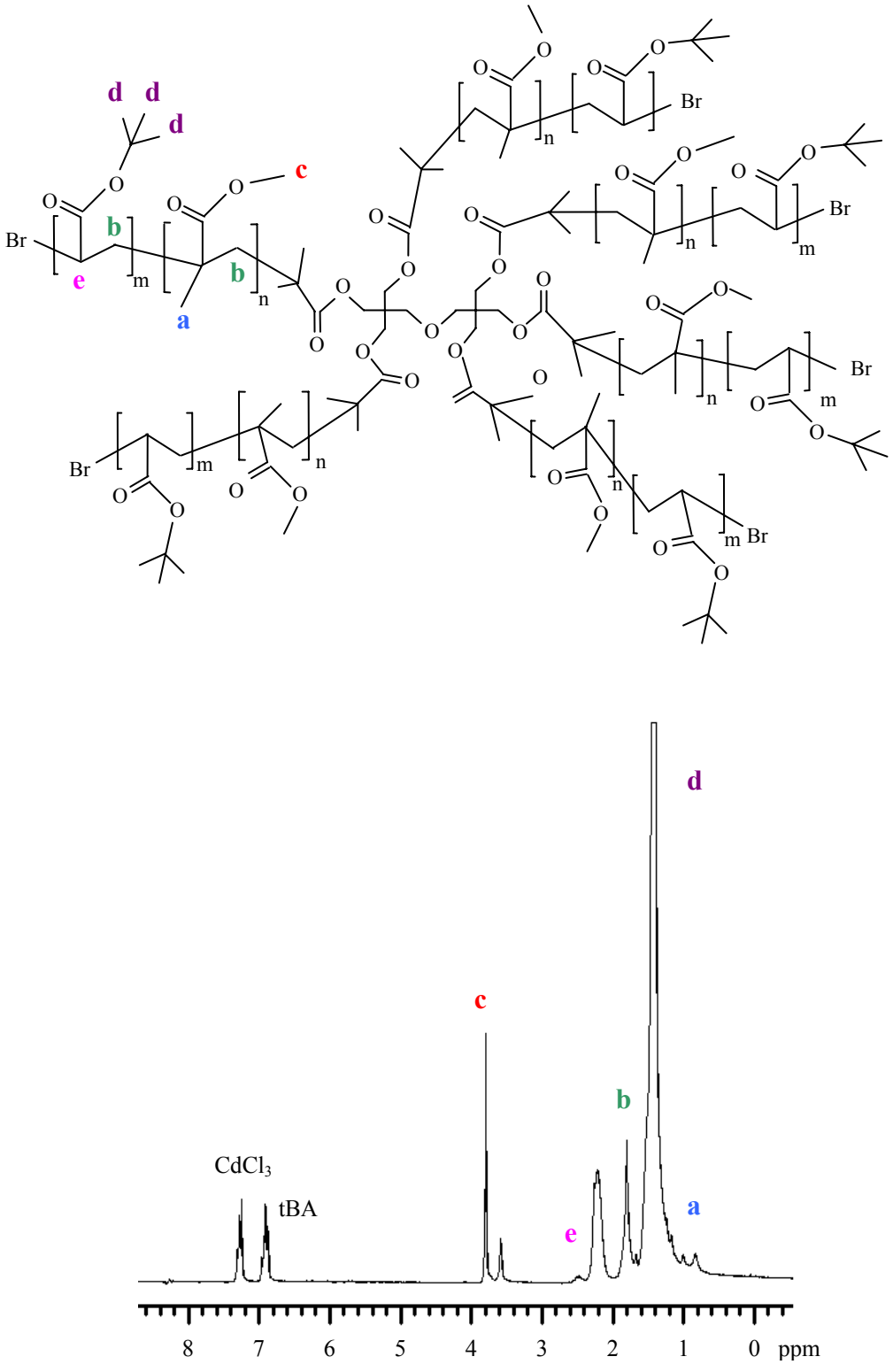

Figure 5.24. ^{1}H-NMR spectrum of 6 arm PMMA-PtBA.

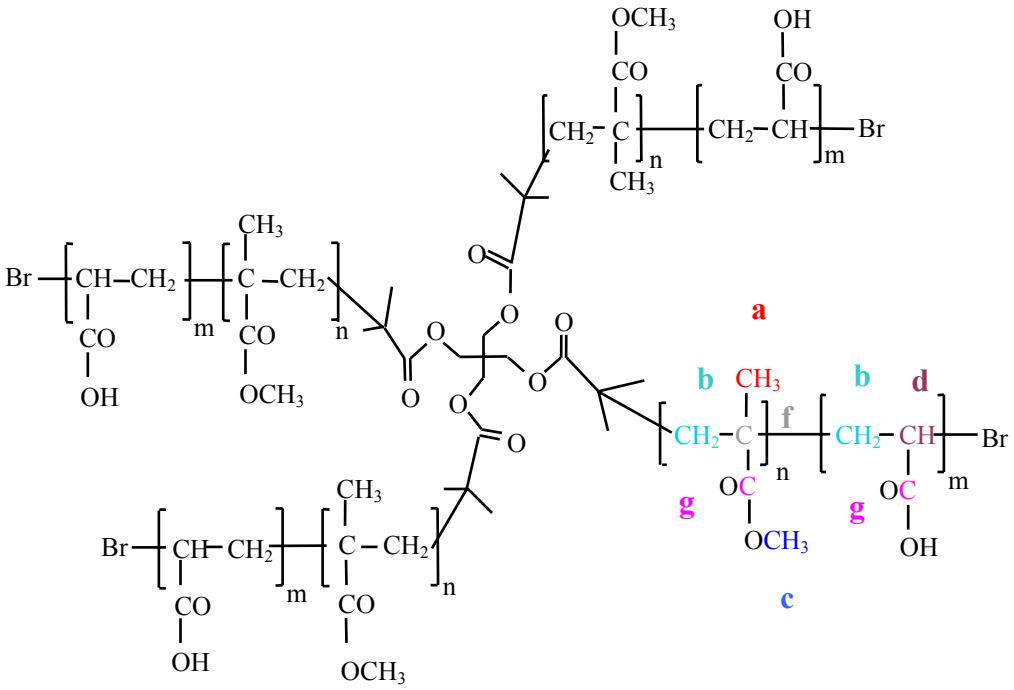

Figure 5.25. Chemical structure of 4 arm PMMA-*b*-PAA synthesized by hydrolysis of 4 arm PMMA-*b*-PtBA.

Peaks of H groups and C atoms of PMMA and PAA chains of 4 arm PMMA-*b*-PAA labeled on NMR spectra given in Figure 5.26 have been defined on molecular structure depicted in Figure 5.25. CH_2 groups of hydrophobic PMMA and hydrophilic PAA labeled with the letter 'b' appeared as two distinct peaks about 1.6 and 1.8 ppm. ^{1}H-NMR spectrum given in 5.25-a showed that CH_3 peak belonging to tBA almost disappeared after hydrolysis.

^{13}C-NMR spectrum explains the structure of amphiphilic molecule more clearly. C peak of CH_3 groups from both PtBA and residual tBA are not observed as in Figure 5.26.b. The only unexpected peak that was not consistent with molecular structure of PMMA-*b*-PAA copolymer was the peak observed at 159 ppm. This peak indicates presence of (-COOC-) structure due to crosslinking of acrylic acid chains. Since the peak is small degree of crosslinking is expected to be low and can be more accurately determined by FTIR analysis.

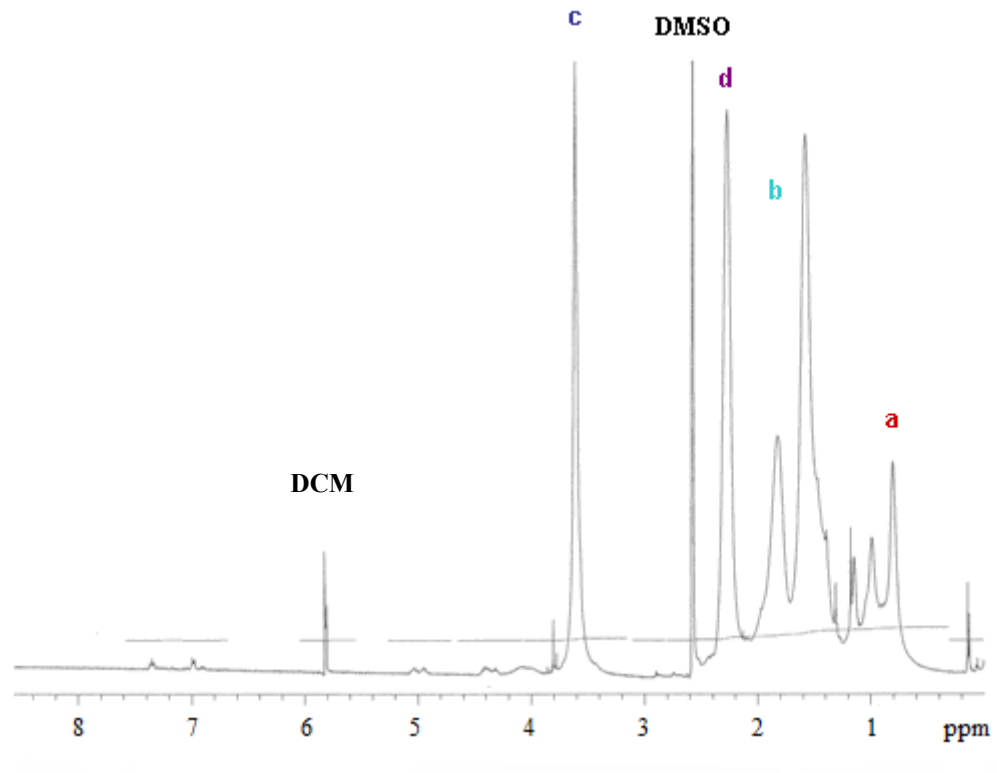

(a)

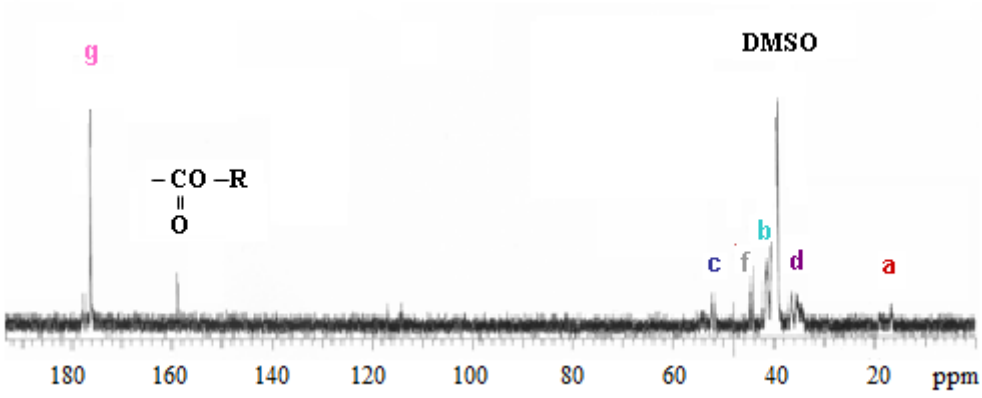

(b)

Figure 5.26. (a) ^{1}H-NMR spectrum of 4 arm PMMA-*b*-PAA (b) ^{13}C-NMR spectrum of 6 arm PMMA-*b*-PAA.

Efficiency of hydrolysis reaction was also examined by FTIR spectra of block copolymers before and after hydrolysis (Figure 5.27-5.29). Peaks of each sample were investigated and named with repect to Table 5.3 (Silverstein et al., 2005; Storey et al., 2005; Ishizu et al., 2005; Wei et al., 2007; Yu et al., 2007; Kang et al., 2006; Yu et al, 2004; Yin et al., 2006)

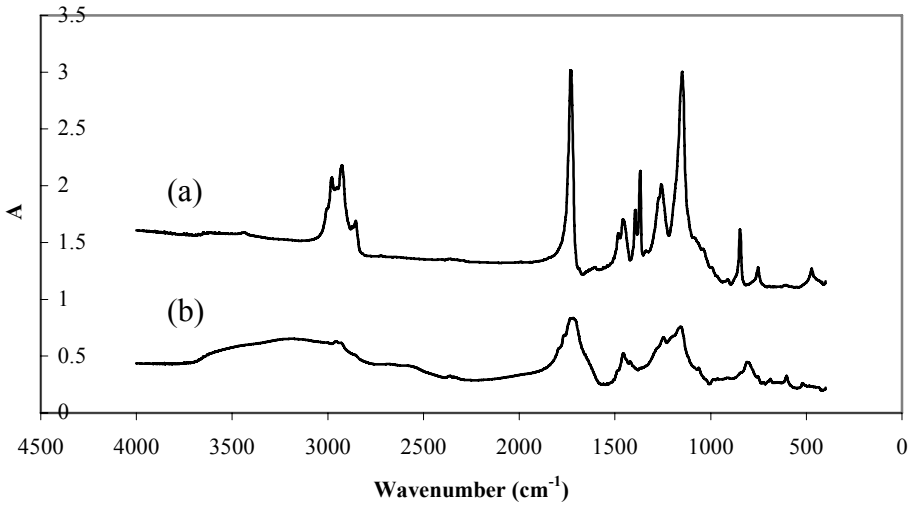

Figure 5.27. FTIR spectra of (a) 3 arm PMMA-*b*-PtBA with 5600 Da PMMA core and total molecular weight of 22000 Da, (b) 3 arm PMMA-*b*-PAA produced by hydrolysis.

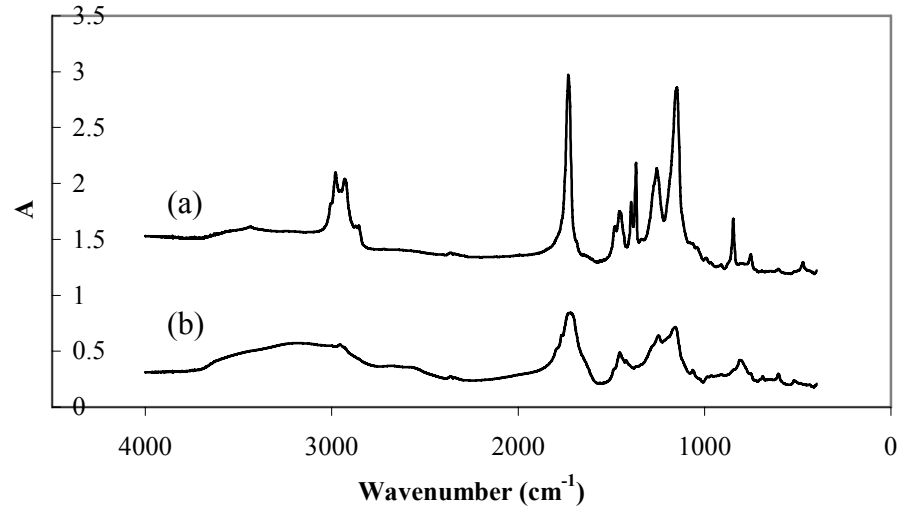

Figure 5.28. FTIR spectra of (a) 4 arm PMMA-*b*-PtBA with 7000 Da PMMA core and total molecular weight of 30000 Da, (b) 4 arm PMMA-*b*-PAA produced by hydrolysis.

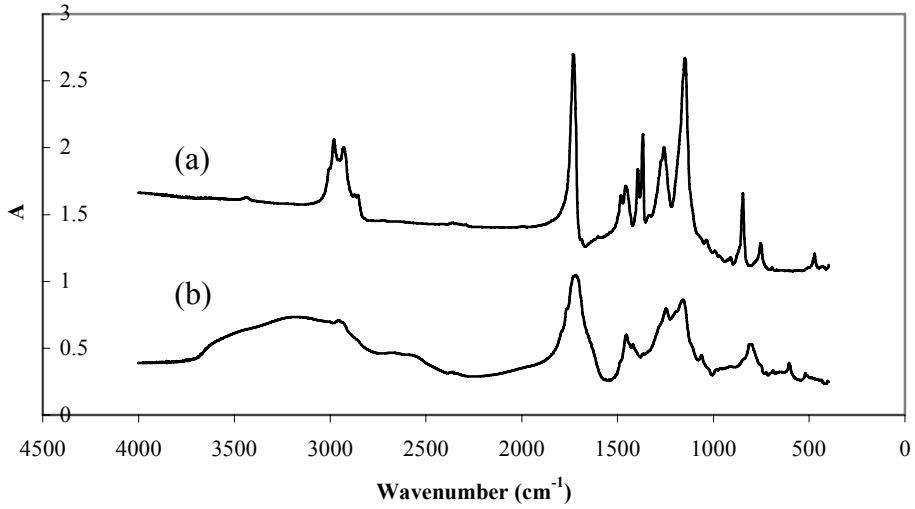

Figure 5.29. FTIR spectra of (a) 6 arm PMMA-*b*-PtBA with 8100 Da PMMA core and total molecular weight of 77000 Da, (b) 6 arm PMMA-*b*-PAA produced by hydrolysis.

Table 5.3. Specific FTIR peaks related to PMMA-*b*-PtBA copolymers.

Wavenumber (cm^{-1})	**Band**	**Monomer**
752	CH vibration of C-CH_3	Methyl methacrylate
990	CH vibration of O-CH_3	Methyl methacrylate
1150	C-O stretching	*tert*-Butyl acrylate
1168	COO ester stretching	Acrylic acid
1260	C-O stretching	Acrylic acid
1400	Stretching vibration of $C(CH_3)_3$	*tert*-Butyl acrylate
1440-1460	Symmetric stretching of COO^-	Acrylic acid
1570	Asymmetric stretching of COO^-	Acrylic acid
1715	Carboxyl peak	Acrylic acid
1730	C=O stretching	All acrylic monomers
2800-3200	OH	Acrylic acid
2925	C-H asymmetric stretching of methyl groups	*tert*-Butyl acrylate

5.3. Maximum Loading Capacity

Maximum loading capacities of seven polymers were compared to select the ideal hydrophobic drug carrier. In that manner number of arms, total molecular weights and hydrophobic core ratios were the main issues for comparison. Table 5.4 gives a list of seven block copolymers synthesized with different number of arms, molecular weights and hydrophobic core ratios.

In order to determine maximum loading capacities, pyrene was used as fluorescent probe and pyrene loading capacity of polymer samples were determined by fluorescent method. Pyrene is a highly hydrophobic substance whose chemical structure is as in Figure 5.30 and is used as an indicator for loading capacity of polymers with hydrophobic drugs.

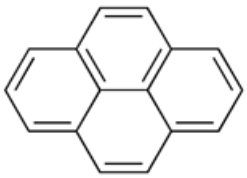

Figure 5.30. Chemical structure of pyrene.

Table 5.4. List of polymers compared for maximum loading capacity.

Sample	Number of Arms	MW of PMMA core (Da)	MW of PMMA-*b*-PtBA form (Da)	Hydrophobic Core Ratio (%)
PMMA-*b*-PAA 3.1	3	5600	22000	25.2
PMMA-*b*-PAA 4.1	4	4700	27000	17.4
PMMA-*b*-PAA 4.2	4	7000	30000	23.3
PMMA-*b*-PAA 4.3	4	7000	17000	41.2
PMMA-*b*-PAA 6.1	6	8000	77000	10.1
PMMA-*b*-PAA 6.2	6	8000	45000	18.0
PMMA-*b*-PAA 6.3	6	8000	18000	46.0

Determination of maximum loading capacity was performed by loading certain concentrations of polymer samples by various pyrene concentrations in aqueous medium. After elimination of unloaded quantity of pyrene by centrifugation, loading capacity was determined from fluorescence emission intensity of pyrene at 393 nm. Loading capacities were determined at two polymer concentrations which were 500 mg/L and 200 mg/L.

A sample graph for change in emission intensities of 4 arm PMMA-*b*-PAA with 4700 Da PMMA core and 27000 Da total molecular weight at different pyrene concentrations excited at 330 nm is given in Figure 5.31. Figures 5.32 and 5.33 show the variations of emission intensities (at 393 nm) of 3 arm, 4 arm and 6 arm PMMA-*b*-PAA samples with respect to pyrene concentration at a polymer concentration of 500 mg/L. Maximum loading capacity is observed to increase with increasing hydrophobic core ratio. 4 arm and 6 arm PMMA-*b*-PAA samples exhibit better loading capacities when compared to 3 arm PMMA-*b*-PAA.

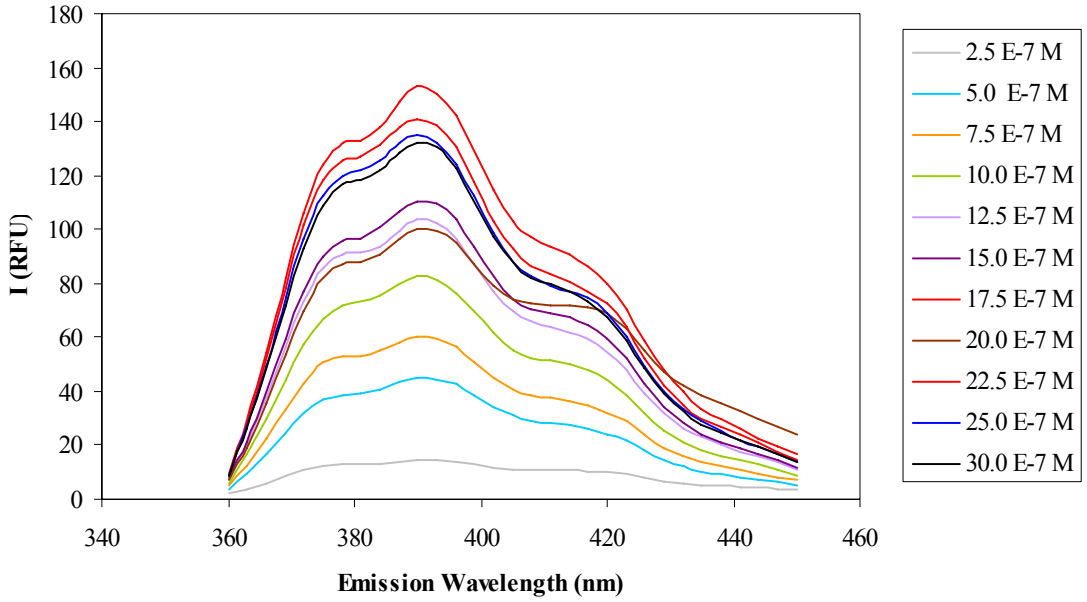

Figure 5.31. Emission spectra of PMMA-*b*-PAA 4.1 loaded at different pyrene concentrations designated in different colors.

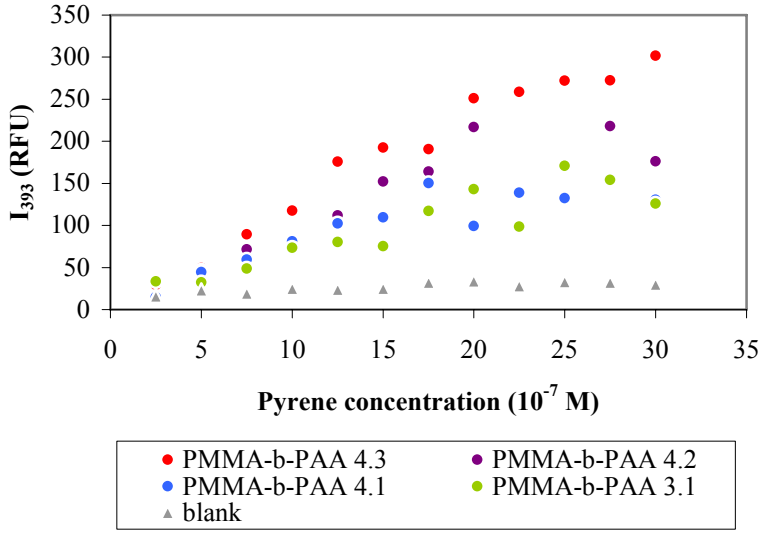

Figure 5.32. Variation of emission intensities of 3 arm and 4 arm PMMA-*b*-PAA samples loaded at 500 mg/L polymer concentration with respect to pyrene concentration.

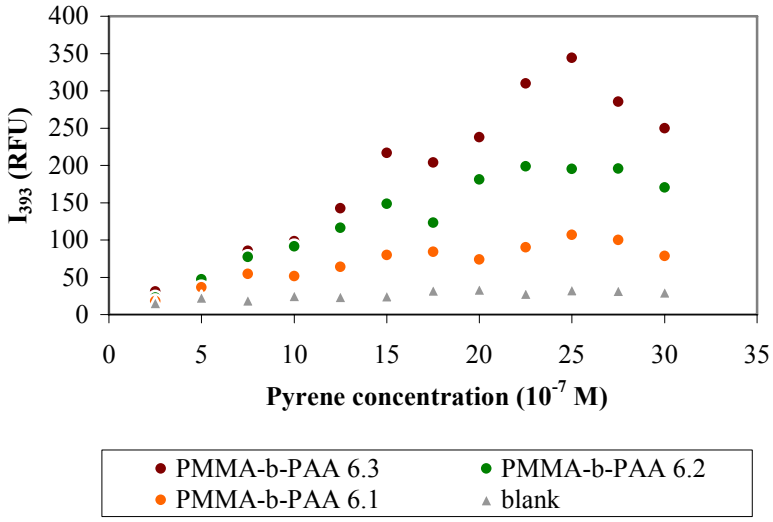

Figure 5.33. Variation of emission intensities of 6 arm PMMA-*b*-PAA samples loaded at 500 mg/L polymer concentration with respect to pyrene concentration.

Figures 5.34 and 5.35 show the variations of emission intensities (at 393 nm) of 3 arm, 4 arm and 6 arm PMMA-*b*-PAA samples with respect to pyrene concentration at a polymer concentration of 200 mg/L. Maximum loading capacities of 3 arm, 4 arm and 6 arm PMMA-*b*-PAA samples at both concentrations of 500 mg/L and 200 mg/L are listed in Table 5.5. Maximum loading capacities in terms of emission intensity at 393 nm given in relative fluorescence units were achieved at and above pyrene concentrations of 20 $\times 10^{-7}$ M.

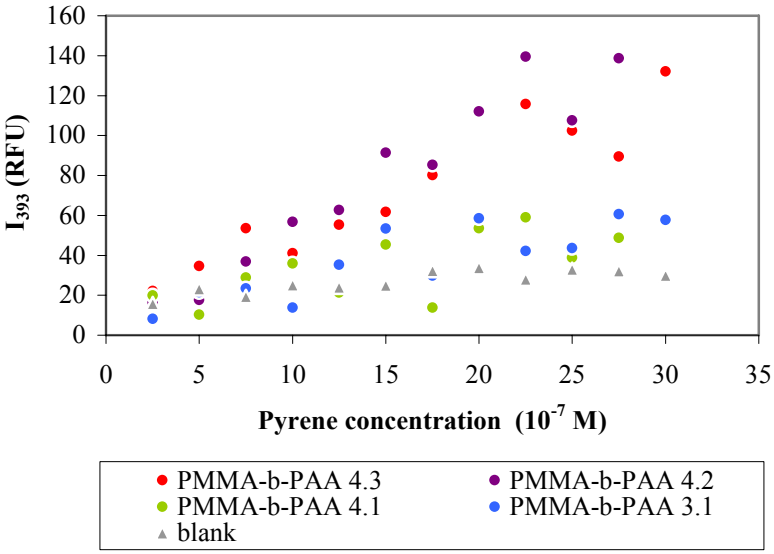

Figure 5.34. Variation of emission intensities of 3 arm and 4 arm PMMA-*b*-PAA samples loaded at 200 mg/L polymer concentration with respect to pyrene concentration.

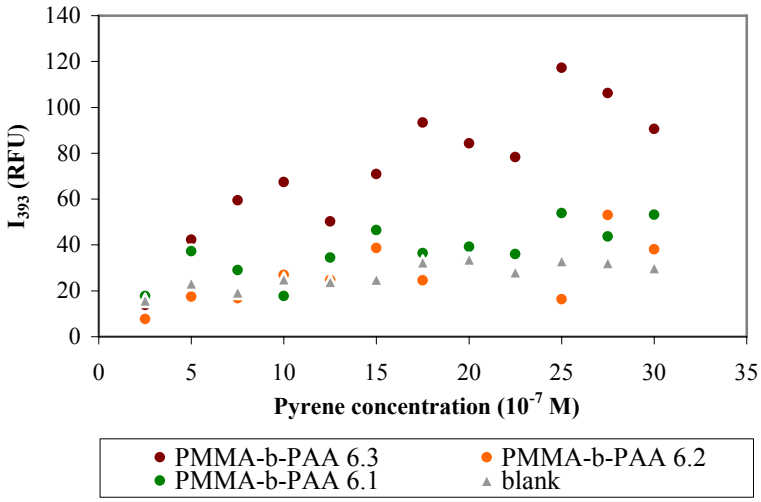

Figure 5.35. Variation of emission intensities of 6 arm PMMA-*b*-PAA samples loaded at 200 mg/L polymer concentration with respect to pyrene concentration.

Table 5.5 shows that highest loading capacities were attained by highest hydrophobic core ratios at 500 mg/L polymer concentration. 4 arm and 6 arm PMMA-*b*-PAA samples with similar hydrophobic core ratios exhibit comparable maximum loading capacities at that polymer concentration. But when system is diluted to a 200 mg/L polymer concentrations, it was observed that maximum loading capacities of 4-arm PMMA-*b*-PAA were higher than that of 6 arm PMMA-*b*-PAA with similar hydrophobic core ratios.

At lower polymer concentration it was also observed that hydrophobic core ratio is not the only criteria that improves maximum loading capacity. At relatively dilute systems importance of stability of the polymer emerges. Although hydrophobic core ratio determines the loading capacity of the polymer, it reduces the stability of the polymer when it exceeds an optimum value. Therefore an ideal multiarm PMMA-*b*-PAA to be used as an hydrophobic drug carrier is estimated to have 4 arms and a a hydrophobic core ratio about 0.25.

Table 5.5. Maximum loading capacities of 3 arm, 4 arm and 6 arm PMMA-*b*-PAA samples loaded at different polymer concentrations.

Sample	MW_{PMMA} / $MW_{PMMA\text{-}b\text{-}PAA}$ (Da)	Max. Loading Capacity (500 mg/L) (I_{393})	Max. Loading Capacity (200 mg/L) (I_{393})	f_c
PMMA-*b*-PAA 3.1	5600/22000	154.11	60.56	0.26
PMMA-*b*-PAA 4.1	4700/27000	150.43	59.05	0.17
PMMA-*b*-PAA 4.2	7000/30000	216.97	139.54	0.23
PMMA-*b*-PAA 4.3	7000/17000	301.80	132.12	0.41
PMMA-*b*-PAA 6.1	8100/77000	106.825	53.84	0.11
PMMA-*b*-PAA 6.2	8100/45000	198.53	53.09	0.18
PMMA-*b*-PAA 6.3	8100/18000	344.41	117.30	0.45

5.4. Critical Micelle Concentration

Critical micelle concentration is a very important characteristics of micelle forming polymers for drug transportation systems. Critical micelle concentration is a minimum concentration that polymer forms a micelle and is able to carry a hydrophobic drug in aqueous medium and are generally determined by pyrene fluorescence methods. Critical micelle concentrations (CMC) of PMMA-*b*-PAA samples loaded with pyrene at different polymer concentrations could have been analyzed by evaluation of both emission and excitation spectra. Emission spectra were obtained for an excitation wavelength of 330 nm, and excitation spectra were obtained for an emission wavelength of 393 nm. Variation of excitation spectra for a pyrene loaded 4 arm PMMA-*b*-PAA sample with 5000 Da PMMA and 45000 Da total molecular weight with respect to polymer concentration is shown in Figure 5.36. Pyrene loading was performed by mixing polymer solutions at different concentrations with constant amount of pyrene at

4°C for 16 hours. Emission intensities (393 nm) of the samples were followed during loading to make sure equilibrium is reached within 16 hours. Pyrene concentration was 2×10^{-7} M to prevent excimer formation which leads erroneous results in fluorescence measurements.

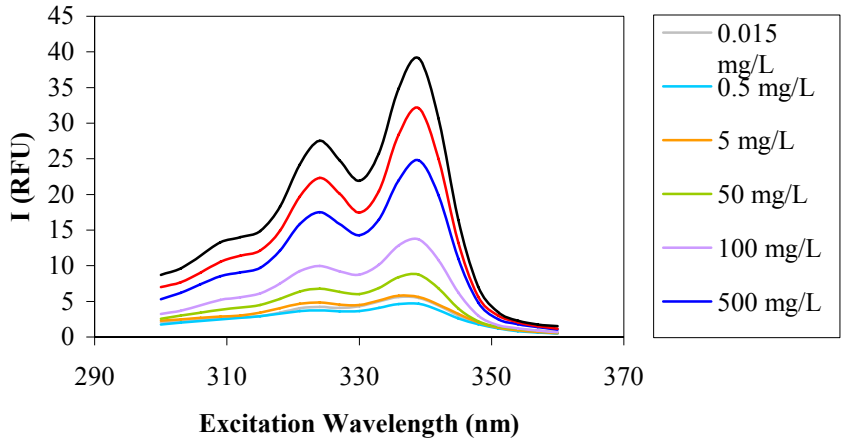

Figure 5.36. Excitation spectra of pyrene loaded 4 arm PMMA-*b*-PAA samples (MW: 5000/45000 Da) at polymer concentrations designated in different colors.

Critical micelle concentrations were determined from changes in I_{336}/I_{333} ratio with increasing polymer concentrations as in method given by Lele and coworkers (Lele et al., 2002) The blue shift in I_{336} band of excitation spectra of pyrene indicates the change in excitation behavior of the probe due to loading. Figure 5.37 shows this change in I_{336}/I_{333} ratio for 4 arm PMMA-*b*-PAA sample (MW: 5000/45000 Da). CMC is accepted to be the polymer concentration where initial constant I_{336}/I_{333} line intersects the increasing slope emerged due to loading. Sketches of I_{336}/I_{333} ratio versus polymer concentration of other PMMA-*b*-PtBA samples that were investigated for comparison are given in Appendix A.

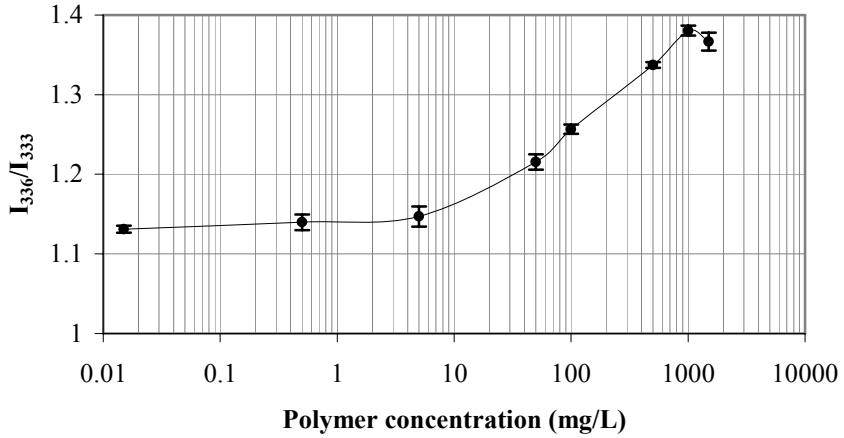

Figure 5.37. Determination of CMC from shifts in I_{336} band in excitation spectra (n=2).

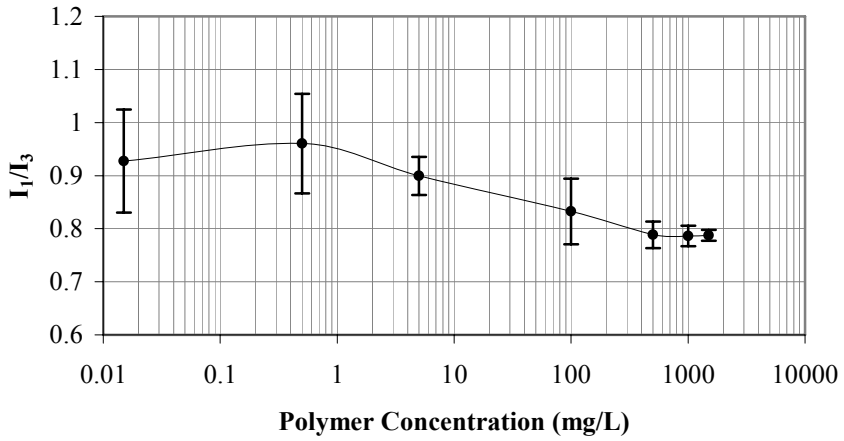

Figure 5.38. Determination of CMC from I_1/I_3 ratios in emission spectra (n=2).

CMC of the 4 arm PMMA-*b*-PAA sample has also been determined from the ratio of first and third emission bands (I_1/I_3) versus polymer concentration in mg/L as in Figure 5.38. Intensities of the first and third bands of pyrene correspond to fluorescence emissions at 372 nm and 385 nm wavelengths (LópezDíaz and Velázquez, 2007; Zhang et al., 2007; Aguiar et al., 2003). Distinct I_1 and I_3 bands were observed more clearly as in Figure 5.39 when pyrene was dissolved in chloroform. The drop in I_1/I_3 ratio designates a change in pyrene's location due to loading and CMC is supposed to be intersection of horizontal and steep slopes of initial constant and increasing I_1/I_3 values on non-logarithmic scale.

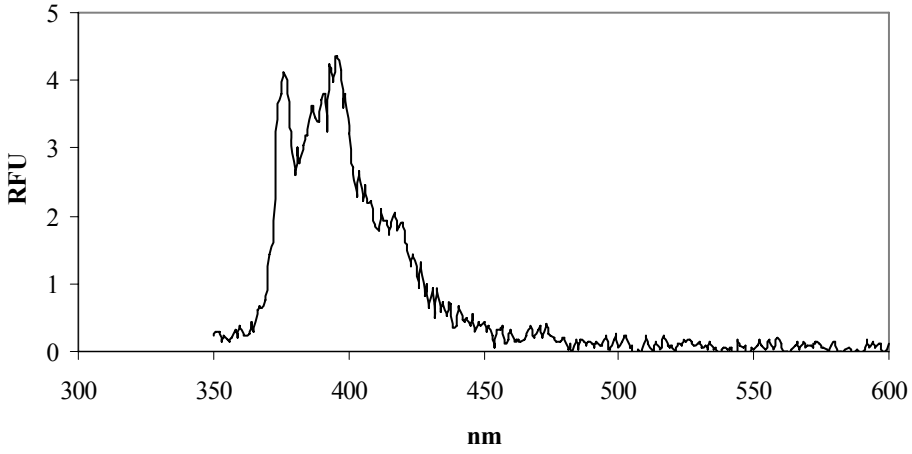

Figure 5.39. I_1 and I_3 bands at 372 nm and 385 nm on emission spectrum of pyrene in chloroform (excited at 330 nm).

As a final approach, pyrene loaded PMMA-*b*-PAA sample was analyzed by UV-spectrophotometry and absorbance spectra of pyrene solubilized by certain concentrations of polymer were measured. Change in absorbance spectra increasing with polymer concentration was observed as in Figure 5.40. An increase in UV-absorbance at 266 was observed after 10 mg/L polymer concentration on Figure 5.41 which verifies CMC obtained by fluorescence spectroscopy.

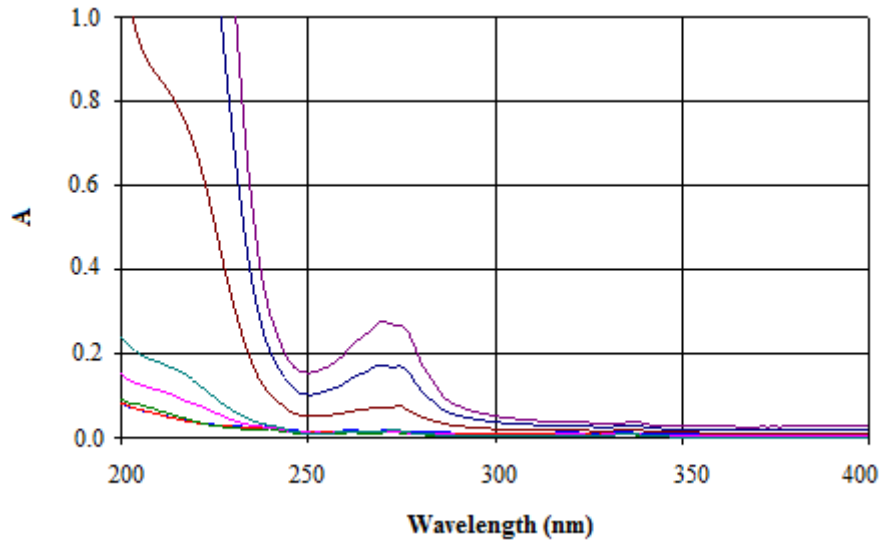

Figure 5.40. UV-Absorbance spectra of pyrene loaded 4 arm PMMA-*b*-PAA samples (MW: 5000/45000 Da) at polymer concentrations designated in different colors.

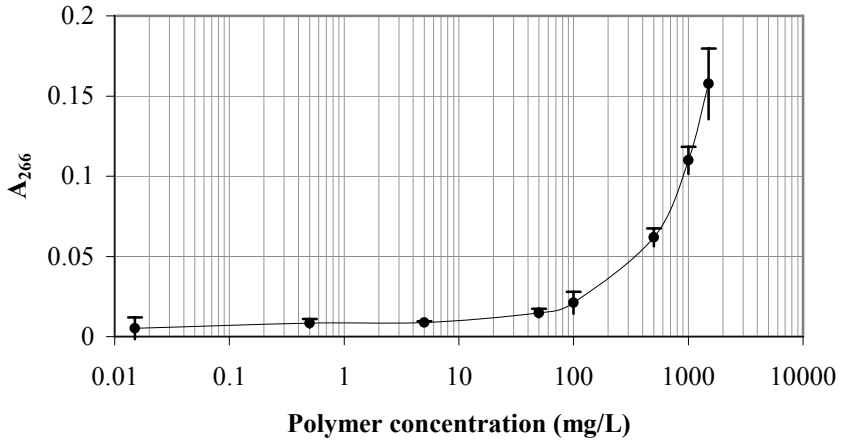

Figure 5.41. Determination of CMC from change in UV-absorbance A_{266} with respect to polymer concentration (n=2).

Comparison of CMC values listed in Table 5.6 suggests that a hydrophobic core ratio at 0.25 provides improved stability indicated by minimum critical micelle concentrations. Another characteristics that affect stability in terms of CMC is molecular weight. It was observed that increasing molecular weight of block copolymer increases stability but it has to be reminded that increased molecular weights reduce loading capacity of multiarm PMMA-*b*-PAA copolymers and increased molecular weight of PMMA core would prevent degradation of polymer particles.

Table 5.6. Critical micelle concentrations of 3 arm, 4 arm and 6 arm PMMA-*b*-PAA samples having various molecular weight and hydrophobic core ratios.

Sample	MW_{PMMA} / $MW_{PMMA\text{-}b\text{-}PAA}$ (Da)	CMC (mg/L)	f_c
PMMA-*b*-PAA 3.1	5600/22000	5	0.26
PMMA-*b*-PAA 4.1	4700/27000	10	0.17
PMMA-*b*-PAA 4.2	7000/30000	5	0.23
PMMA-*b*-PAA 4.4	6400/33000	10	0.19
PMMA-*b*-PAA 4.5	5000/45000	10	0.11
PMMA-*b*-PAA 6.1	8100/77000	10	0.11
PMMA-*b*-PAA 6.2	8100/45000	20	0.18

5.5. Drug Loading

5.5.1 Determination of Optimum Drug Loading Method

Drug loading methods were listed as simple equilibrium, co-precipitation, dialysis, solvent deposition and salting out methods which have been described in Chapter 2.2. PMMA-*b*-PAA copolymers cannot form micelles by direct mixing with water. A micellization technique has to be applied during loading which follows dissolution of drug and polymer samples in appropriate solvents. Polymer samples can be dissolved in ethanol and dimethyl sulfoxide with slight heating while dimethyl formamide readily dissolves the polymer. After dissolution of polymer and drug, they have to be mixed at definite loading conditions that consist of type of loading medium, polymer and drug concentrations, temperature and duration of the process. Before an analysis of effectiveness of those parameters, the most efficient loading technique has to be determined.

Model drug used for selection of loading method was indomethacin. Indomethacin is an anti-enflammatory drug that is slightly soluble in aqueous medium. The chemical structure is shown in Figure 5.42.

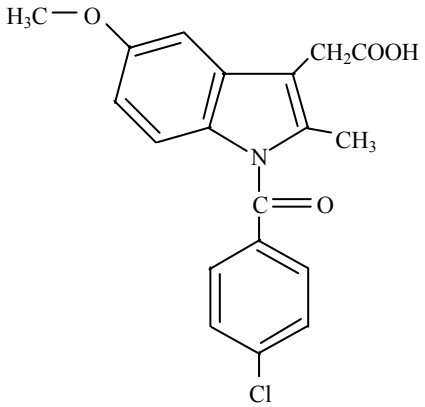

Figure 5.42. Chemical structure of indomethacin.

In order to make a comparison among loading methods listed above, indomethacin was loaded to 4 arm PMMA-*b*-PAA (MW: 7000/30000 Da) which has exhibited the highest maximum loading capacity with pyrene at a polymer concentration

of 200 mg/L. Reaction conditions and conversions of 4 arm PMMA-*b*-PAA (MW: 7000/30000 Da) synthesis are given in Table 5.7 for information.

Co-precipitation is not a suitable method for loading acrylic block copolymers for an appropriate nonsolvent, like diethyl ether for PEG derivatives (Djordevic et al. 2003), does not exist. Therefore PMMA-*b*-PAA samples were loaded by other three techniques and drug loading efficiencies were determined by UV-spectrophotometer.

Table 5.7. Reaction conditions and conversions of synthesis and hydrolysis reactions of 4 arm PMMA-*b*-PAA (7000/30000).

	4 arm PMMA-Br	**4 arm PMMA-*b*-PtBA**	**4- arm PMMA-PAA**
Initiator (I)	Pentaerythritol tetrakis (2-Bromoisobutyrate)	4 arm PMMA-Br (MW 7000 Da)	Reactants: Trifluoro acetic acid + 4 arm PMMA-*b*-PtBA
Mo/I	1000	2300	-
Solvent	Anisole (1:1 V_m/V_s)*	Anisole (1:1 V_m/V_s)*	Dichloromethane
Catalyst	CuCl (4×I)	CuBr (4.4×I)	-
Ligand	PMDETA (4×I)	PMDETA (40×I)	-
Reaction Temperature	70ºC	90ºC	25ºC
Reaction time	10 min	12 hours	24 hours
MW experimental	7000 Da (PI: 1.135)	30000 Da (PI: 1.12)	-
Molar Conversion	3.75 %	14.15 %	91.7 %
Weight of product	0.42 gr	1.014 gr	0.638 gr

*Volumetric solvent to monomer ratio.

For loading 4 arm PMMA-*b*-PAA samples with indomethacin by dialysis method both polymer and drug was dissolved in dimethylformamide and excess drug was eliminated by dialysis in 24 hours. Loading was carried for 1 hour for each sample at room temperature or at 4°C. Samples were freeze dried after dialysis and drug content of each sample was measured by UV-spectroscopy. Absorbance of sample at 320 nm was compared to calibration curve of indomethacin given in Figure 5.43. Drug content of loaded micelle solutions were calculated by using Equation 5.4 that was obtained from regression formula given by Figure 5.42 ($MW_{indomethacin}$=357.8).

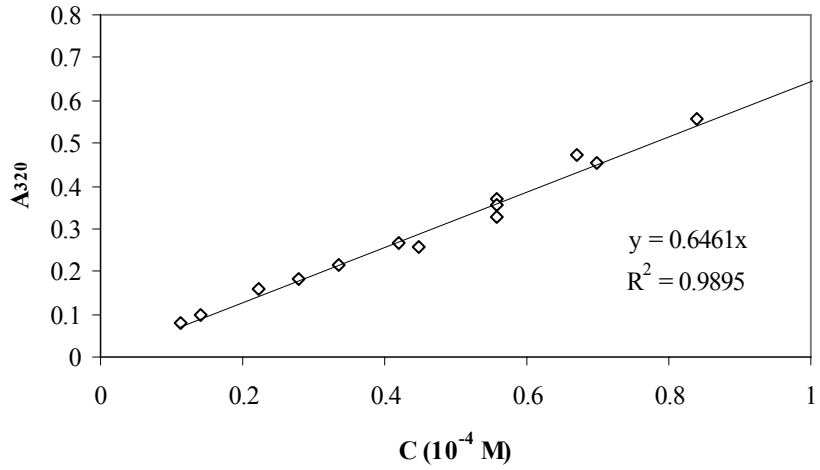

Figure 5.43. Calibration curve of indomethacin dissolved in dimethylformamide.

$$C_{indomethacin}\,(mg/ml) = 0.055 \times A_{320} \qquad (5.4)$$

Dialysis method not only yields high drug loading efficiencies but also provides micellization of freeze dried samples of drug loaded PMMA-*b*-PAA. Drug loaded samples were easily dissolved and formed stable dispersions when introduced to aqueous medium. When Table 5.8 was examined, it was also observed that dialysis method yielded superior drug contents compared to salting out and solvent deposition methods.

Table 5.8**.** Drug loading performances of dialysis, salting out and solvent deposition methods.

Method	**Solvent (Polymer/Drug)**	**Sample Amount (Polymer/Drug) (mg)**	**Temperature (°C)**	**Loading Efficiency (%)**
Dialysis	DMF / DMF	10 /10	25	13.4
Dialysis	DMF / DMF	10 /10	4	20.6
Dialysis	DMF / DMF	50 / 50	4	24.8
Salting Out	Water	50 / 50	25	2.5
Salting Out	PBS	50 / 50	25	5.5
Solvent Deposition	EtOH / DMF	10 /10	25	4.7

Characterization of indomethacin loaded 4 arm PMMA-*b*-PAA (MW:7000/30000 Da) was achieved by FTIR and DSC analysis given by Figures 5.44 and 5.45. Comparison of FTIR spectra of loaded and unloaded polymer samples to that of model drug indomethacin shows that drug is entrapped within polymer particles since sharp peaks of indomethacin were repressed. However specific peaks of indomethacin can be distinguished.

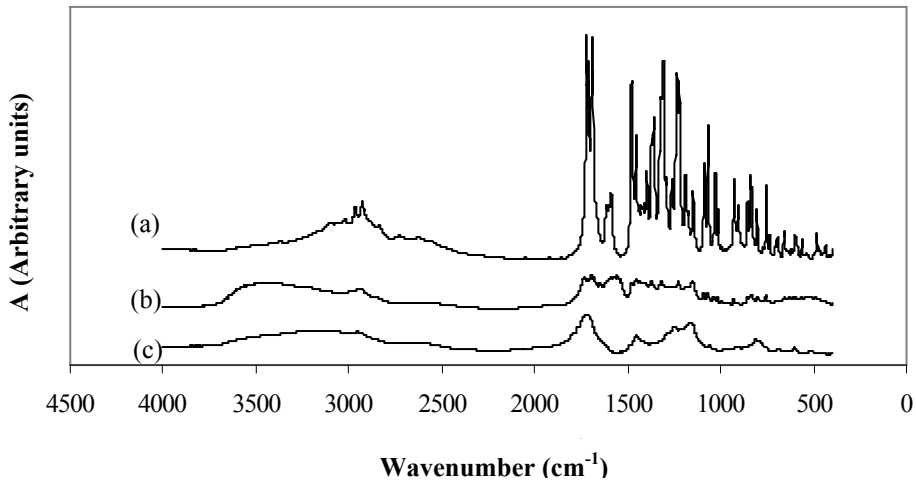

Figure 5.44. FTIR spectra of (a) indomethacin, (b) indomethacin loaded 4 arm PMMA-*b*-PAA.and (c) neat polymer.

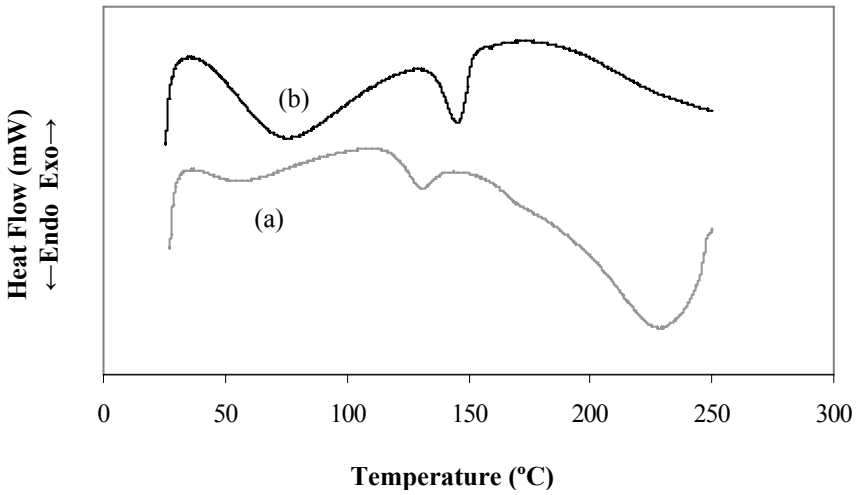

Figure 5.45**.** DSC thermograms of (a) neat polymer and (b) indomethacin loaded 4 arm PMMA-*b*-PAA.

Such high loading efficiencies may indicate strong electrostatic interactions between polymer and drug, which is expected to affect thermal stability of polymer. Eerikäinen reports interaction of an acidic anti-inflammatory drug with methacrylates emphasizing the interactions between drug and polymer in forms of hydrogen bonds and electrostatic forces (Eerikäinen et al., 2004). These interactions may increase glass transition, melting and even degradation temperatures of the original polymer increasing thermal stability of the polymer.

An interaction has been observed with DSC thermograms of our neat and drug loaded 4 arm PMMA-*b*-PAA samples given in Figure 5.45. Afterwards loading, T_g of 4 arm PMMA-*b*-PAA increased from 55 ºC to 75ºC and T_m of PMMA core increased from 130ºC to 145ºC which designates a strong interaction between hydrophobic PMMA core and indomethacin. The third peak at 228ºC observed at neat polymers DSC thermogram belongs to PAA which was expected to melt above 200ºC. Hence T_m of PAA was also improved through loading for the onset of melting could not be observed until 250ºC.

After approval of dialysis method as the most efficient drug loading method, the same procedure was repeated with anticancer drug 5 Fluorouracyl (5FU). But loading efficiency was very poor (less than 1 %) with both 4 arm and 6 arm PMMA-*b*-PAA samples having hydrophobic core ratios changing from 0.10 to 0.25. That may have arose from smaller molecular weight, or weaker electrostatic interactions related to chemical structure of 5FU shown in Figure 5.46. It was obvious that loading conditions had to be optimized for acceptable loading contents in terms of duration, temperature and composition of loading medium.

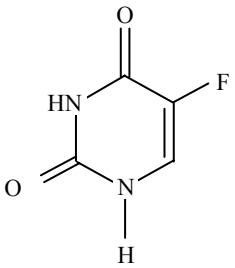

Figure 5.46. Chemical structure of 5 Fluorouracil or 5 Fluoro-2,4-pyrimidinedione.

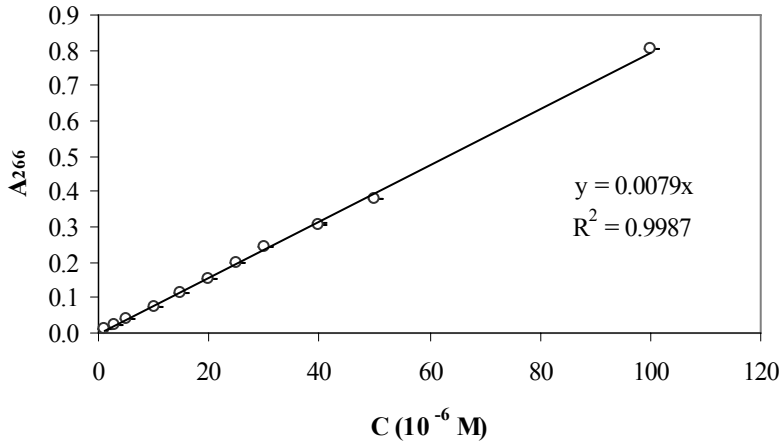

Figure 5.47. Calibration curve of 5FU dissolved in PBS (n=3).

$$C_{5FU}\,(mg/ml) = 0.0165 \times A_{266} \qquad (5.5)$$

Calibration curve and equation used for determination of drug concentration in dialysis medium are given by Figure 5.47 and Equation 5.5. Drug loading contents of loaded polymer samples have been determined from analysis of dialysis media and subtraction of removed amount of drug from initial quantity introduced.

5.5.2 Determination of Optimum Duration of 5FU Loading

Loading interval is an important parameter that has to be optimized considering other conditions such as mixing rate, temperature and composition of loading medium. For monitoring loading efficiency versus time a 6 arm PMMA-*b*-PAA (MW:5700/34000 Da, HCR:0.17) sample was used. In order to determine interval of loading to reach equilibrium, equal quantities of drug and polymer solutions were mixed in distilled water with a concentration of 500 mg/L at room temperature. In certain time intervals a sample of specific volume was taken from solution, dialyzed against water and freeze dried. After weighing dry samples, drug content was determined by UV-spectroscopy. Drug loading contents versus sampling intervals were tabulated in Table 5.9.

Table 5.9. Drug Loading Content (DLC, %) with changing loading time for 5FU loaded 6 arm PMMA-*b*-PAA (MW:5700/34000 Da) at 25°C and 500 mg/L polymer concentration. Loading medium is distilled water.

Time of Loading (min)	**Weight Released (mg)**	**Loaded Weight (mg)**	**Sample Weight (mg)**	**DLC (%)**
5	2.2511	0.2489	2.6	9.96
10	2.2682	0.2318	2.8	9.26
20	2.3032	0.1968	3.1	7.87
30	2.200	0.3000	1.9	12.00
40	2.2483	0.2517	1.9	10.07
50	2.2302	0.2698	2.6	10.79
60	2.1717	0.3283	2.4	13.13
80	2.1258	0.3742	2.7	14.97
105	2.1554	0.3446	2.9	13.78
120	2.0241	0.4759	3.0	19.04
150	2.1158	0.3842	3.0	15.37
185	2.1460	0.354	2.4	14.16
220	2.1300	0.3700	1.4	14.8
260	2.1955	0.3045	2.8	12.8
300	2.0987	0.4013	2.6	16.05
360	1.8561	0.3439	1.9	17.5
TOTAL	34.93	5.07	40.00	12.7

Variation of drug loading contents versus time of loading in distilled water at 25°C is shown in Figure 5.48, too. It can be suggested that loading performance reaches its maximum efficiency in 120 minutes and remains about the equilibrium value. Therefore further investigations to optimize loading conditions were performed with 4 hours of loading intervals at room temperatures.

The samples taken from polymer and drug solution prepared for the experiment to determine optimum loading interval were purified from excess drug by dialysis as mentioned before. Amount of excess drug was determined from UV-absorbance of dialysis media that has been refreshed every one hour until all excess drug was removed from samples. In order to optimize interval of dialysis for removal of excess drug, 5FU concentration of portions of dialysis medium were monitored. Figure 5.49 displays instantaneous amounts of drug removed by dialysis and measured every hour and total amount of drug released from polymer sample loaded for 120 minutes at 25°C and 500 mg/L polymer concentration. It was estimated that at least 10 hours of dialysis was required to remove excess drug completely from loaded particles.

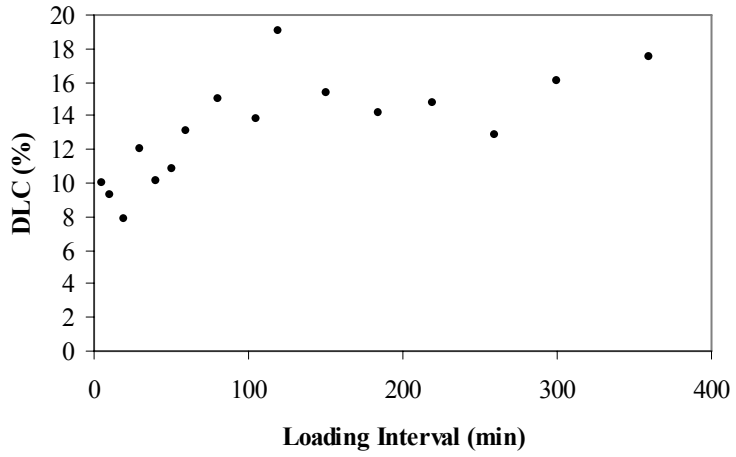

Figure 5.48. Variation of DLC versus time of 5FU loading for 6 arm PMMA-*b*-PAA (MW:5700/34000 Da) at 25°C and 500 mg/L polymer concentration.

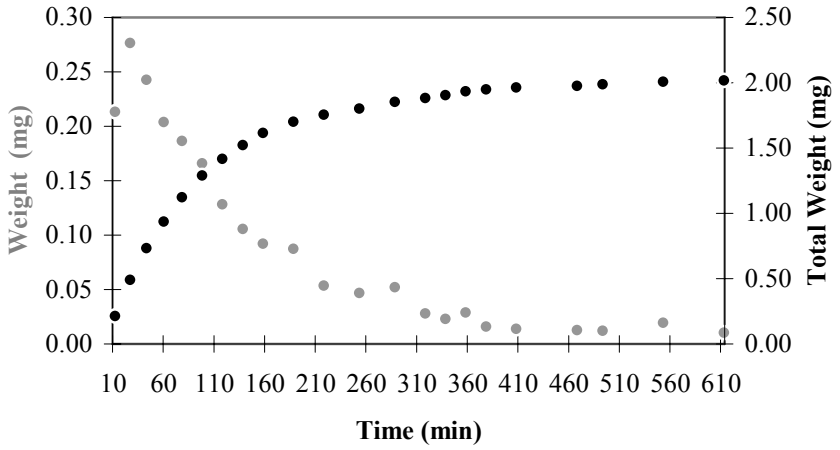

Figure 5.49. Instantaneous amounts of drug released within each 1 hour interval of dialysis (•) and total (cumulative) amount of drug removed within corresponding time interval of dialysis (•).

5.5.3 Selection of Ideal Medium for 5FU Loading

For an efficient loading both polymer and drug has to be completely dissolved prior to mixing. Polymer samples were dissolved in ethanol and drug samples were dissolved in dimethyl formamide, which was a perfect solvent both for indomethacin and 5FU, for all loading experiments reported up to now. To select the ideal composition of loading medium, polymer samples were again dissolved in ethanol and drug samples were dissolved in the solvent investigated, at least for the experiments carried at 25°C. Solvents that were used as loading medium for the comparison of their performances in terms of drug loading content were water, ethanol, 1% acetic acid, dimethyl sulfoxide and dimethyl formamide. Initial polymer and drug concentrations were 5000 mg/L. The results are tabulated in Table 5.10 stating that 1%acetic acid and dimethyl formamide are the best loading media for 5FU loading to PMMA-*b*-PAA copolymers. Yield of loading is very low in ethanol and water since 5FU is slightly soluble in water and almost insoluble in ethanol.

Table 5.10. Loading performance of 6 arm PMMA-*b*-PAA (MW: 5700/34000) at various loading conditions.

Drug/Polymer/Solvent (mg/mg/ml)	Temperature (ºC)	Time (h)	Medium (Solvent)	DLC (%)
10/10/2	25	4	Water	3.6
10/10/2	25	4	Ethanol	<1
10/10/2	25	4	1% Acetic acid	8.0
10/10/2	25	4	DMSO	4.7
10/10/2	25	4	DMF	7.3
10/10/2	15	4	Water	16.9
10/10/2	15	4	Ethanol	14.0
10/10/2	15	4	1% Acetic acid	17.5
10/10/2	15	4	DMSO	16.4
10/10/2	15	4	DMF	16.4
10/10/2	4	16	Water	20.0
10/10/2	4	16	Ethanol	10.1
10/10/2	4	16	1% Acetic acid	7.5
10/10/2	4	16	DMF	17.2

The experiment was repeated at 15°C and 4°C, too. Loading interval was kept 4 hours for 15°C and 16 hours for 4°C. Equilibrium was reached at shorter intervals (between 4 and 12 hours depending on polymer concentration) at 4°C. Since stability of

polymer is permanent at that temperature loading intervals were preferred to be kept elongated.

For the loading experiments performed at 15°C and 4°C, drug was dissolved in little amount of DMF for loading experiments performed in water and ethanol. Otherwise loading performance would be minute due to poor dissolution of drug in water or ethanol. It was observed that failure of loading in water and ethanol was really related to dissolution performance of drug since drug loading contents in various media were comparable when drug was dissolved in appropriate solvent.

But incorporation of dimethylformamide is not desired for biomaterials designed to be used for medical purposes. Hence, optimum drug loading medium was selected as 1% acid solution which could also be used for dissolution of drug. Optimum loading temperature was obviously 15°C.

5.5.4 Determination of Optimum Polymer Concentration for Loading

Determination of optimum polymer concentration was achieved among three concentrations which were 500 mg/L, 2000mg/L and 3500 mg/L. Both drug and polymer sample was introduced into loading medium at the same quantities. In this condition the drug was in excess amount, exceeding the required amount at a great extent. However introduction of equal amounts of drug and polymer simplifies evaluation of results since drug loading contents and drug loading efficiencies shall be identical. Reducing initial amount of drug introduced into loading medium would certainly increase drug loading efficiency and has to be optimized separately to prevent reduction of drug loading contents.

An amphiphilic PMMA-*b*-PAA copolymer with 4 arms, hydrophobic core ratio of 0.25 and molecular weight about 20000 Da has already been anticipated as an ideal drug carrier for hydrophobic drugs considering the comparison of multiarm PMMA-*b*-PAA samples in terms of maximum loading capacity and CMC. Therefore a polymer sample, namely 4 arm PMMA-*b*-PAA (MW:4900/18000 HCR:0.27) has been synthesized to determine optimum drug loading conditions. Reaction conditions and conversions of three stage synthesis of the polymer sample is given by Table 5.11.

Table 5.11. Reaction conditions and conversions of synthesis and hydrolysis reactions of 4 arm PMMA-*b*-PAA (MW 4900/18000).

	4 arm PMMA-Br	**4 arm PMMA-*b*-PtBA**	**4- arm PMMA-*b*-PAA**
Initiator (I)	Pentaerythritol tetrakis (2-Bromoisobutyrate)	4 arm PMMA-Br (MW 4900 Da)	Reactants: Trifluoro acetic acid + 4 arm PMMA-*b*-PtBA
Mo/I	1000	2300	-
Solvent	Anisole (1:1 V_m/V_s)*	Anisole (1:1 V_m/V_s)*	Dichloromethane
Catalyst	CuCl (4×I)	CuBr (4.4×I)	-
Ligand	PMDETA (4.4×I)	PMDETA (40×I)	-
Reaction temperature	70ºC	90ºC	25ºC
Reaction time	12 min	4.5 hours	24 hours
MW experimental	4900 Da (PI: 1.135)	18000 Da (PI: 1.104)	-
Molar Conversion %	3.8 %	11.2 %	29.6 %
Weight of product	0.43 gr	0.8 gr	0.3 gr

*Volumetric solvent/ monomer ratio.

Previously optimized loading conditions were 4 hours of loading at 15°C for dialysis method. Polymer samples were dissolved in small amounts of ethanol and drug samples were dissolved in 1% HCl to provide dissolution of drug in acidic conditions instead of toxic solvents. Hydrochloric acid was preferred for it is commonly used for drug dissolution in pharmacology. Loading experiments were performed with two replicates and drug loading contents were as given in Table 5.12. Concentration of polymer is observed to be effective on drug loading content, but further increase in polymer concentration after 2000 mg/L does not increase loading capacity significantly.

Table 5.12. Effect of polymer concentration on drug loading performed at 15 °C, 4 hours.

Polymer Conc. (mg/L)	**Mass of Polymer (mg)**	**Volume (ml)**	**pH**	**Drug Loading Content (%)**	
500	20.0	40.0	1.968	6.4	11.3
2000	20.0	10.0	1.431	13.6	20.6
3500	20.0	3.0	1.213	14.8	20.7

Polymer samples loaded at 2000 and 3500 mg/L polymer concentrations were also loaded in acidic media since the drug was dissolved in 1% HCl. Loading medium of 2000 mg/L polymer concentration was loaded in 0.15% HCl and 3500 mg/L polymer concentration was loaded in 0.15% HCl (corresponding pH values were given in Table 5.12).

4 arm PMMA-*b*-PAA samples loaded at different polymer concentrations at 15°C and for 4 hours were analysed by FTIR to observe any change in chemical structure due to drug loading. FTIR spectra shown in Figure 5.50 display that characteristic peaks of 5FU (at 1726 and 1656 cm^{-1}) (Gao et al., 2007) do not appear significantly in loaded samples. That was expected since drug is proposed to be entrapped in the hydrophobic core. But a change in structure of COO^- appeared due to chemical shift from symmetric to asymmetric bonds of C=O through loading (Ishizu et al, 2005). Specific bands of symmetric and asymmetric C=O bonds of carboxyl groups appear at wavenumbers of 1460 and 1570 cm^{-1}, respectively. Ratio of asymmetric bond that appear through interaction of carboxyl group with the acidic drug 5FU to symmetric bond of C=O (A_{1570}/A_{1460}) is assumed a measure of loading. A_{1570}/A_{1460} ratios listed in Table 5.13. shows that most efficient loading was performed in dimethyl formamide. But loading in 1% acetic acid solution was comparable.

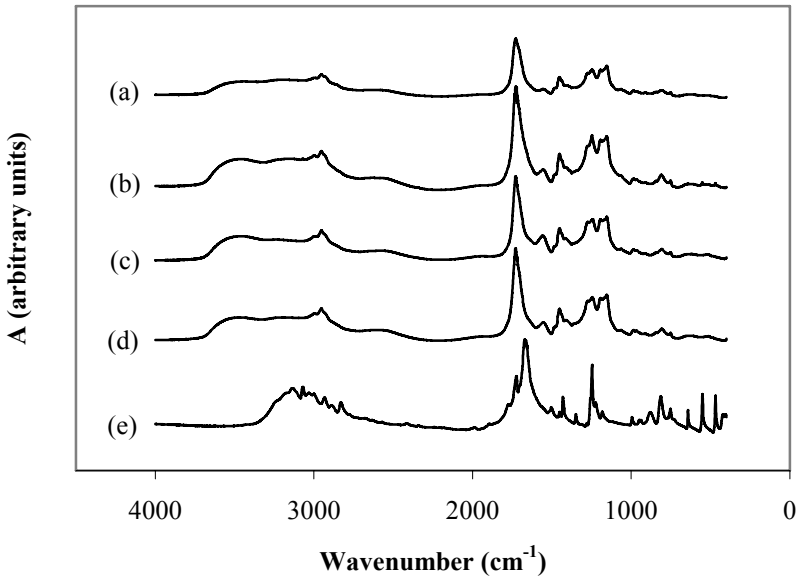

Figure 5.50. FTIR spectra of 4 arm PMMA-*b*-PAA (a) unloaded, (b) loaded at 500 mg/L polymer concentration, (c) loaded at 2000 mg/L polymer concentration, (d) loaded at 3500 mg/L polymer concentration for 4 h at 15°C and (e) FTIR spectrum of 5FU.

Table 5.13. Ratio of asymmetric(A_{1570})/symmetric(A_{1460}) bonds of C=O of carboxyl groups of acrylic acid chains due to loading conditions of 4 arm PMMA-*b*-PAA (MW:4900/18000).

Loading Conditions	Loading Medium*	Polymer Concentration	A_{1460}	A_{1570}	A_{1570}/A_{1460}
Unloaded	-	-	0.494224	0.26019	0.526462
4 h, 15°C	1 % AA	5000 mg/L	0.944267	0.860732	0.911535
4 h, 15°C	DMF	5000 mg/L	0.903261	0.906998	1.004137
4 h, 15°C	0.5 % HCl	3500 mg/L	1.192225	0.9119	0.764872
4 h, 15°C	0.15% HCl	2000 mg/L	1.120375	1.034097	0.922992
16 h, 4°C	0.15% HCl	2000 mg/L	1.410556	1.279316	0.906959
4 h, 15°C	0.05% HCl	500 mg/L	1.320948	1.025745	0.776522

*AA: Acetic Acid, DMF: Dimethyl Formamide, HCl: Hydrochloric Acid.

According to magnitude of change in chemical structure of carboxyl groups of acrylic acid (A_{1570}/A_{1460} ratios), 2000 mg/L seems to be the ideal polymer concentration for 5FU loading into 4 arm PMMA-*b*-PAA samples with molecular weight around 20000 Da and a hydrophobic core ratio of 0.25.

Differential scanning calorimeter thermograms of unloaded and loaded samples were also compared (Figure 5.51). Thermograms show that due to interaction with 5FU degradation temperature of 4 arm PMMA-*b*-PAA depicts a shift about 30°C. Endothermic peaks of unloaded and loaded polymer samples are listed in Table 5.14.

Table 5.14. Endothermic peaks observed on DSC thermograms of the model drug, unloaded and 5-FU loaded polymer samples at 15°C for 4 hours in aqueous medium.

Sample	Peak 1	Peak 2	Peak 3	Peak 4
Polymer Unloaded	75	215	367	-
Polymer loaded at 500 mg/L	74	227	388	444
Polymer loaded at 2000 mg/L	76	225	396	447
Polymer loaded at 3500 mg/L	74	226	396	449
Drug (5 FU)	-	288	318	-

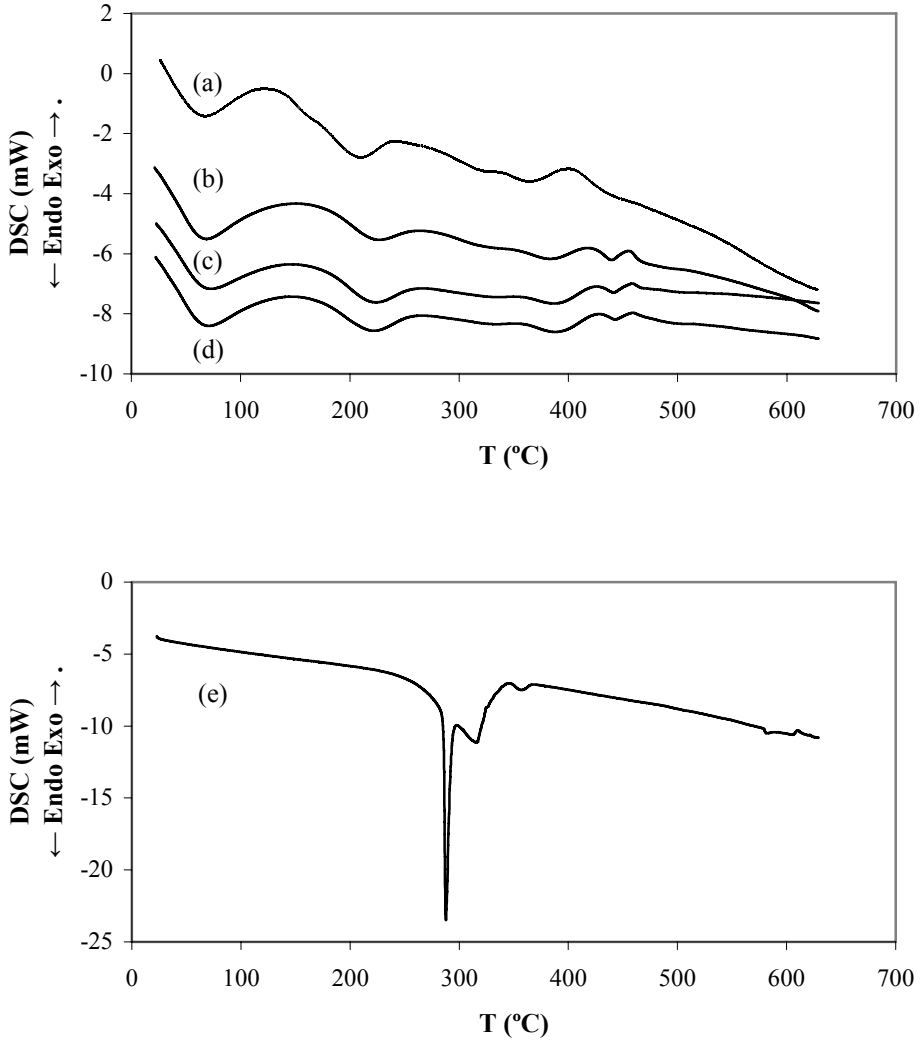

Figure 5.51. DSC thermograms of 4 arm PMMA-*b*-PAA (a) unloaded, (b) loaded at 500 mg/L polymer concentration, (c) loaded at 2000 mg/L polymer concentration, (d) loaded at 3500 mg/L polymer concentration and (e) of 5FU.

Differential Thermal Gravimetry and Thermal Gravimetric Analysis of loaded and unloaded samples are shown in Figure 5.52. In DTG thermograms of loaded samples any peak due to degradation of drug could not be detected at 288°C and 340°C. Weight fractions after degradation shows that fraction of residue after degradation of polymer increased with increasing polymer concentrations during loading. The drug shows a distinct degradation at 350°C and at 18% of initial quantity remains at 600°C. The difference in residue fractions of loaded polymer samples may have originated from degradation of varying drug contents of the samples. Although we cannot make a quantitative determination of drug contents of polymer samples from differences, it has

been obvious that loading efficiency has increased with increasing polymer and drug concentrations of loading.

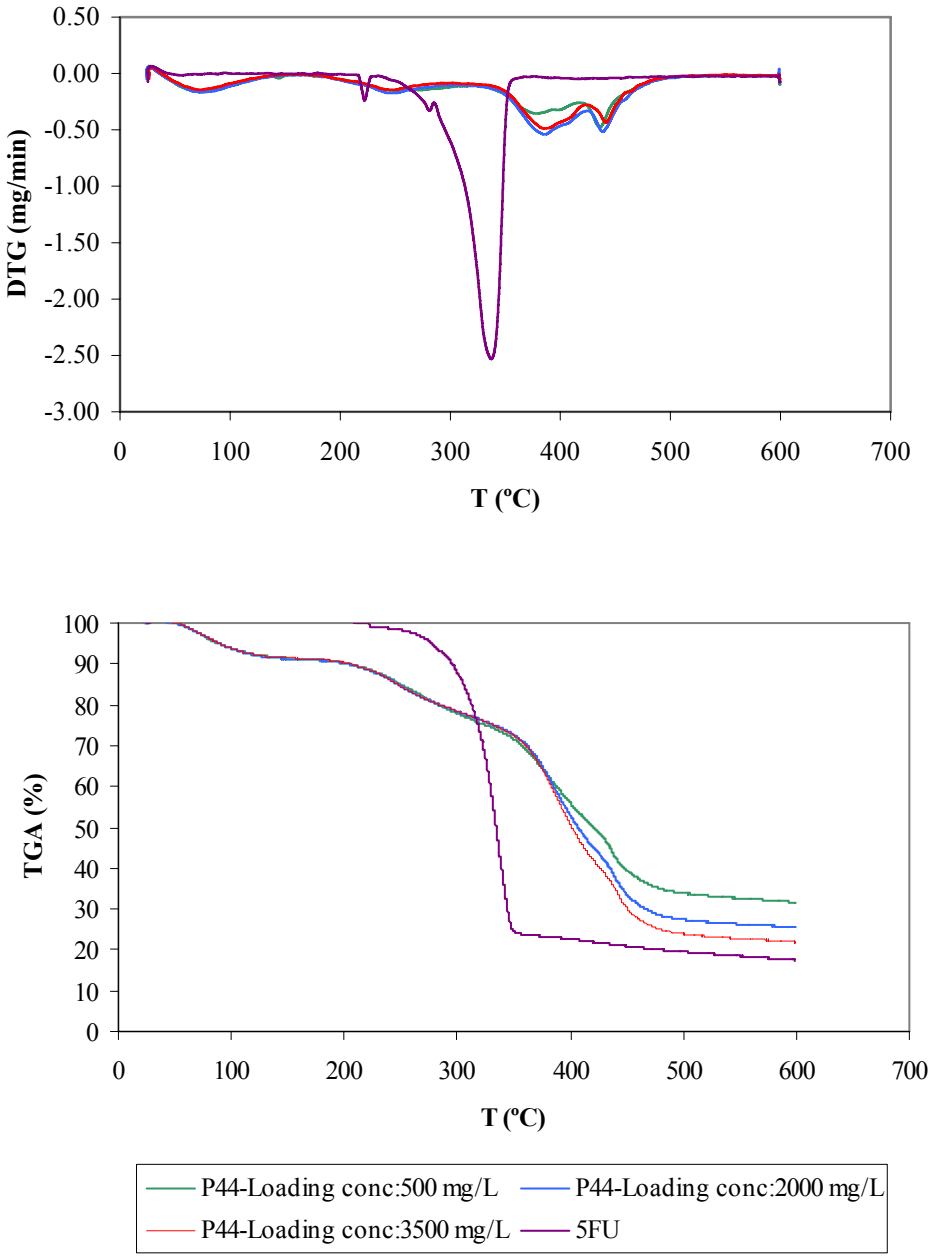

Figure 5.52. Comparison of DTG and TGA thermograms of 4 arm PMMA-*b*-PAA (MW 4900/18000) loaded at different polymer concentrations with that of model drug (5FU).

5.6. Drug Release

Prior to achievement of drug release experiments certain assumptions related to theory of drug release performed in a diffusion cell under continuous flow of fresh buffer solution, and criterion involved by determination of released amount of drug through UV-measurements has to be verified by experimental methods. The first prerequisite to determine amount of drug is zero absorbance of neat polymer which is defined with the term 'control'. UV-absorbance of receptor compartment versus time was measured as described in Chapter 4.9 for the two cases called 'control' and 'blank'. When neat polymer was placed in donor compartment for control experiment no absorbance throughout experiment was observed. Permeation of neat drug (5FU) solution put in donor compartment was also monitored to compare kinetics of drug release from loaded polymer particles with that of blank. Release profiles of both control and blank experiments are given in Figure 5.53.

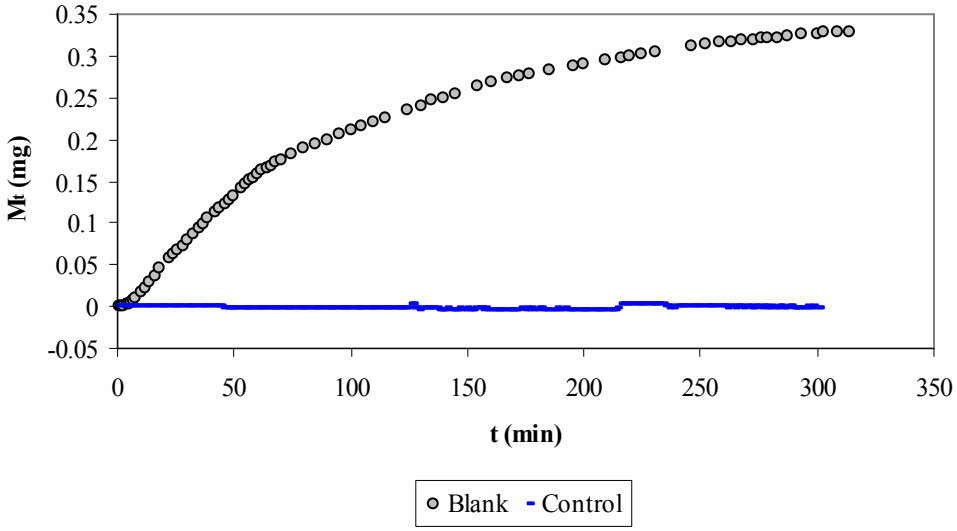

Figure 5.53. Drug release profiles of neat polymer (control) and neat drug (blank) determined by UV-spectroscopy from receptor compartment of diffusion cell.

Effect of temperature of medium on UV-absorbance of drug that permeated from donor compartment of diffusion cell to the receptor compartment through membrane that separates the two compartments was observed as in Figure 5.54. Experiments performed at 22°C and 37°C indicate that permeation increases at higher temperatures.

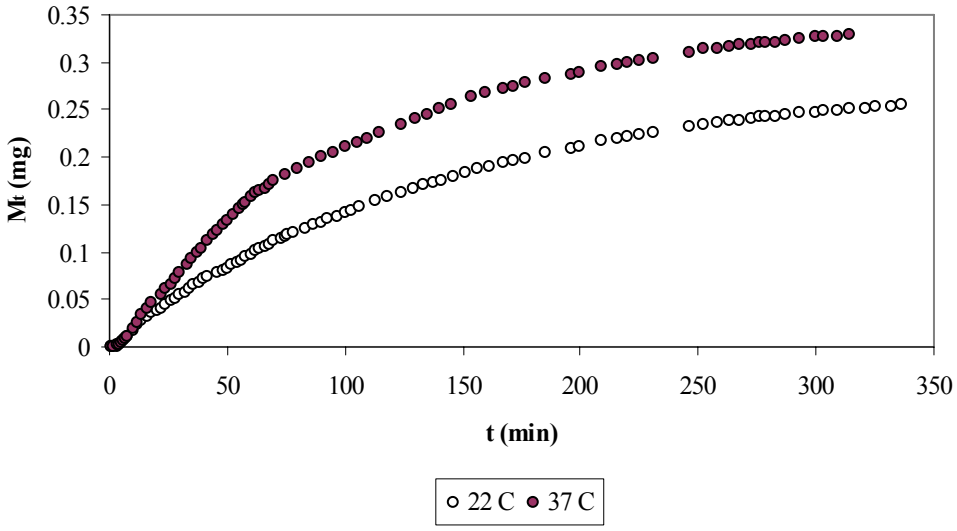

Figure 5.54. Release profiles of neat drug passed through membrane of diffusion cell at different medium temperatures.

Measurements of UV-absorbance were performed with 1 ml/min flowrate of fresh PBS passing through receptor compartment of diffusion cell for all experiments performed to validate assumptions employed to describe mass transfer system. It was the maximum flowrate at which amount of release could be detected. At higher flowrates concentration of drug was too low to be detected by UV-spectrometry.

One last parameter that could have an effect on mass transfer rate was rate of mixing in donor and receptor compartments. Theoretical model proposed in Chapter 3 assumes homogeneous drug concentrations in both donor and receptor compartments which require continuous mixing. Same model assumes that mass transfer through membrane depends on concentration difference only. Effect of mixing in compartments of diffusion cell were observed by employing no mixing, mixing in donor compartment only and mixing in both compartments when a known amount of neat drug was placed in donor compartment and PBS passed through receptor compartment at 1 ml/min flowrate. Amount of drug permeated through membrane was monitored for each condition as shown in Figure 5.55. The three profiles did not exhibit significant variations especially within the initial interval of experiment which confirms that the only driving force is concentration difference at the two sides of membrane. However, when donor compartment was not mixed, permeation profile was more linear since the drug solubility was poor. Probably drug precipitated at the upper side of membrane providing an approximately constant flux.

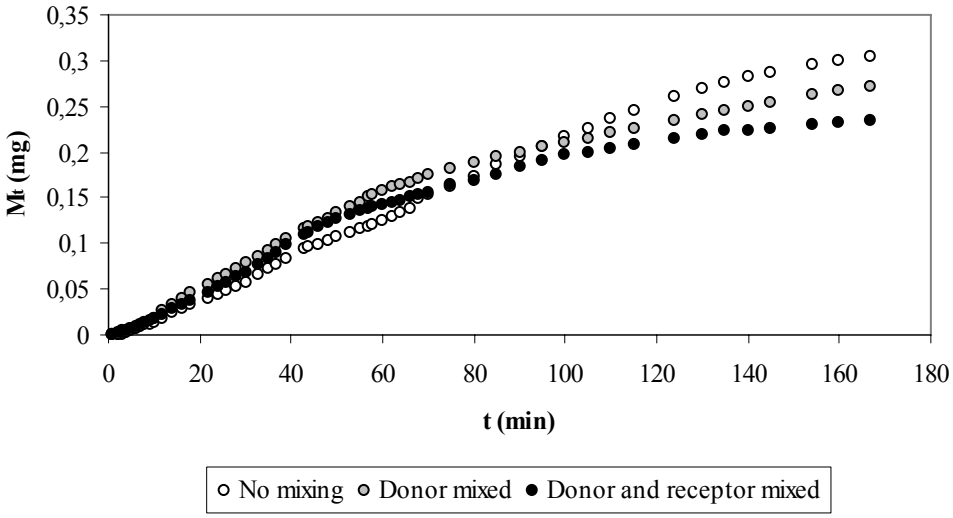

Figure 5.55. Effect of mixing in donor and receptor compartments of diffusion cell.

Permeation profiles in cases of mixing exhibited similar mass transfer behavior; until 40% of the total drug placed in donor compartment permeated through membrane, profile was linear with a constant mass transfer coefficient. Then, depending on the decrease in drug concentration in donor compartment, mass transfer rate decreased. However, since mass fluxes in initial interval are identical, effect of mixing rate has no effect on mass transfer rate (dM/dt) and it is a function of concentration difference only.

The experiment indicates that mixing in donor compartment is essential since concentration difference at the two sides of membrane cannot represent average concentrations of donor and receptor compartments if there is no mixing. Homogeneity of the receptor compartment is also necessary to eliminate effect of variations in flowrate that passes through receptor compartment. Therefore, both compartments are well mixed in drug release experiments in order to provide homogeneous drug concentrations at both sides of the membrane.

Drug release experiments from 5FU loaded 4 arm PMMA-*b*-PAA were performed for the samples with the highest drug loading contents. Figure 5.56 shows release profiles of 5FU from loaded 4 arm PMMA-*b*-PAA samples at two different flowrates. Data was collected continuously at 1 min intervals for 400 hours. Cumulative amount of released drug was determined from downstream at every 1000 minutes intervals. Experimental data of experiments have been given in Appendix B.

Loading conditions of the sample can be reminded as 3500 mg/L polymer & drug concentration in 3 ml volume, being loaded for 4 hours at 15 °C and at pH=1.2.

Release of the loaded drug from particles occurred in donor compartment of the diffusion cell, then released amount was transferred to receptor compartment through semi-permeable membrane. Fresh PBS solution passed through receptor compartment of diffusion cell with 0.25 ml/min flow rate. But it was too hard to detect concentration of released drug when mass decreased. The experiment was repeated with 0.025 ml/min PBS flow rate and it was observed that results of the two experiments were consistent.

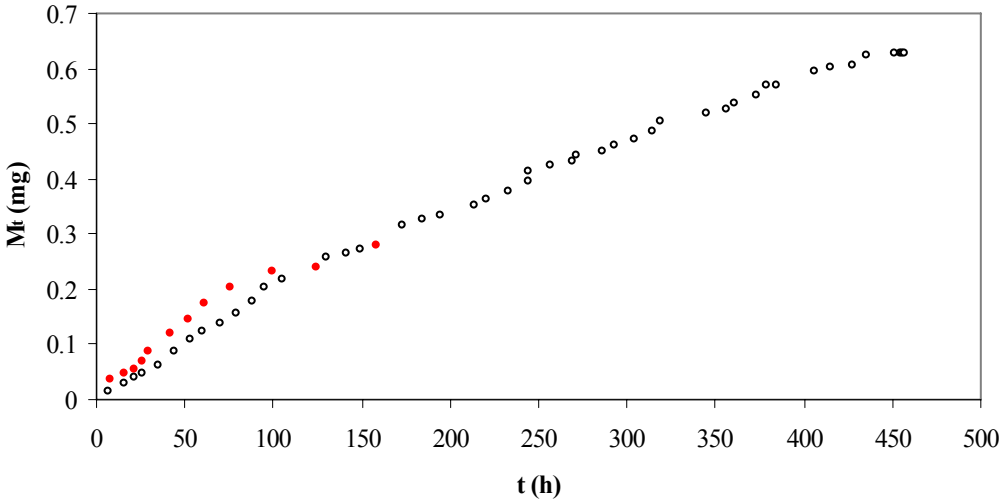

Figure 5.56. Drug release profiles of 4 arm PMMA-*b*-PAA loaded at 3500 mg/L polymer concentration at 15°C, 4 h. (a) Amount of drug released versus time; (○) series belong to the sample with DLC=13.6%, PBS flow rate=0.025 ml/min. (●) series belong to DLC=20.6%, PBS flow rate=0.25 ml/min. M_t amounts were determined from collected 15 ml portions of downstream.

Concentration of drug in receptor compartment monitored by UV-spectroscopy was used to determine amount of released drug per unit time by using Equation 5.6.

$$M_t = A_{266} \times 0.016456\ (mg/ml) \times flowrate\ (ml/min) \times t\ (min) \qquad (5.6)$$

Since flowrate of PBS solution that received released amount of drug is quite small (0.025 ml/min) calculation of released drug per minute may only be approximately representative. In order to confirm the quantities calculated from continuous release data, samples of downstream collected for 600 minute intervals (15

ml) were separately analysed by UV-spectrophotometry. The data gathered that way for the two replicates of release experiments from 5FU loaded 4 arm PMMA-*b*-PAA, loaded at a polymer concentration of 3500 mg/L, are shown in Figure 5.57.

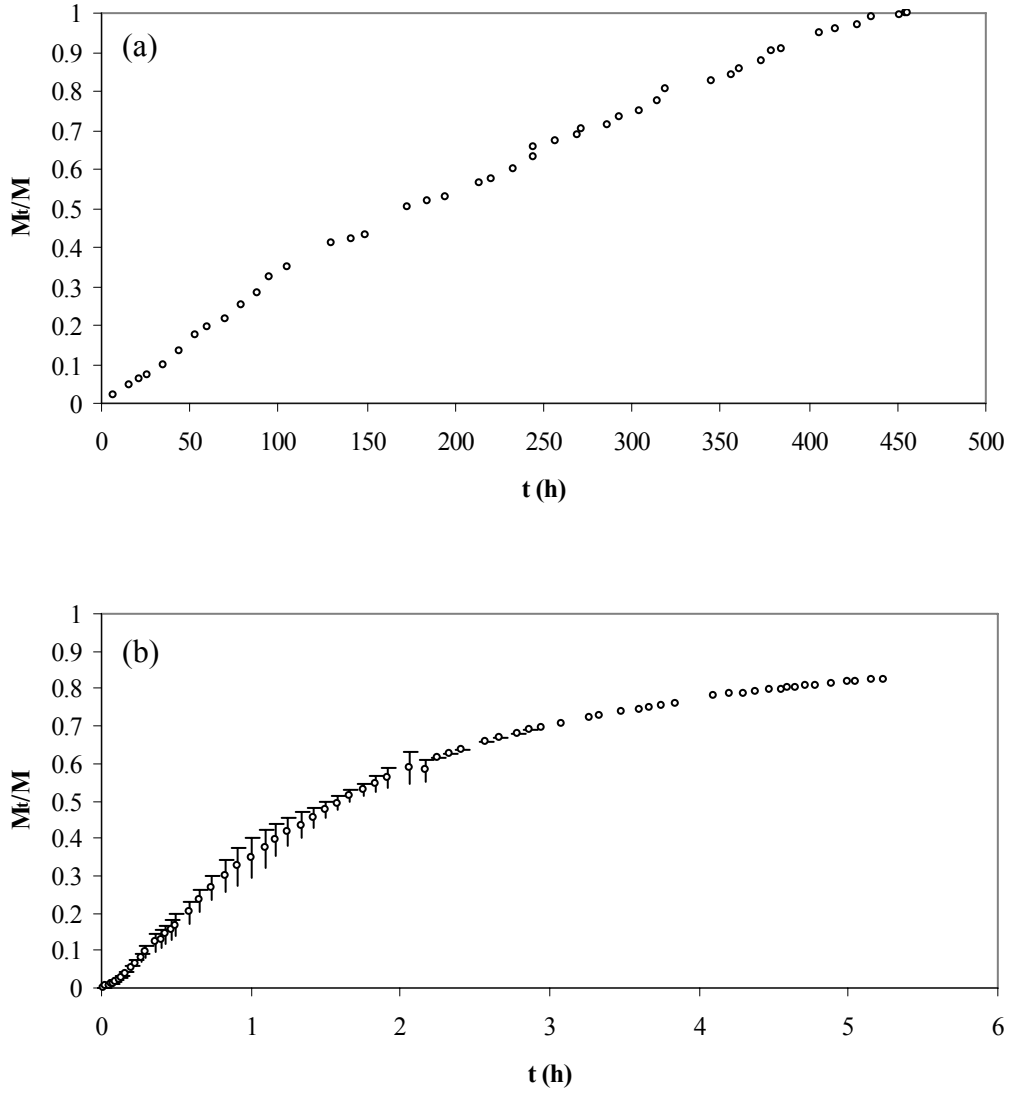

Figure 5.57. Drug release profiles of 4 arm PMMA-*b*-PAA loaded at 3500 mg/L polymer concentration at 15°C, 4 h. (a) Released fraction of drug versus time, (b) Blank experiment of 5FU permeation through membrane (n=3).

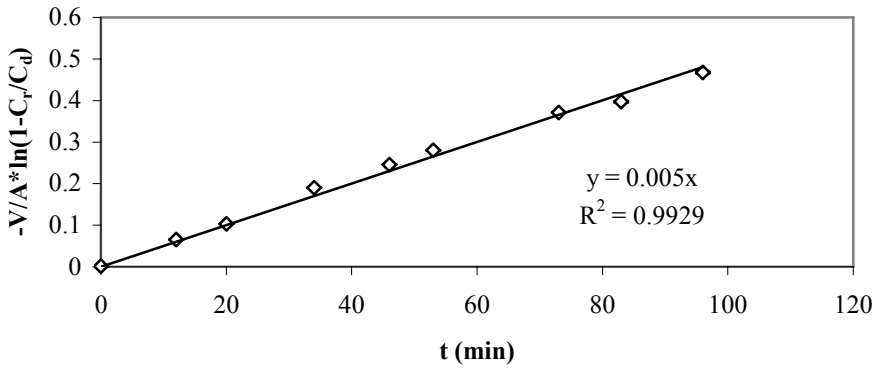

Figure 5.58. Graphical determination of 5FU permeability through membrane that separates donor and receptor compartments of diffusion cell.

Permeability is calculated as P=0.005 from experimental data obtained by keeping drug concentration constant at donor compartment. Initial 5FU concentration introduced to donor compartment was 10 mg/ml. The slope of linear function given in Figure 5.58 provided permeability of the semi-permeable membrane that separated the two compartments of diffusion cell as derived in Chapter 3.3 (Equation 3.36).

As long as permeability was known and it is the only mass transfer resistance that released drug confronts prior to measurement, all constants were available within the model derived in Chapter 3.2. Equation 3.30 was the general form of derived model based on assumption that drug release from particles would be expressed according to power law which can be declared by the mathematical expression kt^n. Since the volume of donor compartment is 1 ml, $C_d = kt^n$ was substituted to derive model equation which included the release rate constant (k) and power index (n) which constituted the degree of release kinetics. Eventually, the ultimate equation (Equation 3.31) had four unknowns the two (C_n and C) being integration constants as expressed in Equation 5.7:

$$M_t(t) = f(C_n, C, k, n) \tag{5.7}$$

Solution of this equation was achieved by a trial and error approach, by using Solver tool (Microsoft Office Excel, 2007) to minimize sum of square errors (SSE) calculated from errors between theoretical and experimental M_t values. Solution of equation yields a zero order release behavior from particles within the donor compartment. The only constraint for the solution was non-negativity of n. For this case

k and C_n values were estimated as $k=9.78\times10^{-4}$ and $C_n=0.217$. C is zero since initial condition claims that drug concentration in donor compartment is zero at t=0. SSE is 0.0658. General equation can then be represented as in Equation 5.8.

$$M_t(t) = \left(9.78\times10^{-4}t\right)F\times9.78\times10^{-4}\frac{F}{\kappa} + 0.217e^{-\kappa t} \tag{5.8}$$

where concentration of the donor compartment is constant and $C_d=kt^n=9.78\times10^{-4}$ mg/ml since n=0. Then mass transfer rate is to be constant throughout experiment and release process occurs at steady state.

Comparison of experimental and theoretical M_t and M_t/M values calculated from Equation 3.31 are shown on Figure 5.59. Here it can be observed that experimental data shows deviation from linearity.

Drug release systems may comply with more than one mechanisms and different release profiles at initial and proceeding stages of drug release is a very common issue. In order to decrease SSE and provide a better fit between theoretical model and experimental results, it is recommended to make a distinction between initial release profile up to where Mt/M<0.6 and late release profile where Mt/M>0.4 and analyze the two regions separately. The overlapping region may be explained by both mechanisms (Ho and Sirkar, 1992).

The first interval starting from t=0 up to t=130 hour covers the first stage of drug release where 40% of the drug loaded to polymer sample was released. Then Equation 3.31 was solved for each interval separately as shown in Appendix B. As a result SSE decreased to 0.016 and deviation from experimental data diminished as in Figure 5.60.

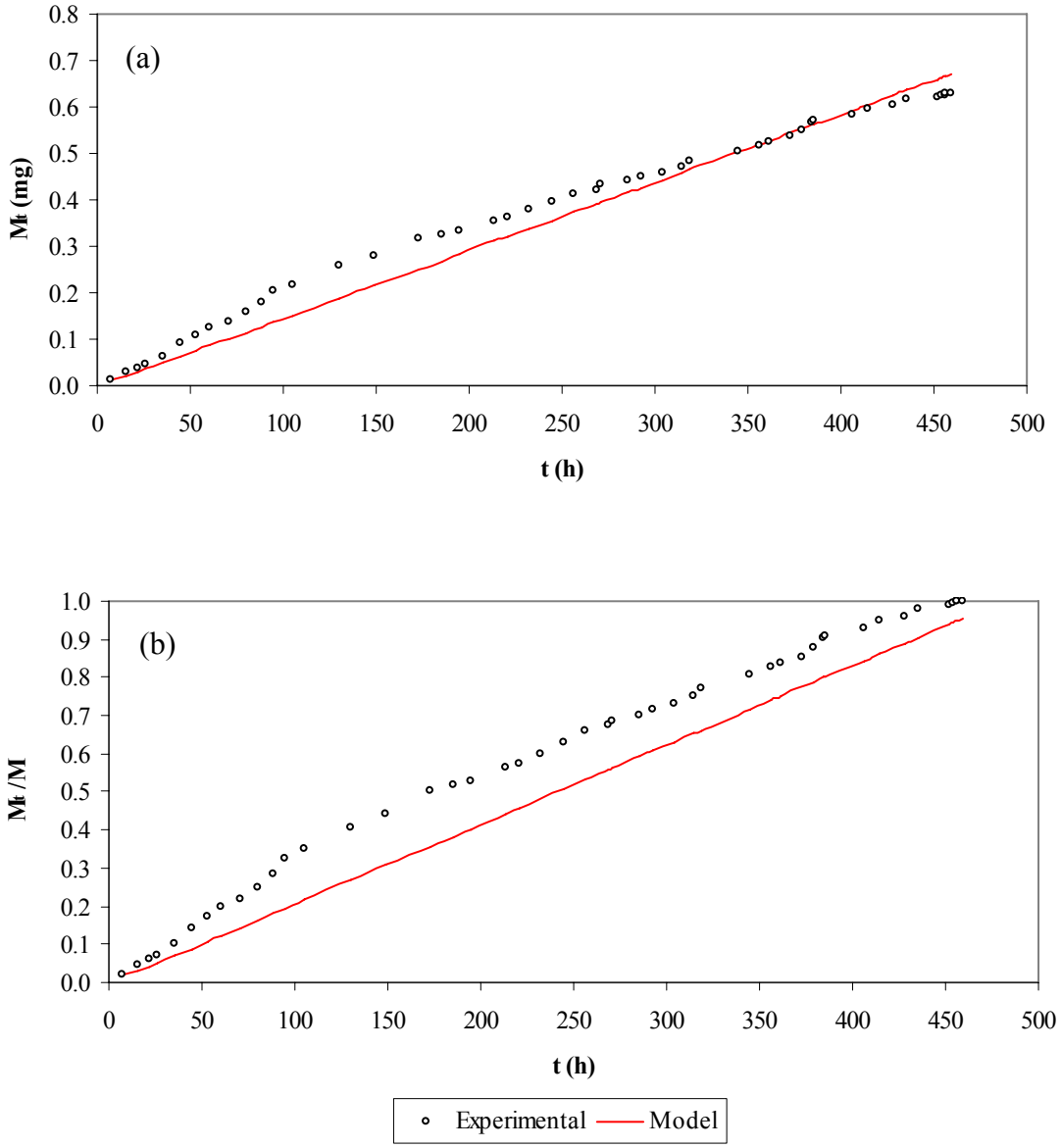

Figure 5.59. Experimental and theoretical values of (a) M_t and (b)M_t/M obtained from model that assumes $C_d=kt^n=9.78\times10^{-4}$ mg/ml, for the drug release from 4 arm PMMA-*b*-PAA nanoparticles.

Solution of equation yields an approximately zero order release behavior again. $n_1=0.0025$ that is quite close to zero is the order of release rate for the initial interval and $n_2=0$ for the rest of the release process. As release rate is a bit higher in the initial region the main difference in two intervals originate from k values which are $k_1=1.35\times10^{-3}$ and $k_2=7.59\times10^{-4}$. The constraints for the solution were non-negativity of n values and C=0 for the initial interval of drug release. For this case C_n values were estimated as $C_1=0.12$ and $C_2=-0.212$ for the two intervals. C was nonzero for the second

interval and was estimated to be C_3=0.118 as shown in Appendix B. The third, fourth and fifth terms of the alternating series that appear in Equation 3.31 were not significant although they were nonzero, therefore they were not considered for constitution of the general equation.

Equation 3.31 for the solution of equation in two separate intervals that cover the first 130 hours and the rest of release process respectively, yields the two equations given in Equations 5.8 and 5.9.

$$M_t = \frac{1.35\times10^{-3}\,t^{1.0025}}{1.0025}F - 1.35\times10^{-3}\,t^{0..0025}\,\frac{F}{\kappa} + 0.12e^{-\kappa t} \qquad \left[\frac{M_t}{M} \le 0.40\right] \tag{5.8}$$

$$M_t = 7.59\times10^{-4}\,tF - 7.59\times10^{-4}\,\frac{F}{\kappa} - 0.212e^{-\kappa t} + 1.18 \qquad \left[\frac{M_t}{M} > 0.40\right] \tag{5.9}$$

where F is volumetric flow rate of PBS stream passing through receptor compartment (0.025 ml/min), κ=AP/Vr, Vr is volume of receptor compartment (0.47 ml), A is area of membrane (0.785 cm^2) and P is permeability calculated previously (0.005 cm/min).

Concentration of donor compartment (C_d) also has two conditions given by the mathematical expressions as in Equations 5.10 and 5.11.

$$C_d \cong 1.35\times10^{-3} \quad \text{mg/ml} \qquad \left[\frac{M_t}{M} \le 0.40\right] \tag{5.10}$$

$$C_d = 7.59\times10^{-4} \quad \text{mg/ml} \qquad \left[\frac{M_t}{M} > 0.40\right] \tag{5.11}$$

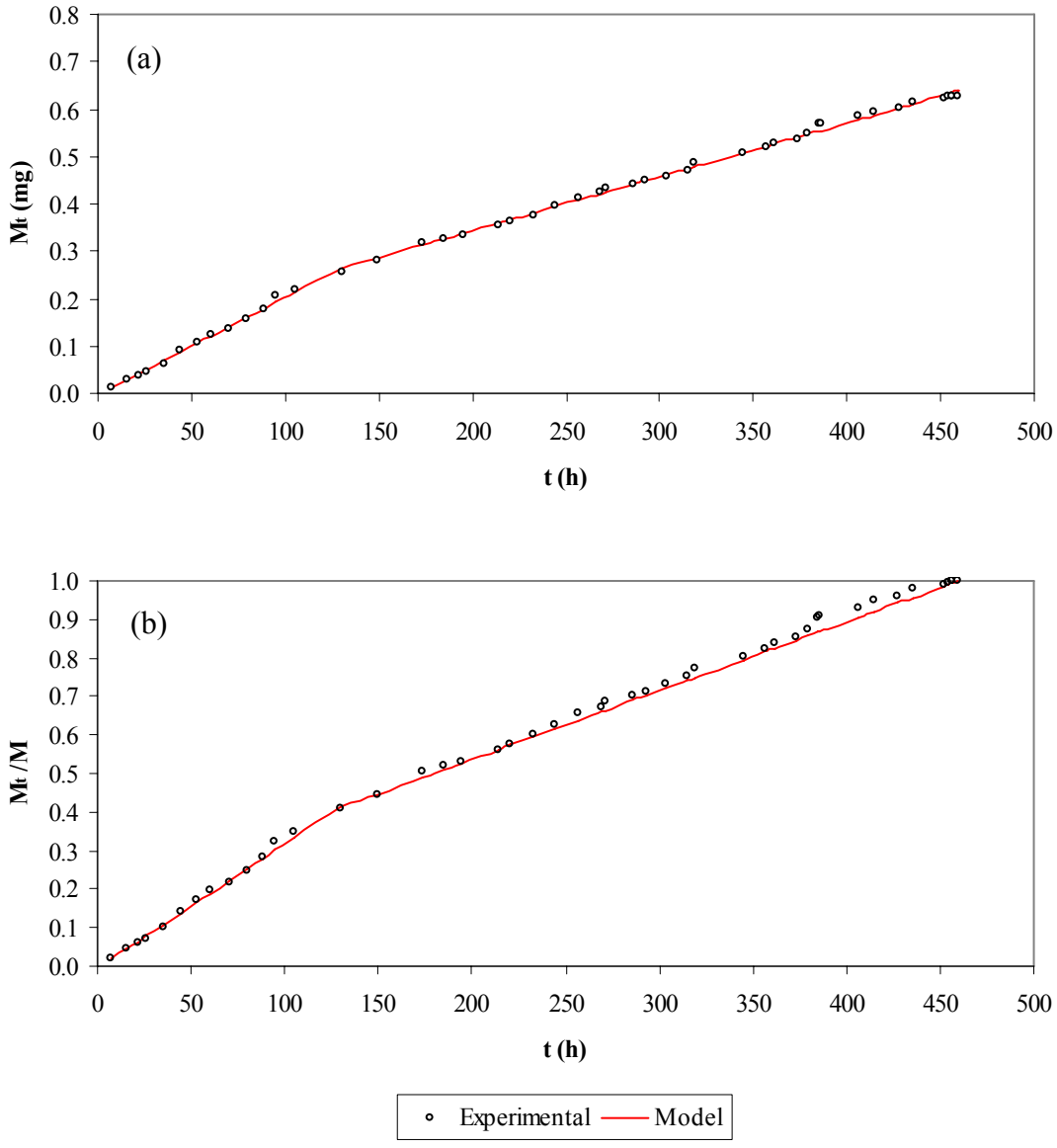

Figure 5.60. Experimental and theoretical values of (a) M_t and (b)M_t/M obtained from model that assumes $C_d=1.35\times10^{-3}$ mg/ml (for the initial interval where Mt/M<40) and $C_d=7.59\times10^{-4}$ mg/ml (for the late interval where Mt/M>40), for the drug release from 4 arm PMMA-*b*-PAA nanoparticles.

5.7 Biodegradation

Biodegradability of particles were evaluated in terms of particle sizes of degraded 4 arm PMMA-*b*-PAA samples at 37°C. For the particle size analysis with DLS polymer samples were degraded in standard PBS solution.

Polymer samples prepared by simple equilibrium method were analyzed in 1 hour to determine particle size of undegraded polymer particles. Initial particle size is about 20-30 nm as dissolved in aqueous medium at 25 ºC. Dissolved polymeric micelle samples were introduced into degradation temperature that was 37 ºC, then they start to agglomerate and reach an average particle size of 35 nm within 36 hours. Within 3 days particle size drops back to an average particle size of 25 nm, and below 10 nm in a 7 days period of degradation. Variation of particle sizes for degraded polymer samples were shown in Figure 5.61.

Volume average particles sizes shown in Figure 5.61 represent the dominant peak that constitutes more than 90% of total volume of particles. That peak also represents the smallest particle size interval. But presence of other peaks having a particle size between 50 nm and 150 nm indicate tendency of 4 arm PMMA-*b*-PAA particles to agglomerate.

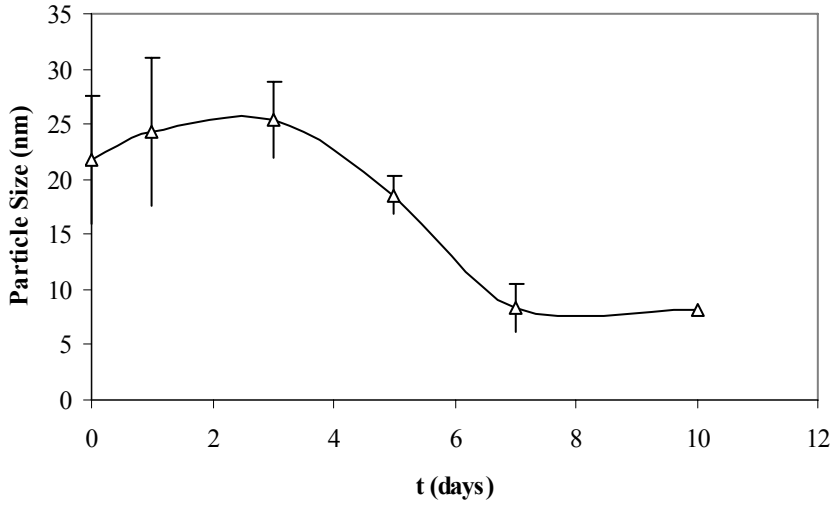

Figure 5.61. Volume average particle size analysis of 4 arm PMMA-*b*-PAA degraded in PBS solution at 37 ºC (n=3). Concentrations of polymer samples were 2 mg/ml.

The effect of polymer concentration on agglomeration and micelle forming behavior versus degradation has to be investigated. For this reason, polymer solutions at different concentrations (varying between 1-8 mg/ml) were degraded at 37°C and monitored in terms particle size.

Particle size distribution of undegraded 4 arm PMMA-*b*-PAA show that, average particle size does slightly increase with increasing polymer concentration, but average size of agglomerates which constitutes only a 10% of all particles by volume strongly depends on polymer concentration as can be observed from Figure 5.62. Then it can be declared that undegraded particles form unimolecular micelles with almost constant particle size about 20-30 nm that is virtually independent of polymer concentration. But agglomeration tendency increases drastically with increasing concentration of polymer in solution.

After three days of degradation, micelle size remains constant, and dependency of agglomerate sizes on polymer concentration is not significant. Particle size still occurs in 20-30 nm, while agglomerates at every concentration were observed to be about 100-150 nm (Figure 5.63). This case is just identical to the initial particle size distributions observed at low polymer concentrations, only volumetric ratios of agglomerates to particles are smaller. Particle size distributions of the samples determined by zetasizer have been reported in Appendix C.

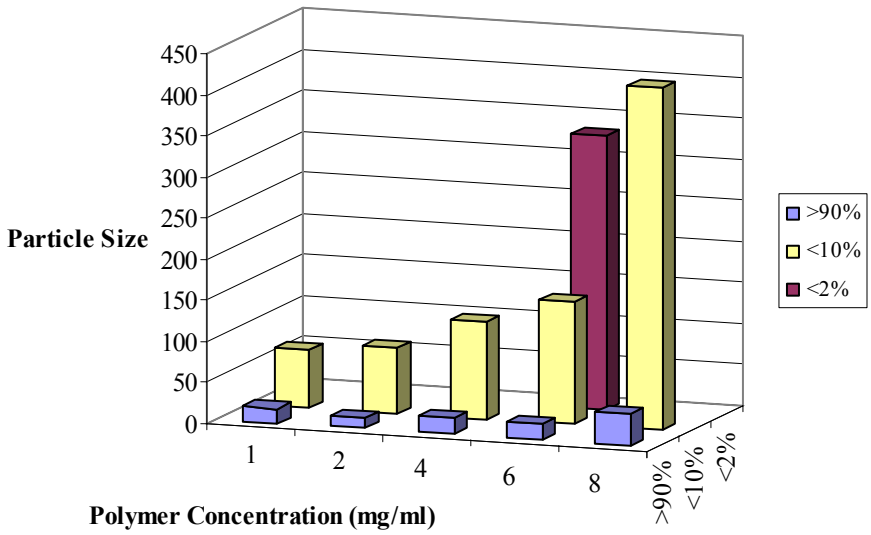

Figure 5.62. Variation of particle size with increasing polymer concentration of 4 arm PMMA-*b*-PAA nanoparticles before degradation.

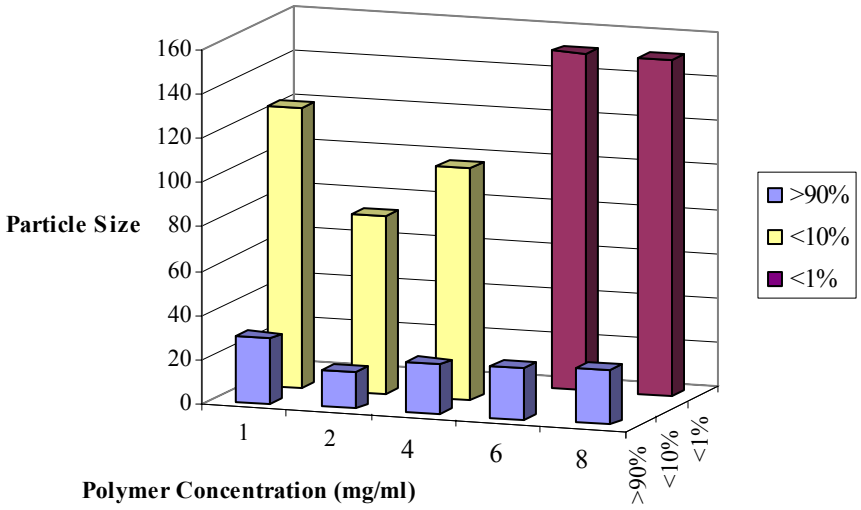

Figure 5.63. Variation of particle size with increasing polymer concentration of 4 arm PMMA-*b*-PAA nanoparticles degraded for 3 days.

At the seventh day of degradation, agglomerates were completely diminished and particle sizes were decreased down to below 10 nm as (Figure 5.64). Thereby the biodegradability of 4 arm PMMA-*b*-PAA with a PMMA core smaller than 5000 Da was substantiated. A dependency of particle size on polymer concentration still holds but the polymer solution at this point has lost all its capability to produce a micellar structure that can entrap hydrophobic molecules.

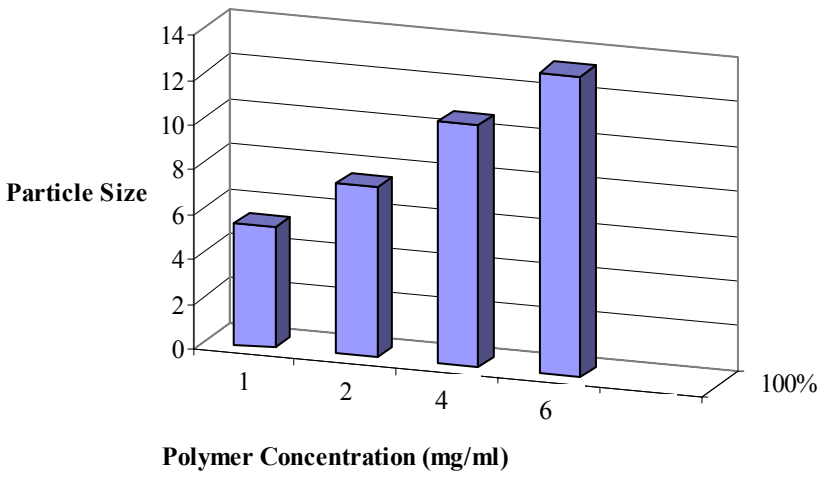

Figure 5.64. Variation of particle size with increasing polymer concentration of 4 arm PMMA-*b*-PAA nanoparticles degraded for 7 days.

5FU loaded particles in dimethyl formamide and acetic acid solution were also investigated by DLS. Hydrodynamic radius of unloaded 4 arm PMMA-b-PAA particles was 14 nm with a slight agglomeration (about 6.3 volume % agglomerates having 79 nm size) as given in Table C.2. The polymer samples loaded in dimethyl formamide (DLC=7.3%) and 1% acetic acid solution (DLC=8.0%) yielded almost the same particle size as unloaded sample, and exhibited no agglomeration. Volume average particle sizes of 4 arm PMMA-b-PAA particles were 11.3 nm (loaded in DMF) and 12.3 nm (loaded in 1% acetic acid). Detailed description of particle size distributions of the samples have been shown in Tables C.12-C.13.

All the samples that were employed for the biodegradation experiments were loaded with pyrene (as described in Chaper 4.6) after the particle size analysis to check their loading capacity. Figure 5.65 shows the capability of 4 arm PMMA-*b*-PAA as dissolved in PBS solution at various polymer concentrations. UV absorbance of pyrene loaded samples show the increasing abilities of micelle forming and entrapping capacity of polymer samples with increasing polymer concentration. It is obvserved in Figure 5.66 that biodegraded polymer samples have lost their capability to entrap and solubilize pyrene molecules.

Particle sizes were also determined by AFM images in order to confirm particle size and particle size distribution data obtained by DLS. In order to observe single particles and agglomerates, dilute solutions (such as 5×10^{-3} mg/ml) were prepared (Demir and Erman 2002). Figure 5.67 and 5.68 show how agglomeration proceeds even within 1 hour of degradation at 37°C.

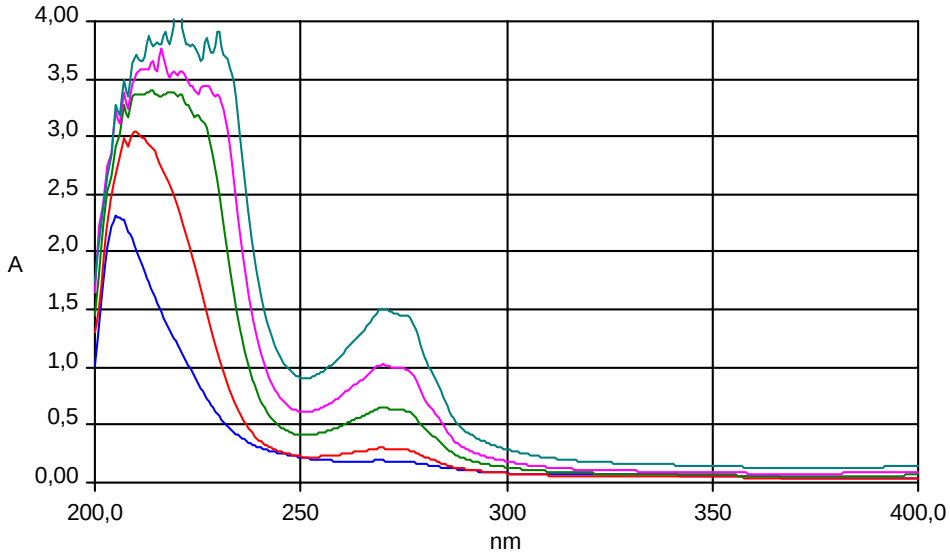

Figure 5.65. Entrapment efficiency of 4 arm PMMA-*b*-PAA in PBS solution having polymer concentrations 8,6,4,2,1 mg/ml (from top to bottom), before degradation.

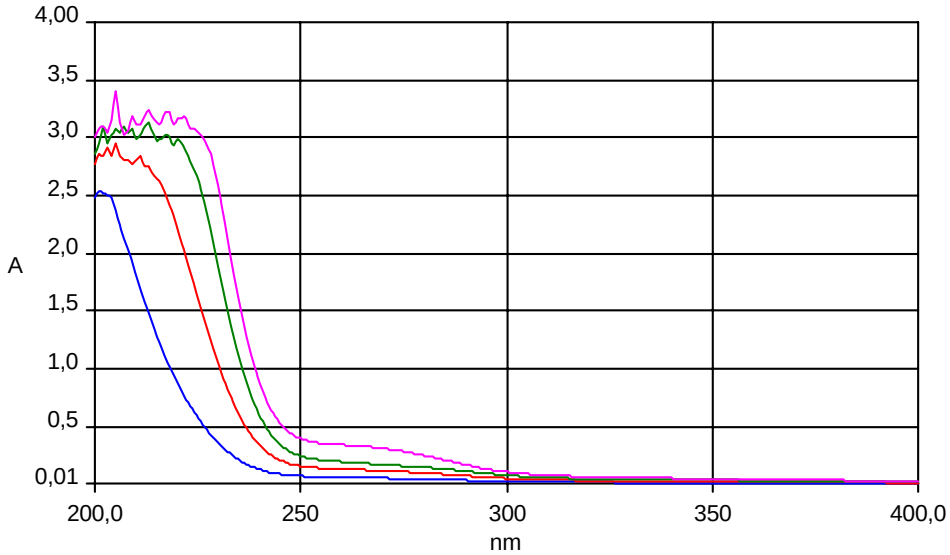

Figure 5.66. Entrapment efficiency of 4 arm PMMA-*b*-PAA in PBS solution having polymer concentrations 6,4,2,1 mg/ml (from top to bottom), after 7 days of degradation.

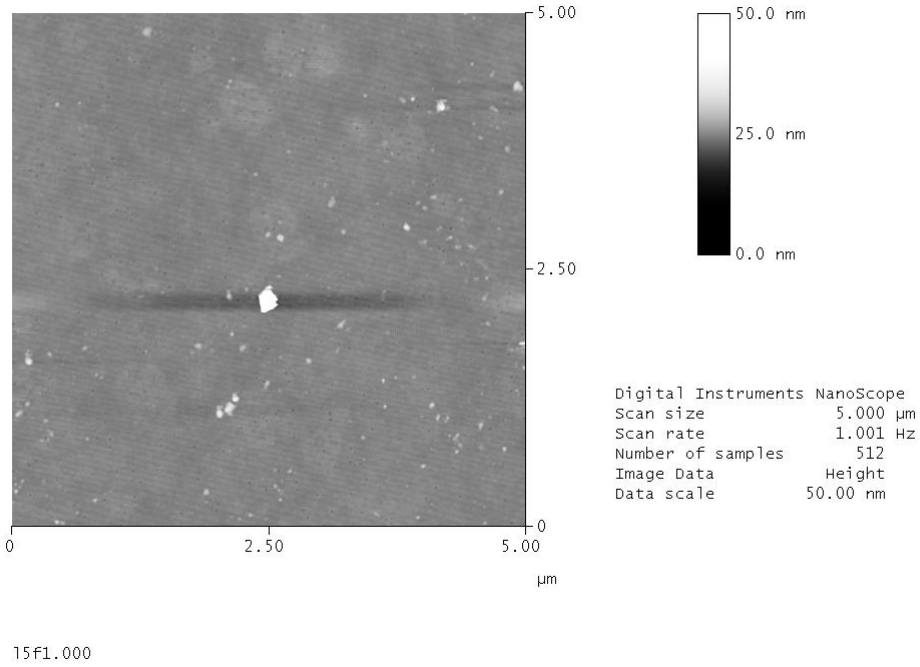

Figure 5.67. AFM micrograph of 4 arm PMMA-*b*-PAA (MW 4900/18000 Da) as dissolved in aqueous medium at 25 °C.

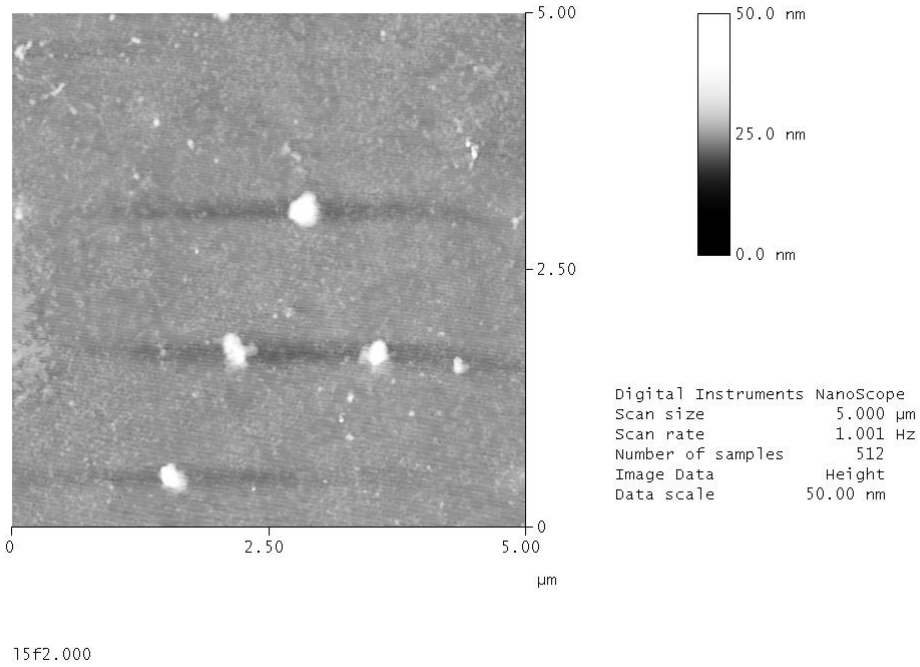

Figure 5.68. AFM micrograph of 4 arm PMMA-*b*-PAA (MW 4900/18000 Da) degraded for 1 hour in aqueous medium at 37 °C.

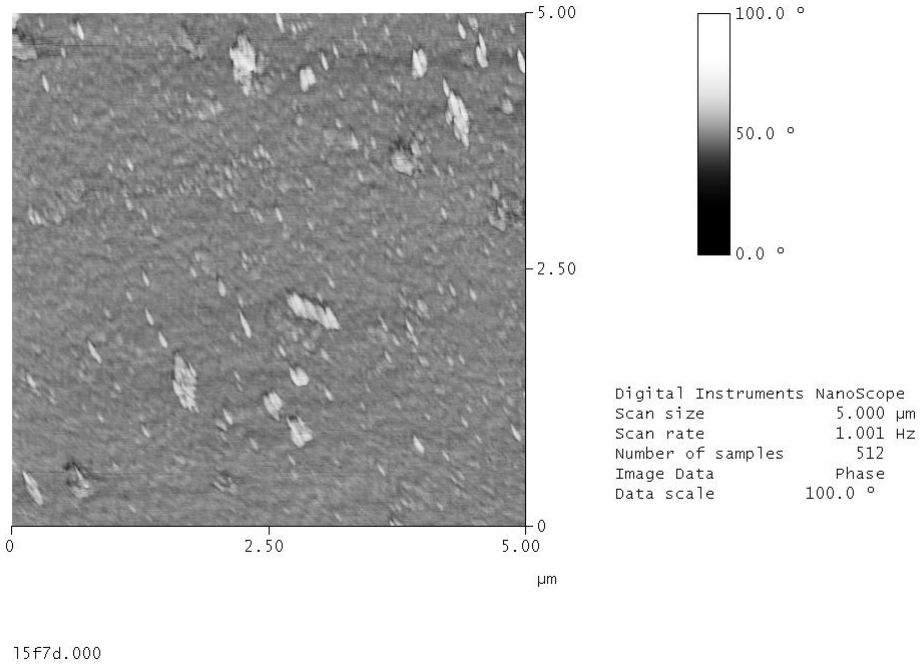

Figure 5.69. AFM micrograph of 4 arm PMMA-*b*-PAA (MW 4900/18000 Da) as degraded for 7 days in aqueous medium at 37 °C.

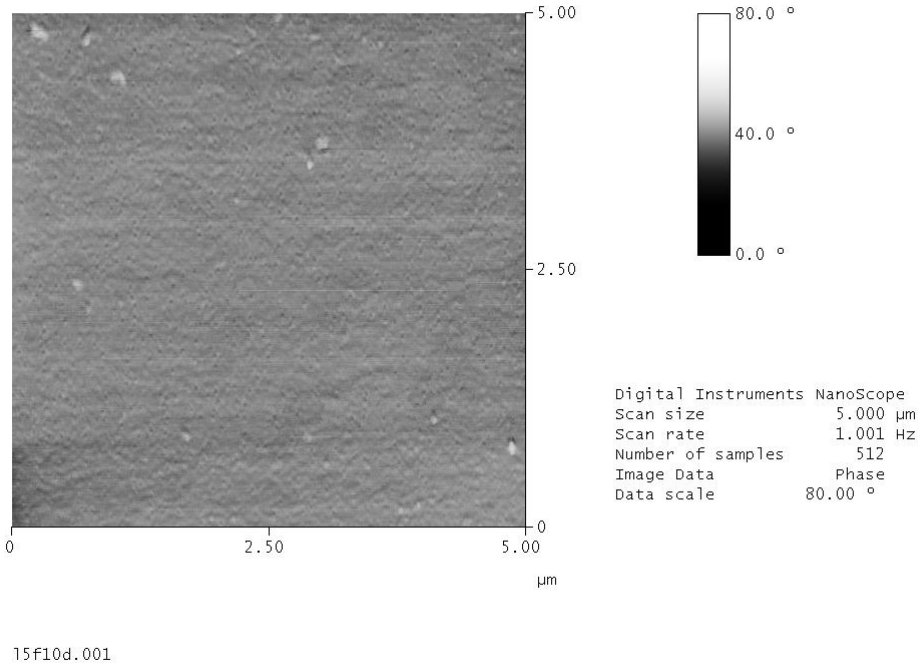

Figure 5.70. AFM micrograph of 4 arm PMMA-*b*-PAA (MW 4900/18000 Da) as degraded for 10 days in aqueous medium at 37 °C.

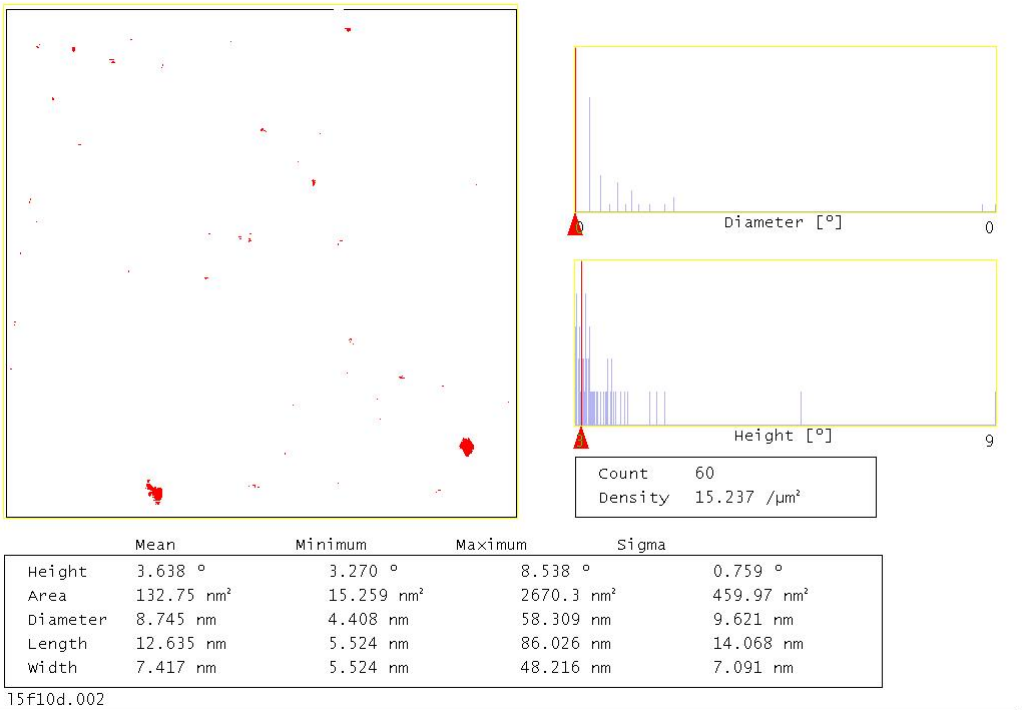

Figure 5.71. Particle analysis of 4 arm PMMA-b-PAA (MW 4900/18000 Da) as degraded for 10 days in aqueous medium at 37 °C.

Table 5.15. Particle size analysis of 4 arm PMMA-*b*-PAA (MW: 18000, f_c:0.27).

Degradation Time	Count	Average Particle Size (nm)	Minimum Particle Size (nm)	Minimum Particle Size (nm)	σ
5×5 µm^2					
As dissolved	88 158	26.0 31.1	11.0 11.0	150.3 207.3	25.4 24.3
1 hour	161 53	35.2 58.3	11.0 11.0	305.8 298.7	44.1 69.4
1 day	38	42.9	11.0	122.7	28.3
5 days	44	37.8	11.0	288.6	54.2
7 days	382	36.3	11.0	342.7	46.7
10 days	83	22.65	11.0	85.4	17.9
2×2 µm^2					
As dissolved	53 133	14.2 9.9	4.4 4.4	78.0 68.8	13.4 10.9
1 hour	55 59	12.4 17.9	4.4 4.4	64.8 197.5	12.8 29.6
1 day	55	16.13	4.4	93.1	21.0
5 days	16	19.0	4.4	107.5	26.4
7 days	107	13.12	4.4	189.2	19.8
10 days	60	8.7	4.4	58.3	9.6

Particle sizes from 5×5 μm^2 and 2×2 μm^2 scans were determined by particle analysis and are given by Table 5.15. Particle analysis of 5×5 μm^2 AFM scans can be examined in detailed from sketches and statistics given in Appendix D. In all samples exposed to particle analysis, threshold height was kept at 1±0.2 nm. σ values were given as a measure of variation of particle sizes indicating an evaluation of particle size distribution.

Agglomerates remaining at 7^{th} day of degradation can be observed in Figure 5.69. They seem like accumulated particles when compared to solid agglomerates observed previously. By the 10^{th} day of degradation, agglomerates significantly decreased both in number and particle size (Figures 5.70 & 5.71).

AFM images and particle analysis cannot yield definite results for particle size and distribution analysis since samples can never be perfectly representative. Besides agglomerates observed from micrographs might have occurred via drying process. But when AFM micrographs were compared with particle size determinations achieved by DLS, it was observed that results were comparative after all.

CHAPTER 6

CONCLUSIONS

3 arm, 4 arm and 6 arm PMMA-*b*-PAA copolymers having molecular weights between 18kDa-80kDa and hydrophobic core ratios varying from 0.1 to 0.45 were synthesized by ATRP method.

Brominated 3 arm, 4 arm and 6 arm initiators of first stage of ATRP reaction were synthesized from 1,3,5-trihydroxybenzene, pentaerythritol and dipentaerythritol with 94.5, 76.3 and 67.3% conversions. Pentaerythritol tetrakis (2-bromoisobutyrate) from pentaerythritol and dipentaerythritol hexakis (2-bromoisobutyrate) from dipentaerythritol were synthesized with 100% purity while attained purity of 1,3,5- (2-bromo-2-methyl propionate) benzene from 1,3,5-trihydroxybenzene was 82 %.

Sythesis of PMMA cores were achieved in anisole by using PMDETA as ligand and CuCl as catalyst in stoichiometric ratio. Monomer to initiator molar ratio was kept 250 for each arm. Reactions were carried at 60-70°C for 10-12 minutes to obtain PMMA-Br macroinitiators at 5000 Da molecular weights and with acceptable polydispersity indexes. Molecular weights were tried to be kept about 5000 Da for providing particle sizes of degraded polymers under 5 nm after biodegradation at 37 °C following administration into body for therapeutically purposes. This is an important requirement for biodegradable polymers to be used for drug delivery for only the particles smaller than 5 nm can be removed from circulatory system by renal route.

3 arm PMMA-*b*-PtBA synthesis from PMMA-Br macroinitiators were also carried in anisole by using PMDETA as ligand. CuBr was used as catalyst with 10% excess and monomer to initiator molar ratio varied about 500-600 for each arm. Reaction times changing from 5 hours to 20 hours determined molecular weights of PMMA-*b*-PtBA copolymers. Synthesized PMMA-*b*-PtBA copolymers were reacted into PMMA-*b*-PAA copolymers by selective hydrolysis reaction of tBA chains by trifluoroacetic acid.

Critical micelle concentrations and maximum loading capacities of polymer samples were determined by fluorescence method. Pyrene was used as a fluorescent probe and critical micelle concentration was determined by both comparing ratio of first

and third bands in emission spectra and detecting the shift in I_{336} band in excitation spectra of pyrene loaded polymer samples at different concentrations. Critical micelle concentration was observed to increase with increasing molecular weight and maximum loading capacity was observed to increase with increasing hydrophobic core ratio. Therefore an optimum PMMA-*b*-PAA copolymer was proposed to have 20000 Da molecular weight and 0.25 hydrophobic core ratio in order to provide a minimum critical micelle concentration and maximum loading capacity for hydrophobic drugs.

Drug loading method was optimized with 4 arm PMMA-*b*-PAA having 30 kDa molecular weight and 0.23 hydrophobic core ratio and indomethacin as model drug. Drug and polymer was easily loaded at high loading content (24.8%) with 1 hour of mixing at room temperature following dissolution in a strong solvent which was dimethylformamide. Removal of solvent and excess drug was achieved by dialysis. Dialysis method yielded excellent loading performance when compared to salting out and solvent deposition methods which constitute alternatives for drug loading.

Drug loading contents of synthesized PMMA-*b*-PAA samples with 4 and 6 arms were very poor when they were tried to be loaded with the anticancer drug 5 Fluorouracyl at the same conditions. Therefore determination of ideal loading conditions were required. 6 arm PMMA-*b*-PAA having molecular weight of 34 kDa with hydrophobic core PMMA of 5400 Da, and 4 arm PMMA-*b*-PAA having molecular weight of 18000 Da with hydrophobic core PMMA of 4900 Da), were used for determination of ideal drug loading conditions for 5FU loading. The polymers were characterized by FTIR to confirm they were completely hydrolyzed and contained neither monomer nor solvent residue.

Drug loading conditions were optimized as 4 hours of loading at 15°C, within aqueous medium with pH value of 1.0-1.5. Polymer samples were dissolved in minute amounts of ethanol and drug samples at equal quantities were dissolved in 1% HCl. Effect of polymer concentration on loading performance was investigated and it was observed that higher polymer concentrations yielded higher drug loading contents. Three polymer concentrations (500, 2000 and 3500 mg/L) yielded 8.8 %, 17.7% and 17.1% drug contents (average drug contents of two replicates), respectively. In FTIR spectra of loaded polymer samples, asymmetric stretching of COO^- bands appeared due to interaction of carboxyl groups of the polymer with 5FU. In DSC and DTG thermograms specific degradation peaks of 5FU could not be observed and TGA

thermograms indicated an improvement in thermal stability of the polymer probably due to interaction with 5FU molecules.

Although drug loading contents determined from concentration analysis of dialysis media of samples by UV-spectroscopy were very close, TGA thermogram of 4 arm PMMA-*b*-PAA loaded at a polymer concentration of 3500 mg/L exhibited relatively low residue depicting relatively higher drug content. Therefore 4 arm PMMA-*b*-PAA loaded at a polymer concentration of 3500 mg/L samples were tested for their drug release performances.

Drug release from 4 arm PMMA-*b*-PAA loaded at a polymer concentration of 3500 mg/L, at 15°C for four hours were determined by a continuous system equipped by a Franz diffusion cell, a syringe pump and a flow cell continuously monitored by UV spectroscopy. Absorbance of PBS solution passed through receptor compartment at 37°C was analyzed with one minute intervals. To confirm continuous measurement, 15 ml samples of downstream were separately analyzed to calculate released amount of drug versus time. The experiment was repeated at two different flow rates, 0.25 ml/min and 0.025 ml/min, which yielded comparable amounts of drug released. Release profile from particles has been estimated by considering continuous mass transfer of released drug to the receptor compartment of diffusion cell through a semipermeable membrane. Concentration of PBS flow passing through receptor compartment was monitored throughout release process and release profile was modelled following determination of permeability as 0.005 cm/min which constituted the mass transfer coefficient of overall system.

Drug release from 4 arm PMMA-b-PAA was modeled separately for the initial and proceeding intervals of release process. Solution of parameters (n, k and integration constants) by trial and error indicated that release from polymer particles approached zero order kinetics with negligibly small n for the initial interval and constant release for the rest of the process. Therefore drug release mechanism was dominated by k constants which were determined as 1.35×10-3 and 7.59×10-4 for the initial and late intervals of drug release, respectively. Precise values of coefficient (k) and degree (n) of release kinetics within donor compartment provided by the solutions has been tabulated in Table 6.1. They show the release behavior from PMMA-*b*-PAA nanoparticles according to the mathematical model derived by assuming drug concentration in donor compartment to be time dependent obeying the power low equation which was represented by the mathematical expression, kt^n.

Table 6.1. Constants of release kinetics equation from 5FU loaded PMMA-*b*-PAA nanoparticles.

Release Profile Along the Whole Release Period (SSE=0.066)		**Release Profiles for the Initial and Late Periods (SSE=0.016)**			
		$\left[\frac{M_t}{M} \le 0.40\right]$		$\left[\frac{M_t}{M} > 0.40\right]$	
k	n	k_1	n_1	k_2	n_2
9.78×10^{-4}	0	1.35×10^{-3}	0.0025	7.59×10^{-4}	0

Biodegradation profiles of 4 arm PMMA-*b*-PAA were consistent with release profiles which indicated erosion of polymeric particles. 4 arm PMMA-*b*-PAA particles exposed to buffer solution of 7.4 pH and body temperature tended to agglomerate for the first day of degradation. This behavior explains 6 hours of delay in release profile, when agglomeration was severe. Then agglomerates slowly reduced in seven days when drug release appeared almost with a constant rate.

Average particle size of 4 arm PMMA-*b*-PAA having a PMMA core of 5000 Da molecular weight and 0.25±0.05 hydrophobic core ratio was 20-30 nm as dissoleved in aqueous medium. Due to agglomeration, particle size could rise up to 150 nm, but agglomerates were rather few (<10 v%). compared to small particles After 10 days of degradation average particle size were smaller than 10 nm, dilute samples resulting in 5 nm. AFM micrographs confirmed these results.

For a final word, amphiphilic 4 arm PMMA-*b*-PAA nanoparticles have been proved promising drug carriers especially for hydrophobic anticancer drugs. They exhibit substantial drug loading content (14 % for 5FU and 22% for indomethacin) and provided controlled release for 18 days. All polymer samples studied for their release performance exhibited sustained release with a 4-6 hours of delay prior to beginning of drug release. This delay is attributed beneficial for the application of release system in cancer therapy since sustained delivery permits carrier particles accumulate in tumors. Agglomerated particles not exceeding 100 nm particle size provides another benefit for cancer therapy ensuring passive tumor targeting. On the other hand further agglomeration of particles within the first few hours of administration may cause problems in reticuloendothelial system. A surface modification of 4 arm PMMA-*b*-PAA nanoparticles may be necessary to prevent severe agglomeration for parenteral applications of drugs carried by 4 arm PMMA-*b*-PAA nanoparticles.

REFERENCES

Aguiar, J.; Carpena, P.; Molina-Bolívar, J. A.; Carnero, R. C. On the Determination of the Critical Micelle Concentration by the Pyrene 1:3 Ratio Method. *J. Colloid Interf. Sci.* **2003**, *258*, 116–122.

Allen, C.; Maysinger, D.; Eisenberg, A. Nano-Engineering Block Copolymer Aggregates for Drug Delivery. *Colloid Surface B*. **1999**, *16*, 3–27.

Arias, J. L.; Ruiz, M. A.; López-Viota, M.; Delgado, Á. V.; Poly(Alkylcyanoacrylate) Colloidal Particles as Vehicles for Antitumour Drug Delivery: A Comparative Study. *Colloids and Surface B*. **2008**, *62*, 64–70.

Asthana, A.; Chauhan, A. S.; Diwan, P.V.; Jain, N.K. Poly(Amidoamine) (PAMAM) Dendritic Nanostructures for Controlled Site-Specific Delivery of Acidic Anti-Inflammatory Active Ingredient. *AAPS Pharm.Sci.* **2005**, *6*, 536-542.

Aulenta, F.; Hayes, W.; Rannard, S. Dendrimers: A New Class of Nanoscopic Containers and Delivery Devices. *Eur. Polym. J.* **2003**, *39*, 1741–1771.

Babu, V. R.; Sairam, M.; Hosamani, K. M.; Aminabhavi, T. M. Development of 5-Fluorouracil Loaded Poly(Acrylamide-co-Methylmethacrylate) Novel Core-Shell Microspheres: In Vitro Release Studies. *Int. J. Pharm.* **2006**, *325*, 55–62.

Bartolozzi, I.; Solaro, R.; Schacht, E.; Chiellini, E. Hydroxyl End-Capped Macromers of N-Vinyl-2-Pyrrolidinone as Precursors of Amphiphilic Block Copolymers. *Eur. Polym. J.* **2007**, *43*, 4628–4638.

Bontha, S.; Kabanov, A. V.; Bronich, T. K. Polymer Micelles With Cross-Linked Ionic Cores for Delivery Of Anticancer Drugs. *J. Control. Release.* **2006**, *114*, 163-174.

Brannon-Peppas L.; Blanchette J. O. Nanoparticle and Targeted Systems for Cancer Therapy. *Adv. Drug Deliver. Rev.* **2004**, *56*, 1649– 1659.

Brannon-Peppas L. Polymers in Controlled Drug Delivery. *Medical Plastics And Biomaterials Magazine.* **1997**, *4*, 34-44.

Brar, A. S.; Saini, T. Atom Transfer Radical Polymerization of 2-Methoxy Ethyl Acrylate and Its Block Copolymerization with Acrylonitrile. *Eur. Polym. J.* **2007**, *43*, 1046–1054.

Braunecker, W. A.; Matyjaszewski K. Controlled/Living Radical Polymerization: Features, Developments and Perspectives. *Prog. Polym. Sci.* **2007**, *32*, 93-146

Breitenbach, A.; Li, Y. X.; Kissel, T. Branched Biodegradable Polyesters for Parenteral Drug Delivery Systems. *J. Control. Release.* **2000**, *64*, 167–178.

Burguière, C., Chassenieux, C., Charleux, B. Characterization of Aqueous Micellar Solutions of Amphiphilic Block Copolymers of Poly(Acrylic Acid) And Polystyrene Prepared via ATRP. Toward the Control of the Number of Particles in Emulsion Polymerization. *Polymer.* **2003**, *44*, 509–518.

Candau, F.; Ottewill, R. H. *Scientific Methods for the Study of Polymer Colloids and their Applications ;* Kluwer : Strasbourg, 1988, pp 311-314.

Castelli, F.; Messina, C.; Sarpietro, M. G.; Pignatello, R.; Puglisi, G. Eudragit as Controlled Release System for Anti-Inflammatory Drugs. A Comparison between DSC and Dialysis Experiments. *Thermochim. Acta.* **2003**, *400*, 227–234.

Castelli, F.; Conti, B.; Maccarrone, D.; Lacamera, O.; Conte, U. Indomethacin-Dipalmitoylphosphatidylcholine Interaction. A Calorimetric Study of Drug Release From Poly(Lactide-co-Glycolide) Microspheres into Multilamellar Vesicles. *Drug Deliv.* **1997**, *4*, 273-279.

Celik, C.; Hızal, G.; Tunca, U. Synthesis of Miktoarm Star and Miktoarm Star Block Copolymers via a Combination of Atom Transfer Radical Polymerization and Stable Free-Radical Polymerization. *J. Polym. Sci. Pol. Chem.* **2003**, *41*, 2542–2548.

Chatterjee, U.; Jewrajka, S. K.; Mandal, B. M. The Amphiphilic Block Copolymers of 2-(Dimethylamino)Ethyl Methacrylate and Methyl Methacrylate: Synthesis by Atom Transfer Radical Polymerization and Solution Properties. *Polymer*. **2005**, *46*, 10699–10708.

Cheng, Y.; Xu, T. The Effect of Dendrimers on the Pharmacodynamic and Pharmacokinetic Behaviors of Non-Covalently or Covalently Attached Drugs. *Eur. J. Med. Chem*. **2008**, *43*, 2291-2297.

Chu, J.; Chen, J.; Zhang K. N,N,N,N,N-Penta(Methyl Acrylate)Diethylenetriamine: A Novel Ligand for Atom Transfer Radical Polymerization of Methyl Methacrylate. *J. Polym. Sci. Pol. Chem*. **2004**, *42*, 1963–1969.

Chytil, P.; Etrych, T.; Koňák, Č.; Šírová, M.; Mrkvan, T.; Říhová, B.; Ulbrich, K. Properties of HPMA Copolymer–Doxorubicin Conjugates with pH-Controlled Activation: Effect of Polymer Chain Modification. *J. Control. Release*. **2006**, *115*, 26–36.

Coessens, V.; Pintauer, T.; Matyjaszewski K. Functional Polymers by Atom Transfer Radical Polymerization. *Prog. Polym. Sci*. **2001**, *26*, 337-377.

Crank J. *The Mathematics of Diffusion*; Clarendon Pres: Oxford, 1975; pp 89-91.

Demir, M. M.; Erman, B. Dimensions of Polystyrene Particles Deposited on Mica from Dilute Cyclohexane Solution at Different Temperatures. *Macromolecules,* **2002**, *35*, 7986-7992.

Deng, G.; Ma, D.; Xu, Z. Synthesis of ABC-Type Miktoarm Star Polymers By ‘‘Click’’ Chemistry, ATRP and ROP. *Eur. Polym. J*. **2007**, *43*, 1179–1187.

Djordjevic, J.; Michniak, B.; Uhrich, K. E. Amphiphilic Star-Like Macromolecules as Novel Carriers for Topical Delivery of Nonsteroidal Anti-Inflammatory Drugs. *AAPS Pharm.Sci.* **2003**, *5*, Article 26, 1-12.

Dodova, M. G.; Calis, S.; Crcarevska, M. S.; Geskovski, N.; Petrovska, V.; Goracinova, K.; Wheat Germ Agglutinin-Conjugated Chitosan–Ca–Alginate Microparticles for Local Colon Delivery of 5-FU: Development and *in vitro* Characterization. *Int. J. Pharm.* **2009**, *381*, 166–175.

Eerikäinen, H.; Peltonen, L.; Raula, J.; Hirvonen, J.; Kauppinen, E. I. Nanoparticles Containing Ketoprofen and Acrylic Polymers Prepared by an Aerosol Flow Reactor Method. *AAPS Pharm. Sci.* **2004**, *5*, Article 68, 1-9.

Erdoğan, T.; Ozyürek, Z.; Hızal G.; Tunca U. Facile Synthesis Of AB_2-Type Miktoarm Star Polymers Through the Combination of Atom Transfer Radical Polymerization and Ring-Opening Polymerization. *J. Polym. Sci. Pol. Chem.* **2004**, *42*, 2313–2320.

Even, M.; Haddleton, D. M.; Kukulj, D. Synthesis and Characterization of Amphiphilic Triblock Polymers by Copper Mediated Living Radical Polymerization. *Eur. Polym. J.* **2003**, *39*, 633–639.

Faisant, N.; Akiki, J.; Siepmann, F.; Benoit, J.P.; Siepmann, J. Effects of the Type of Release Medium on Drug Release From PLGA-Based Microparticles: Experiment and Theory. *Int. J. Pharm.* **2006**, *314*, 189–197.

Faisant, N.; Siepmann, J.; Richard, J.; Benoit, J.P. Mathematical Modeling of Drug Release from Bioerodible Microparticles: Effect of Gamma-Irradiation. *Eur. J. Pharm. Biopharm.* **2003**, *56*, 271–279.

Gast, A. P. Polymeric Micelles. *Curr Opin Colloid In*. **1997**, *2*, 258-263.

Ganguly, M. Controlled Polymerization of Alkyl Methacrylates. Ph.D. Dissertation, University Of Pune, Pune, India. December 2002.

Gao, H.; Gu, Y.; Ping, Q. The Implantable 5-Fluorouracil-Loaded Poly(L-Lactic Acid) Fibers Prepared by Wet-Spinning from Suspension. *J. Control. Release*. **2007**, *118*, 325–332.

Gaucher, G.; Dufresne, M. H.; Sant, V. P.; Kang, N.; Maysinger D.; Leroux J. C. Block Copolymer Micelles: Preparation, Characterization and Application in Drug Delivery. *J. Control. Release*. **2005**, *109*, 169–188.

Gillies, E. R., Fréchet, J. M. J. Development of Acid-Sensitive Copolymer Micelles for Drug Delivery. *Pure Appl. Chem*. **2004**, *76*, 1295–1307.

Grayson, S. M.; Fréchet, J. M. J. Convergent Dendrons and Dendrimers: from Synthesis to Applications. *Chem. Rev*. **2001**, *101*, 3819-3868.

Gudasi, K. B.; Vadavi, R. S.; Shelke, N. B.; Sairam, M.; Aminahbavi, T. M. Synthesis and Characterization of Novel Polyorganophosphazenes Substituted with 4-Methoxybenzylamine and 4-Methoxyphenethylamine for *in vitro* Release of Indomethacin and 5-Fluorouracil. *React. Funct. Polym*. **2006**, *66*, 1149–1157.

Gupte, A.; Ciftci, K. Formulation and Characterization of Paclitaxel, 5-FU and Paclitaxel + 5-Fu Microspheres. *Int. J. Pharm*. **2004**, *276*, 93–106.

Haddleton, D. M.; Clark, A. J.; Crossman, M. C.; Duncalf, D. J.; Heming, A. M.; Morsley, S. R.; Shooter, A. J. Atom Transfer Radical Polymerisation (ATRP) Of Methyl Methacrylate in the Presence of Radical Inhibitors. *Chem. Commun.* **1997**, 1173-1174.

Heng, P. W. S.; Chan, L. W.; Easterbrook, M. G.; Li, X. Investigation of the Influence of Mean HPMC Particle Size and Number of Polymer Particles on The Release of Aspirin from Swellable Hydrophilic Matrix Tablets. *J. Control. Release*. **2001**, *76*, 39–49.

Ho, W. S. W.; Sirkar, K. K. *Membrane Handbook*; Van Nostrand Reinhold; New York, 1992; pp 915-931.

Ibrahim, K. Studies on Atom Transfer Radical Polymerization of Acrylates and Styrenes with Controlled Polymeric Block Structures. Ph.D. Dissertation, Helsinki University Of Technology, Helsinki, Finland, June 2006.

Ishizu, K.; Furukawa, T.; Yamada, H. Silver Nanoparticles Dispersed within Amphiphilic Star-Block Copolymers as Templates for Plasmon Band Materials. *Eur. Polym. J.* **2005**, *41*, 2853–2860.

Ishizu, K.; Uchida, S. Synthesis and Microphase-Separated Structures of Star-Block Copolymers. *Prog. Polym. Sci.* **1999**, *24*, 1439–1480.

Jain, A.; Jain, S. K. *In vitro* and Cell Uptake Studies for Targeting of Ligand Anchored Nanoparticles for Colon Tumors. *Eur. J. Pharm. Sci.* **2008**, *35*, 404–416.

Jankova, K.; Bednarek, M.; Hvilsted, S. Star Polymers by ATRP of Styrene and Acrylates Employing Multifunctional Initiators. *J. Polym. Sci. Pol. Chem*. **2005**, *43*, 3748–3759.

Jie, P.; Venkatraman, S. S.; Min, F.; Freddy, B. Y. C.; Huat, G. L. Micelle-Like Nanoparticles of Star-Branched PEO–PLA Copolymers as Chemotherapeutic Carrier. *J. Control. Release*. **2005**, *110*, 20– 33.

Jones, M. C.; Hui, G.; Leroux, J. C. Reverse Polymeric Micelles for Pharmaceutical Applications. *J. Control. Release*. **2008**, *132*, 208-215.

Kakizawa, Y.; Kataoka, K. Block Copolymer Micelles for Delivery of Gene and Related Compounds. *Adv. Drug Deliver. Rev*. **2002**, *54*, 203–222.

Kang, B. K.; Chon, S. K.; Kim, S. H.; Jeong, S. Y.; Kim, M. S.; Cho, S. H.; Lee, H. B.; Khang, G. Controlled Release of Paclitaxel from Microemulsion Containing PLGA and Evaluation of Anti-Tumor Activity *in vitro* and *in vivo*. *Int. J. Pharm*. **2004**, *286*,147–156.

Kang, H.; Liu, W.; He, B.; Shen, D.; Ma, L.; Huang, Y. Synthesis of Amphiphilic Ethyl Cellulose Grafting Poly(Acrylic Acid) Copolymers and Their Self-Assembly Morphologies in Water. *Polymer.* **2006**, *47*, 7927-7934.

Kang, N.; Leroux, J. C. Triblock and Star-Block Copolymers of N-(2-Hydroxypropyl) Methacrylamide or N-Vinyl-2-Pyrrolidone and D,L-Lactide: Synthesis and Self-Assembling Properties in Water. *Polymer.* **2004**, *45*, 8967–8980.

Kang, Y.; Wu, J.; Yin, G.; Huang, Z.; Yao, Y.; Liao, X.; Chen, A.; Pu, X.; Liao, L. Preparation, Characterization and *in vitro* Cytotoxicity of Indomethacin-Loaded PLLA/PLGA Microparticles Using Supercritical CO_2 Technique. *Eur. J. Pharm.Biopharm*. **2008**, *70*, 85-97.

Kilian, L. Synthesis and Characterization of Responsive Poly(Alkyl Methacrylate) Topologies. Ph. D. Dissertation, Virginia Polytechnic Institute and State University, Virginia, USA, July 2004.

Klose, D.; Siepmann, F.; Elkharraz, K.; Siepmann, J. PLGA-Based Drug Delivery Systems: Importance of the Type of Drug and Device Geometry. *Int. J. Pharm*. **2008**, *354*, 95–103.

Krishnan, R. K.; Srinivasan, S. V. Homo and Block Copolymers of *tert*-Butyl Methacrylate by Atom Transfer Radical Polymerization. *Eur. Polym. J.* **2004**, *40*, 2269–2276.

Langer, R. S.; Peppas, N. A. Present and Future Applications of Biomaterials in Controlled Drug Delivery Systems. *Biomaterials*. **1981**, *2*, 201-214.

Lele, B. S.; Leroux, J. C. Synthesis of Novel Amphiphilic Star-Shaped Poly(L-Caprolactone)-*block*-Poly(N-(2-Hydroxypropyl) Methacrylamide) by Combination of Ring-Opening And Chain Transfer Polymerization. *Polymer*. **2002**, *43*, 5595–5606.

Leroux, J. C.; Ranger, M. Water-Soluble Amphiphilic Nanocarriers – Applications in Drug Delivery, Drug Delivery Companies Report, Autumn-Winter, 2002.

Li, S.; Wang, A.; Jiang, W.; Guan, Z. Pharmacokinetic Characteristics and Anticancer Effects of 5-Fluorouracil Loaded Nanoparticles. *BMC Cancer*. **2008**, *8*, 103-112.

Limer, A. J.; Rullay, A. K.; Sanmiguel V.; Peinado, C.; Keely, S.; Fitzpatrick, E.; Carrington, S. D.; Brayden, D.; Haddleton, D. M. Fluorescently Tagged Star Polymers by Living Radical Polymerisation for Mucoadhesion and Bioadhesion. *React. Funct. Polym.* **2006**, *66*, 51–64.

Lin, C. C.; Fu, C. H. Controlled Release Study of 5-Fluorouracil-Loaded Chitosan/Polyethylene Glycol Microparticles. *Drug Deliv*. **2009**, *16*, 274–279.

Liu, M.; Kono, K.; Fréchet J. M. J. Water-Soluble Dendritic Unimolecular Micelles: Their Potential as Drug Delivery Agents. *J. Control. Release.* **2000**, *65*, 121–131.

Liu, Z.; Rimmer, S. Synthesis and Release of 5-Fluorouracil from Poly(N-Vinylpyrrolidinone) Bearing 5-Fluorouracil Derivatives. *J. Control. Release.* **2002**, *81*, 91–99.

Lópezdíaz, D.; Velázquez, M. M. Variation of the Critical Micelle Concentration with Surfactant Structure: A Simple Method to Analyze the Role of Attractive–Repulsive Forces on Micellar Association. *Chem. Educ*. **2007**, *12*, 327-330.

Lowman, A. M.; Peppas, N. A. *Hydrogels, Encyclopedia of Controlled Drug Delivery*; Wiley; New York, 1999; pp 397-418.

Lukyanov, A. N.; V. P. Torchilin. Micelles from Lipid Derivatives of Water-Soluble Polymers as Delivery Systems for Poorly Soluble Drugs, *Adv. Drug Deliver. Rev.* **2004**, *56*, 1273– 1289.

Malinowska, A.; Vlček, P.; Kříž, J.; Toman, L.; Látalová, P.; Janata, M.; Masař, B. ATRP of (Meth)Acrylates Initiated with a Bifunctional Initiator Bearing Trichloromethyl Functional Groups and Structural Analysis Of The Formed Polymer. *Polymer.* **2005**, *46*, 5–14.

Manocha, B.; Margaritis, A. Production and Characterization of γ -Polyglutamic Acid Nanoparticles For Controlled Anticancer Drug Release. *Crit. Rev. Biotechnol.* **2008**, *28*, 83–99.

Mao, B. W.; Gan, L. H.; Gan, Y. Y.; Tam, K. C.; Tan, O. K. Controlled One-Pot Synthesis of pH-Sensitive Self-Assembled Diblock Copolymers and Their Aggregation Behavior. *Polymer*. **2005**, *46*, 10045–10055.

Marion, S. C.; Okano, T.; Kataoka, K. Functional and Site-Specific Macromolecular Micelles as High Potential Drug Carriers. *Colloid. Surface. B.* **1999**, *16*, 207–215.

McCarron, P. A.; Hall, M. Incorporation of Novel L-Alkylcarbonyloxymethyl Prodrugs Of 5-Fluorouracil into Poly(Lactide-co-Glycolide) Nanoparticles. *Int. J. Pharm.* **2008**, *348*, 115–124.

Musumeci, T.; Ventura, C. A.; Giannone, I.; Ruozi, B.; Montenegro, L.; Pignatello, R.; Puglisi, G. PLA/PLGA Nanoparticles for Sustained Release of Docetaxel. *Int. J. Pharm*. **2006**, *325*, 172–179.

Narrainen, A. P.; Pascual, S.; Haddleton, D. M. Amphiphilic Diblock, Triblock, and Star Block Copolymers by Living Radical Polymerization: Synthesis and Aggregation Behavior. *J. Polym. Sci. Pol. Chem.* **2002**, *40*, 439-450.

Ning, F.; Jiang, M.; Mu, M.; Duan, H.; Xie, J. Synthesis of Amphiphilic Block–Graft Copolymers [Poly(Styrene-*b*-Ethylene-co-Butylene-*b*-Styrene)-G-Poly(Acrylic Acid)] and Their Aggregation in Water. *J. Polym. Sci. Pol. Chem.* **2002**, *40*, 1253–1266.

Nishiyama, N.; Kataoka, K. Current State, Achievements, and Future Prospects of Polymeric Micelles as Nanocarriers for Drug and Gene Delivery. *Pharmacol. Therapeut.* **2006**, *112*, 630-648.

Nurmi, L.; Holappa, S.; Mikkonen, H.; Seppälä, J. Controlled Grafting of Acetylated Starch by Atom Transfer Radical Polymerization Of MMA. *Eur. Polym. J.* **2007**, *43*, 1372–1382.

Pascu, M. L.; Carstocea, B.; Brezeanu1, M.; Gazdaru, D.; Voicu, L.; Smarandache, A. Studies On Activated Fluorouracil with Optical Beams, for Use in The Eye Tumours Treatment. *Romanian Reports In Physics.* **2003**, *55*, 270-274.

Patri, A. K.; Kukowska-Latallo, J. F.; Baker, J. R. Jr. Targeted Drug Delivery with Dendrimers: Comparison of the Release Kinetics of Covalently Conjugated Drug and Non-Covalent Drug Inclusion Complex. *Adv. Drug Deliver. Rev.* **2005**, *57*, 2203–2214.

Prabakaran, D.; Singh, P.; Kanaujia, P.; Vyas, S. P.; Effect of Hydrophilic Polymers on the Release of Diltiazem Hydrochloride from Elementary Osmotic Pumps. *Int. J. Pharm.* **2003**, *259*, 173–179.

Qiu, L. Y.; Bae, Y. H.; Polymer Architecture And Drug Delivery. *Pharmaceut. Res.* **2006**, *23*, 1-30.

Quaglia, F.; Ostacolo, L.; Derosa, G.; Larotonda, M.; Ammendolab, M.; Nese, G; Maglio, G.; Palumbo, R.; Vauthier, C. Nanoscopic Core-Shell Drug Carriers Made of Amphiphilic Triblock and Star-Diblock Copolymers. *Int. J. Pharm.* **2006**, *324*, 56–66.

Radhakumary, C.; Prabha, D. N .; Mathew, S.; Nair C. P. R. Biopolymer Composite of Chitosan and Methyl Methacrylate for Medical Applications. *Trends Biomater. Artif. Organs.* **2005**, *18*, 117-124.

Ritger, P. L.; Peppas, N. A. A Simple Equation for Description of Solute Release I. Fickian and Non-Fickian Release from Non-Swellable Devices in the Form of Slabs, Spheres, Cylinders or Discs. *J. Control. Release.* **1987**, *5*, 23-36.

Rösler, A.; Vandermeulen, G. W. M.; Klok, H. A. Advanced Drug Delivery Devices via Self-Assembly of Amphiphilic Block Copolymers. *Adv. Drug Deliver. Rev.* **2001**, *53*, 95–108.

Sahoo, S. K.; Labhasetwar, V. Nanotech Approaches to Drug Delivery and Imaging. *Drug Discov. Today*. **2003**, *8*, 1112-1120.

Sairam, M.; Babu R., Krishna, V.; Rao, K. S. V.; Aminabhavi, T. M. Poly(Methylmethacrylate)-Poly(Vinyl Pyrrolidone) Microspheres as Drug Delivery Systems: Indomethacin/Cefadroxil Loading and *in vitro* Release Study. *J. Appl. Polym. Sci.* **2007**, *104*, 1860–1865.

Salaam, L. E.; Dean, D.; Bray, T. L. *In vitro* Degradation Behavior of Biodegradable 4-Star Micelles. *Polymer.* **2006**, *47*, 310–318.

Sanmiguel, V.; Limer, A. J.; Haddleton, D. M.; Catalina, F.; Peinado, C. Biodegradable and Thermoresponsive Micelles of Triblock Copolymers Based on 2-(N,N-Dimethylamino)Ethyl Methacrylate and E-Caprolactone for Controlled Drug Delivery. *Eur. Polym. J.* **2008**, *44*, 3853–3863.

Sant, V. P.; Smith, D.; Leroux, J. C. Enhancement of Oral Bioavailability of Poorly Water-Soluble Drugs by Poly(Ethylene Glycol)-*block*-Poly(Alkyl Acrylate-co-Methacrylic Acid) Self-Assemblies. *J. Control. Release*. **2005**, *104*, 289–300.

Santos, C.; Martins, M. A.; Franke, R. P.; Almeida, M. M.; Costa, M. E. V. Calcium Phosphate Granules for Use as a 5-Fluorouracil Delivery System. *Ceram. Int.* **2009**, *35*, 1587–1594.

.

Sezgin, Z.; Yüksel, N.; Baykara, T. Preparation and Characterization of Polymeric Micelles for Solubilization of Poorly Soluble Anticancer Drugs. *Eur. J. Phar. Biopharm.* **2006**, *64*, 261–268.

Shim, W. S.; Kim, S. W.; Choi, E.-K.; Park, H.- J.; Kim, J.-S.; Lee D. S. Novel pH Sensitive Block Copolymer Micelles for Solvent Free Drug Loading. *Macromol. Biosci.* **2006**, *6*, 179–186.

Silverstein, R. M., Webster, F. X., Kiemle, D. J. *Spectrometric Identification of Organic Compounds*, 7th ed.; John Wiley & Sons Inc, 2005; Chapters 2-4.

Storey, R. F.; Scheuer, A. D.; Achord, B. C. Amphiphilic Poly(Acrylic Acid-b-Styrene-b-Isobutylene-b-Styrene-b-Acrylic Acid) Pentablock Copolymers from a Combination of Quasiliving Carbocationic and Atom Transfer Radical Polymerization. *Polymer*, **2005**, *46*, 2141–2152.

Sun, X.; Zheng, H.; Huang, X.; Wang, X.; Zhou, Q.-F. Synthesis of Poly(Ethylene Oxide)-block-Poly(Methyl Methacrylate)-block-Polystyrene Triblock Copolymers by Two Step Atom Transfer Radical Polymerization. *Polymer*. **2005**, *46*, 5251-5257.

Svenson, S.; Tomalia, D. A. Dendrimers in Biomedical Applications. *Adv. Drug Deliver. Rev.* **2005**, *57*, 2106– 2129.

Tao, L.; Uhric, K. E. Novel Amphiphilic Macromolecules and Their *in vitro* Characterization as Stabilized Micellar Drug Delivery Systems. *J. Colloid Interf. Sci.* **2006**, *298*, 102–110 .

Tomalia, D. A. Dendrimers: Key Properties of Importance to Nanomedicine. *Nanomedicine*. **2006**, *2*, 269–312.

Tomalia, D. A.; Fréchet, J. M. J. Introduction to Dendrimers and Dendritic Polymers. *Prog. Polym. Sci.* **2005**, *30*, 217-219.

Tuma, J. J. *Engineering Mathematics Handbook*, 3rd ed.; McGraw Hill, 1987; p.368.

Tunca, U.; Erdoğan, T.; Hızal, G. Synthesis and Characterization of Well-Defined ABC-Type Triblock Copolymers via Atom Transfer Radical Polymerization and Stable Free-Radical Polymerization. *J. Polym. Sci. Pol. Chem.* **2002**, *40*, 2025–2032.

Ulbrich, K.; Pechar, M.; Etrych, T.; Jelínková, M.; Kováø, M.; Øíhová, B.; Polymer Carriers for Targeted Drug Delivery and Controlled Drug Release. *Materials Structure.* **2003**, *10*, 3-5.

Wang, G.; Henselwood, F.; Liu, G. Water-Soluble Poly(2-Cinnamoylethyl Methacrylate)-*block*-Poly(Acrylic Acid) Nanospheres as Traps for Perylene. *Langmuir*. **1998**, *14*, 1554-1559.

Wei, H.; Zhang, X.; Cheng, C.; Cheng, S. X.; Zhuo, R. X. Self-Assembled, Thermosensitive Micelles of a Star Block Copolymer Based on PMMA and PNIPAAM for Controlled Drug Delivery. *Biomaterials.* **2007**, *28*, 99–107.

Xie, D.; Yang, Y.; Zhao, J.; Park, J. G.; Zhang, J. T. A Novel Comonomer-Free Light-Cured Glass-Ionomer Cement for Reduced Cytotoxicity and Enhanced Mechanical Strength. *Dent. Mater.* **2006**, *23*, 994-1003.

Yang, H. C.; Hon, M. H. The Effect of the Molecular Weight of Chitosan Nanoparticles and Its Application on Drug Delivery. *Microchem. J.* **2009**, *92*, 87–91.

Yang, Z.; Liu, J.; Huang, Z.; Shi, W. Crystallization Behavior and Micelle Formation of Star-Shaped Amphiphilic Block Copolymer Based on Dendritic Poly(Ether-Amide). *Eur. Polym. J.* **2007**, *43*, 2298–2307.

Yin, M.; Habichera, W. D.; Voit, B.; Preparation of Functional Poly(Acrylates and Methacrylates) and Block Copolymers Formation Based on Polystyrene Macroinitiator by ATRP. *Polymer.* **2005**, *46*, 3215–3222.

Yin, N.; Chen, K.; Kang, W. Preparation of BA/ST/AM Nano Particles by Ultrasonic Emulsifier-Free Emulsion Polymerization. *Ultrason. Sonochem.* **2006**, *13*, 345–351.

Yu, H.; Peng, J.; Zhai, M.; Li, J.; Wei, G.; Qiao, J. Synthesis and Characterization of Poly (n-Butyl Acrylate)-Poly(Methyl Methacrylate) Latex Interpenetrating Polymer Networks by Radiation-Induced Seeded Emulsion Polymerization. *Radiat. Phys. Chem.* **2006**, *76*, 1746–1750.

Yu, Z.-Q.; Ni, P.-H.; Li, J.-A.; Zhu, X.-L. Miniemulsion Copolymerization of Methyl Methacrylate and Butyl Acrylate in the Presence of Vinyl Siloxane Rubber. *Colloid Surfaces A*, **2004**, *242*, 9–15.

Yuan, W.; Yuan, J.; Zheng, S.; Hong, X. Synthesis, Characterization, and Controllable Drug Release of Dendritic Star-Block Copolymer by Ring-Opening Polymerization and Atom Transfer Radical Polymerization. *Polymer.* **2007**, *48*, 2585-2594.

Zhang, Z.; Zhang, Q.; Wang, J.; Shi, X.; Zhang, J.; Song, H.; Synthesis and Drug Release *in vitro* of Porphyran Carrying 5-Fluorouracil. *Carbohyd. Polym.* **2010**, *79*, 628-632.

Zhang, Y.; Jiang, M.; Zhao, J.; Chen, D. Thermo-Sensitive Core–Shell Nanoparticles as Potential Drug Carrier. *Eur. Polym. J.* **2007**, *43*, 4905-4915.

Zhang, Z.; Grijpma, D. W.; Feijen, J. Poly(Trimethylene Carbonate) and Monomethoxy Poly(Ethylene Glycol)-block-Poly(Trimethylene Carbonate) nanoparticles for the controlled release of dexamethasone. *J. Control. Release.* **2006**, *111*, 263–270.

Zhang, Y.; Zhuo, R. X. Synthesis and Drug Release Behavior of Poly (Trimethylene Carbonate)–Poly(Ethyleneglycol)–Poly(Trimethylene Carbonate) Nanoparticles. *Biomaterials.* **2005a**, *26*, 2089–2094.

Zhang, Y.; Zhuo, R. X. Synthesis, characterization, and *in vitro* 5-FU Release Behavior of Poly(2,2-Dimethyltrimethylene Carbonate)-Poly(Ethylene Glycol)-Poly(2,2-DimethylTrimethylene Carbonate) Nanoparticles. J. *Biomed. Mater. Res*. **2005b**, *76*, 674–680.

Zhao, Y. L.; Gong, A. J.; Jiang, J.; Liu, H. W.; Chen, C. F.; Xi, F. Synthesis of Dendritic-Linear Block Copolymers by Atom Transfer Radical Polymerization. *Chinese Chem. Lett.* **2001**, *12*, 595-596.

Zheng, D.; Li, X.; Xu, H.; Lu, X.; Hu, Y.; Fan, W. Study on Docetaxel Loaded Nanoparticles with High Antitumor Efficiacy agains Malignant Melanoma. *Acta Biochim. Biophys. Sin.* **2009**, *41*, 578-587.

Zheng, Y.; Yang, W.; Wang, C.; Hu, J.; Fu, S.; Dong, L.; Wu, L.; Shen, X. Nanoparticles Based on the Complex of Chitosan and Polyaspartic Acid Sodium Salt: Preparation, Characterization and the Use for 5-Fluorouracil Delivery. Eur. *J. Phar. Biopharm.* **2007**, *67*, 621–631.

Zhuo, R. X.; Du, B.; Lu, Z. R. *In vitro* Release of 5-Fluorouracil with Cyclic Core Dendritic Polymer, *J. Control. Release.* **1999**, *57*, 249–257.

APPENDIX A

CRITICAL MICELLE CONCENTRATIONS

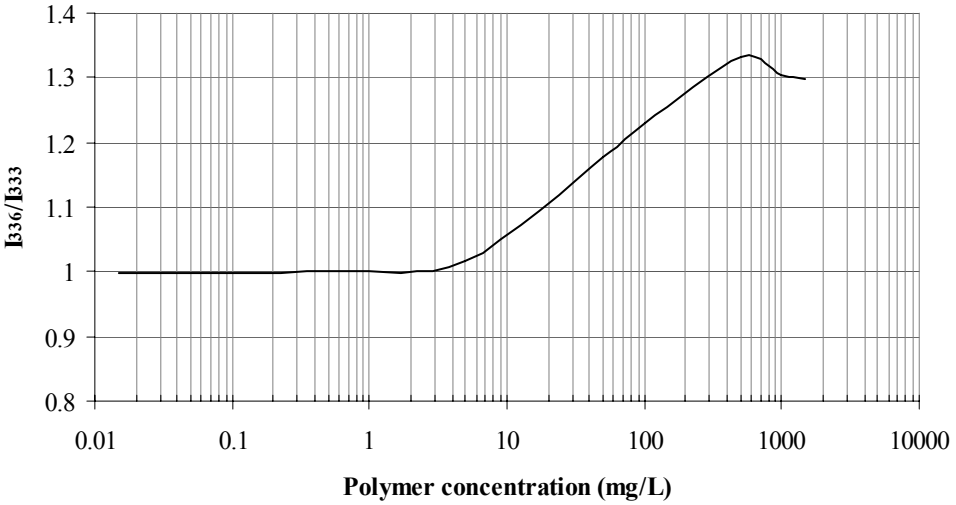

Figure A.1. CMC determination by fluorescence method for 3 arm PMMA-*b*-PAA with molecular weight of 22000 Da and hydrophobic core ratio of 0.26.

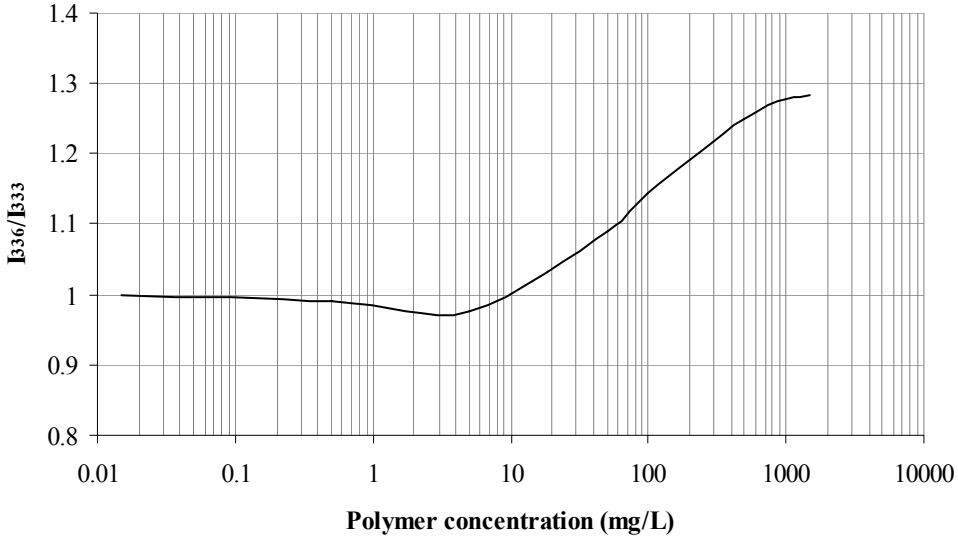

Figure A.2. CMC determination by fluorescence method for 4 arm PMMA-*b*-PAA with molecular weight of 27000 Da and hydrophobic core ratio of 0.17.

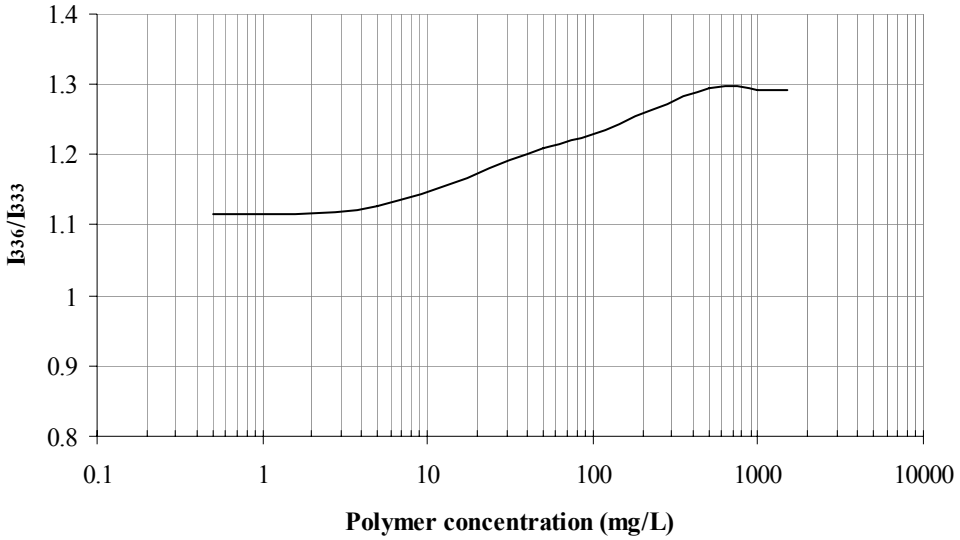

Figure A.3. CMC determination by fluorescence method for 4 arm PMMA-*b*-PAA with molecular weight of 30000 Da and hydrophobic core ratio of 0.23.

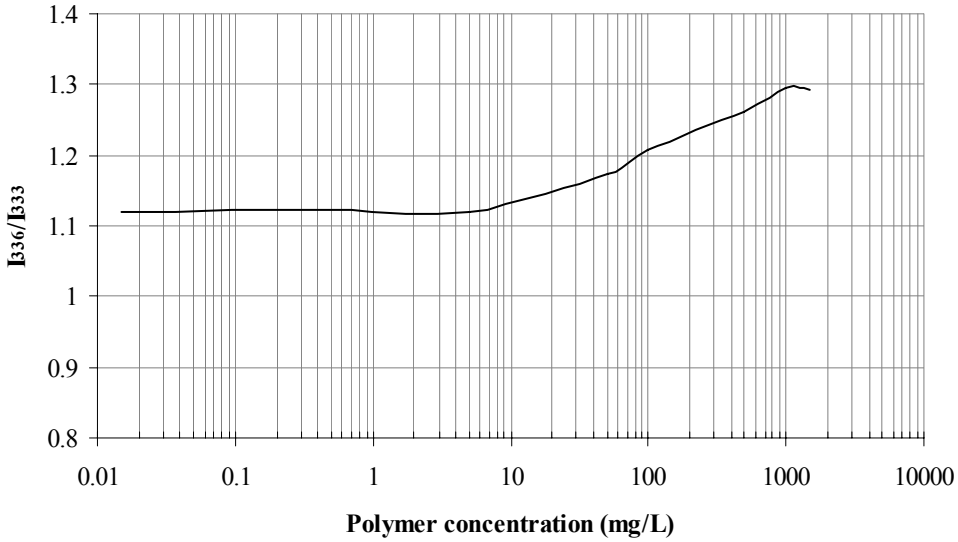

Figure A.4. CMC determination by fluorescence method for 4 arm PMMA-*b*-PAA with molecular weight of 33000 Da and hydrophobic core ratio of 0.19.

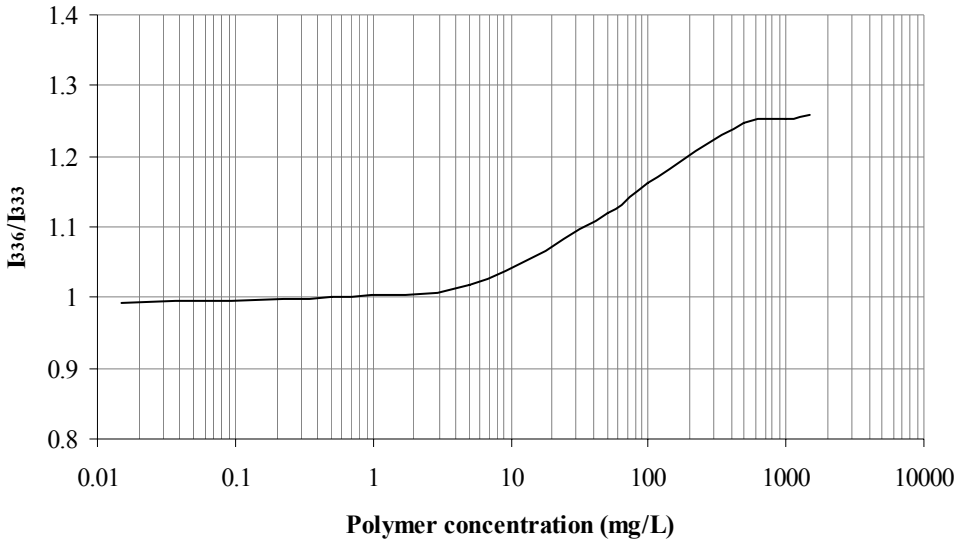

Figure A.5. CMC determination by fluorescence method for 4 arm PMMA-*b*-PAA with molecular weight of 45000 Da and hydrophobic core ratio of 0.11.

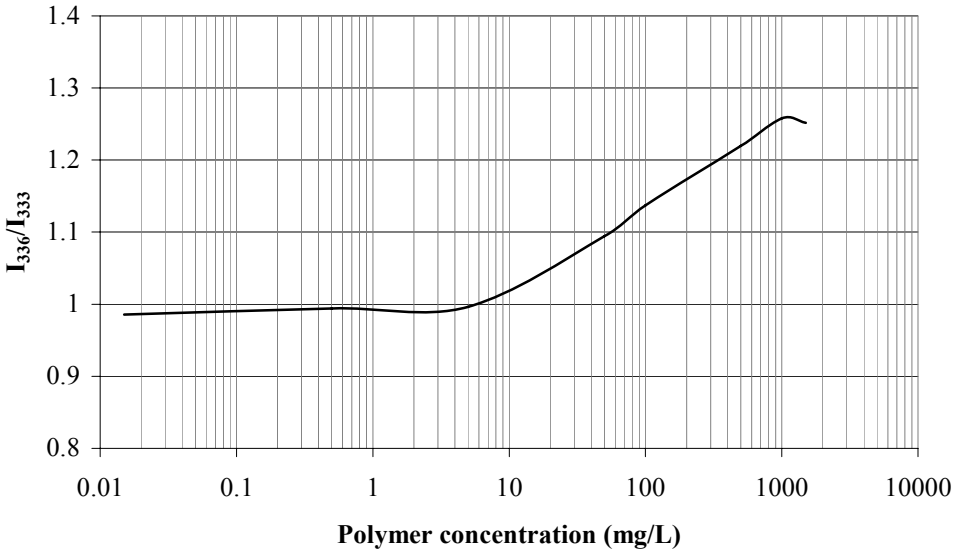

Figure A.6. CMC determination by fluorescence method for 6 arm PMMA-*b*-PAA with molecular weight of 77000 Da and hydrophobic core ratio of 0.11.

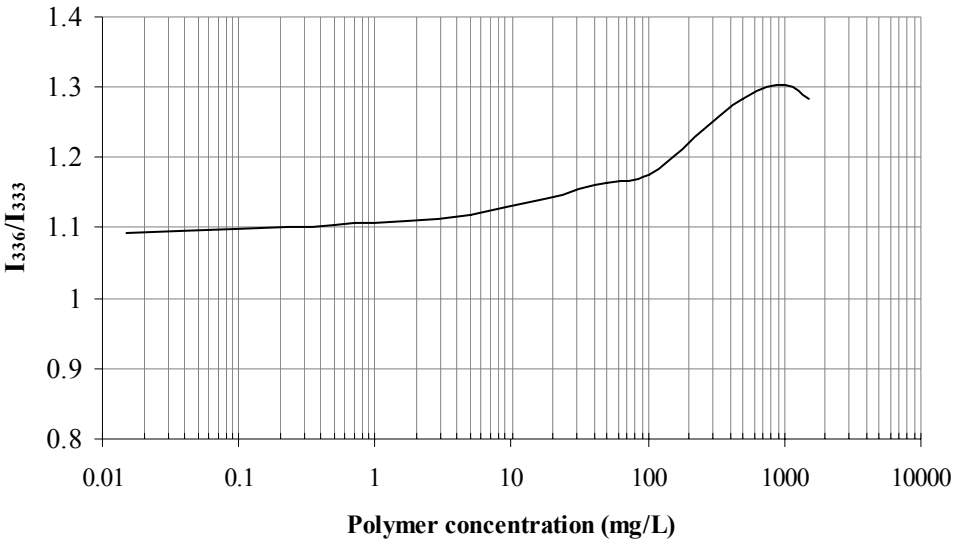

Figure A.7. CMC determination by fluorescence method for 6 arm PMMA-*b*-PAA with molecular weight of 45000 Da and hydrophobic core ratio of 0.18.

APPENDIX B

DRUG RELEASE DATA

Table B.1. Assumptions, constants and constraints occupied in mathematical determination of theoretical model.

ASSUMPTION: X(t)=kt^n
Y(t)=i1+i2+i3+i4+i5+C_n/e^kt+C
n=n1 and k=k1 in 0-40% release interval
n=n2 and k=k2 in 40-100% release interval
$C_n=C_1$ in 0-40% release interval $C_n=C_2$ in 40-100% release interval $C=C_3$ $C_3=0$ in 0-40% release interval

A=	0.785 cm^2
P=	0.005 $cm.min^{-1}$
Vr=	0.471 cm^3

n_1=	0.00256012
k_1=	1.35E-03
n_2=	0
k_2=	7.59E-04
C_1=	1.20E-01
C_2=	-2.12E-01
C_3=	1.18E-01
AP/Vr=	0.00833333
F=	0.025 cm^3min^{-1}

SSQ=	0.0016

Table B.2. Determination of terms in theoretical model derived and given by Equation 3.31 including the first 5 terms of the alternating series.

time (min)	i=1	i=2	i=3	i=4	i=5	C_n/e^kt+C
420	0.01435	0.00411	3.0065E-06	-8.57E-07	4.8898E-07	3.63E-03
930	0.03184	0.00412	1.3606E-06	-1.75E-07	4.5131E-08	5.17205E-05
1290	0.0442	0.00412	9.8169E-07	-9.11E-08	1.6925E-08	2.57501E-06
1580	0.05416	0.00412	8.0192E-07	-6.07E-08	9.216E-09	2.29739E-07
2110	0.07239	0.00413	6.0094E-07	-3.41E-08	3.8725E-09	2.77396E-09
2660	0.09131	0.00413	4.7697E-07	-2.15E-08	1.934E-09	2.8352E-11
3200	0.1099	0.00413	3.9667E-07	-1.48E-08	1.1113E-09	3.14963E-13
3620	0.12436	0.00413	3.5075E-07	-1.16E-08	7.6791E-10	9.51105E-15
4220	0.14503	0.00413	3.01E-07	-8.54E-09	4.8492E-10	6.40849E-17
4785	0.1645	0.00414	2.6555E-07	-6.64E-09	3.3274E-10	5.78033E-19
5310	0.1826	0.00414	2.3936E-07	-5.40E-09	2.4354E-10	7.27636E-21
5700	0.19605	0.00414	2.2302E-07	-4.68E-09	1.9693E-10	2.82135E-22
6330	0.21777	0.00414	2.0088E-07	-3.80E-09	1.4383E-10	1.48051E-24
7820	0.26918	0.00414	1.6269E-07	-2.49E-09	7.6326E-11	5.99683E-30
8955	1.70E-01	0.00228	7.9916E-08	-1.07E-09	2.8591E-11	1.18E-01
10395	0.19714	0.00228	6.8872E-08	-7.93E-10	1.8286E-11	1.18E-01
11095	0.21042	0.00228	6.4537E-08	-6.96E-10	1.5041E-11	1.18E-01
11685	0.22161	0.00228	6.1287E-08	-6.28E-10	1.2878E-11	1.18E-01
12825	0.24323	0.00228	5.5852E-08	-5.21E-10	9.742E-12	1.18E-01
13245	0.2512	0.00228	5.4086E-08	-4.89E-10	8.8451E-12	1.18E-01
13965	0.26485	0.00228	5.1304E-08	-4.40E-10	7.5473E-12	1.18E-01
14685	0.27851	0.00228	4.8795E-08	-3.98E-10	6.4916E-12	1.18E-01
15405	0.29216	0.00228	4.652E-08	-3.61E-10	5.6239E-12	1.18E-01
16125	0.30582	0.00228	4.4448E-08	-3.30E-10	4.9043E-12	1.18E-01
16275	0.30866	0.00228	4.404E-08	-3.24E-10	4.7701E-12	1.18E-01
17145	0.32516	0.00228	4.181E-08	-2.92E-10	4.0807E-12	1.18E-01
17565	0.33313	0.00228	4.0813E-08	-2.78E-10	3.7951E-12	1.18E-01
18225	0.34564	0.00228	3.9339E-08	-2.58E-10	3.3979E-12	1.18E-01
18885	0.35816	0.00228	3.7967E-08	-2.41E-10	3.0542E-12	1.18E-01
19125	0.36271	0.00228	3.7492E-08	-2.35E-10	2.9408E-12	1.18E-01
20685	0.3923	0.00228	3.4672E-08	-2.01E-10	2.3248E-12	1.18E-01
21405	0.40595	0.00228	3.3508E-08	-1.87E-10	2.0982E-12	1.18E-01
21675	0.41107	0.00228	3.3092E-08	-1.83E-10	2.0208E-12	1.18E-01
22395	0.42473	0.00228	3.2031E-08	-1.71E-10	1.8323E-12	1.18E-01
22765	0.43174	0.00228	3.1511E-08	-1.66E-10	1.7444E-12	1.18E-01
23085	0.43781	0.00228	3.1076E-08	-1.61E-10	1.673E-12	1.18E-01
23145	0.43895	0.00228	3.0995E-08	-1.60E-10	1.66E-12	1.18E-01

(Cont. on next page)

Table B.2. (cont.)

time (min)	i=1	i=2	i=3	i=4	i=5	C1/e^Kt+C3
24375	0.46228	0.00228	2.9435E-08	-1.45E-10	1.4214E-12	1.18E-01
24885	0.47195	0.00228	2.8834E-08	-1.39E-10	1.3358E-12	1.18E-01
25665	0.48674	0.00228	2.7959E-08	-1.30E-10	1.2178E-12	1.18E-01
26115	0.49528	0.00228	2.7479E-08	-1.26E-10	1.156E-12	1.18E-01
27105	0.51405	0.00228	2.6478E-08	-1.17E-10	1.034E-12	1.18E-01
27265	0.51709	0.00228	2.6323E-08	-1.16E-10	1.0159E-12	1.18E-01
27375	0.51917	0.00228	2.6217E-08	-1.15E-10	1.0037E-12	1.18E-01
27395	0.51955	0.00228	2.6198E-08	-1.14E-10	1.0015E-12	1.18E-01
27585	0.52316	0.00228	2.6018E-08	-1.13E-10	9.8097E-13	1.18E-01
27585	0.52316	0.00228	2.6018E-08	-1.13E-10	9.8097E-13	1.18E-01
28835	0.54686	0.00228	2.4893E-08	-1.03E-10	8.5894E-13	1.18E-01

Table B.3. Calculation of theoretical values of M_t and M_t/M.

time (h)	time (min)	$M_{t\ exp}$	$M_{t\ theo}$	Error	Square Error	M_t/M_{exp}	M_t/M_{theo}
7.0	420	0.01385	0.01387	0.0000	0.0000	0.0221	0.0217
15.5	930	0.02808	0.02777	0.0003	0.0000	0.0447	0.0435
21.5	1290	0.0383	0.0401	-0.0017	0.0000	0.0611	0.0628
26.3	1580	0.0455	0.0500	-0.0045	0.0000	0.0725	0.0784
35.2	2110	0.0626	0.0683	-0.0057	0.0000	0.0997	0.1069
44.3	2660	0.0897	0.0872	0.0025	0.0000	0.1429	0.1365
53.3	3200	0.1093	0.1058	0.0035	0.0000	0.1741	0.1656
60.3	3620	0.1229	0.1202	0.0027	0.0000	0.1958	0.1883
70.3	4220	0.1367	0.1409	-0.0042	0.0000	0.2177	0.2207
79.8	4785	0.1566	0.1604	-0.0038	0.0000	0.2494	0.2511
88.5	5310	0.1772	0.1785	-0.0013	0.0000	0.2823	0.2795
95.0	5700	0.2044	0.1919	0.0125	0.0002	0.3256	0.3005
105.5	6330	0.2187	0.2136	0.0050	0.0000	0.3484	0.3346
130.3	7820	0.2565	0.2650	-0.0086	0.0001	0.4086	0.4151
149.3	8955	0.2787	0.2852	-0.0066	0.0000	0.4439	0.4467
173.3	10395	0.3160	0.3125	0.0035	0.0000	0.5035	0.4894
184.9	11095	0.3254	0.3258	-0.0005	0.0000	0.5183	0.5102
194.8	11685	0.3328	0.3370	-0.0042	0.0000	0.5302	0.5278
213.8	12825	0.3533	0.3586	-0.0053	0.0000	0.5629	0.5616
220.8	13245	0.3611	0.3666	-0.0055	0.0000	0.5752	0.5741
232.8	13965	0.3772	0.3802	-0.0030	0.0000	0.6009	0.5955
244.8	14685	0.3943	0.3939	0.0004	0.0000	0.6282	0.6169
256.8	15405	0.4135	0.4075	0.0060	0.0000	0.6588	0.6382
268.8	16125	0.4227	0.4212	0.0015	0.0000	0.6734	0.6596
271.3	16275	0.4314	0.4240	0.0073	0.0001	0.6872	0.6641
285.8	17145	0.4408	0.4405	0.0003	0.0000	0.7023	0.6899
292.8	17565	0.4483	0.4485	-0.0002	0.0000	0.7142	0.7024
303.8	18225	0.4594	0.4610	-0.0016	0.0000	0.7319	0.7220
314.8	18885	0.4712	0.4735	-0.0024	0.0000	0.7506	0.7416
318.8	19125	0.4853	0.4781	0.0072	0.0001	0.7732	0.7487
344.8	20685	0.5052	0.5077	-0.0025	0.0000	0.8048	0.7951
356.8	21405	0.5182	0.5213	-0.0031	0.0000	0.8256	0.8164
361.3	21675	0.5267	0.5265	0.0002	0.0000	0.8391	0.8245
373.3	22395	0.5363	0.5401	-0.0038	0.0000	0.8544	0.8459
379.4	22765	0.5498	0.5471	0.0027	0.0000	0.8760	0.8568
384.8	23085	0.5678	0.5532	0.0146	0.0002	0.9045	0.8663
385.8	23145	0.5694	0.5543	0.0151	0.0002	0.9072	0.8681
406.3	24375	0.5844	0.5777	0.0067	0.0000	0.9310	0.9047

(Cont. on next page)

Table B.3. (cont.)

time (h)	time (min)	$M_{t\ exp}$	$M_{t\ theo}$	Error	Square Error	M_t/M_{exp}	M_t/M_{theo}
414.8	24885	0.5949	0.5873	0.0076	0.0001	0.9478	0.9198
427.8	25665	0.6030	0.6021	0.0008	0.0000	0.9606	0.9430
435.3	26115	0.6151	0.6107	0.0044	0.0000	0.9799	0.9563
451.8	27105	0.6227	0.6294	-0.0067	0.0000	0.9921	0.9857
454.4	27265	0.6257	0.6325	-0.0068	0.0000	0.9968	0.9905
456.3	27375	0.6267	0.6346	-0.0079	0.0001	0.9984	0.9938
456.6	27395	0.6277	0.6349	-0.0073	0.0001	1.0000	0.9944
459.8	27585	0.6277	0.6385	-0.0109	0.0001	1.0000	1.0000
459.8	27585	0.6277	0.6385	-0.0109	0.0001	1.0000	1.0000
480.6	28835	0.6277	0.6623	-0.0346	0.0012	1.0000	1.0000

APPENDIX C

PARTICLE SIZE ANALSIS BY ZETASIZER

TABLE C.1. Particle size analysis of 4 arm PMMA-*b*-PAA having 1mg/ml concentration in PBS

Size(nm)	Intensity	Volume	Number
7.5	0.0	0.0	0.0
8.6	0.0	0.0	0.0
9.9	0.0	0.0	0.0
11.4	0.0	0.0	0.0
13.1	0.0	0.0	0.0
15.1	0.0	22.6	25.0
17.4	12.7	45.2	49.9
20.0	0.0	22.6	25.0
23.0	0.0	0.0	16.4
26.4	0.0	0.0	0.0
30.4	0.0	0.0	0.0
34.9	0.0	0.0	0.0
40.2	0.0	0.0	0.0
46.2	0.0	0.0	0.0
53.2	0.0	0.0	0.0
61.2	0.0	2.3	0.0
70.3	79.1	4.7	0.1
80.9	7.8	2.5	0.0
93.1	0.0	0.1	0.0
107.0	0.0	0.0	0.0
123.1	0.0	0.0	0.0
141.6	0.0	0.0	0.0
162.9	0.4	0.0	0.0

Peak Analysis by intensity

Peak	Area	Mean	Width
1	12.7	17.4	2.4
2	86.9	71.3	10.5

Peak Analysis by volume

Peak	Area	Mean	Width
1	90.4	17.4	4.9
2	9.6	71.3	20.6

Peak Analysis by number

Peak	Area	Mean	Width
1	99.8	17.4	4.9

TABLE C.2. Particle size analysis of 4 arm PMMA-*b*-PAA having 2 mg/ml concentration in PBS.

Size(nm)	Intensity	Volume	Number
6.4	0.0	0.0	0.0
8.1	0.0	0.0	0.0
10.2	0.0	16.5	20.7
12.8	4.3	39.9	45.6
16.2	3.6	30.3	29.3
20.3	0.0	6.9	4.3
25.6	0.0	0.0	0.0
32.2	0.0	0.0	0.0
40.6	0.0	0.0	0.0
51.1	0.0	0.5	0.0
64.4	14.9	2.0	0.0
81.0	61.3	2.6	0.0
102.0	15.8	1.3	0.0
128.5	0.0	0.1	0.0
161.7	0.0	0.0	0.0
203.7	0.0	0.0	0.0
256.4	0.0	0.0	0.0
322.8	0.0	0.0	0.0
406.5	0.0	0.0	0.0
511.8	0.0	0.0	0.0
644.3	0.0	0.0	0.0
811.2	0.0	0.0	0.0
1021.4	0.0	0.0	0.0
1286.0	0.0	0.0	0.0

Peak Analysis by intensity

Peak	Area	Mean	Width
1	8.0	14.3	6.3
2	92.0	81.9	25.2

Peak Analysis by volume

Peak	Area	Mean	Width
1	93.5	14.0	7.4
2	6.5	79.0	42.9

Peak Analysis by number

Peak	Area	Mean	Width
1	100.0	13.6	6.8

TABLE C.3. Particle size analysis of 4 arm PMMA-*b*-PAA having 4 mg/ml concentration in PBS.

Size(nm)	Intensity	Volume	Number
5.1	0.0	0.0	0.0
6.5	0.0	0.0	0.0
8.2	0.0	0.0	0.0
10.3	0.0	0.0	0.0
12.9	0.0	0.0	0.0
16.3	0.0	24.3	25.0
20.5	19.9	48.6	50.0
25.8	0.0	24.3	25.0
32.5	0.0	0.0	0.0
40.9	0.0	0.0	0.0
51.5	0.0	0.0	0.0
64.8	0.0	0.0	0.0
81.6	0.0	0.3	0.0
102.8	23.0	0.8	0.0
129.4	50.1	0.9	0.0
162.9	0.0	0.3	0.0
205.1	0.6	0.0	0.0
258.3	0.0	0.0	0.0
325.2	0.0	0.0	0.0
409.4	0.0	0.0	0.0
515.5	0.0	0.0	0.0
649.0	3.9	0.1	0.0
817.1	3.2	0.2	0.0
1028.8	0.0	0.1	0.0

Peak Analysis by intensity

Peak	Area	Mean	Width
1	19.9	20.5	4.8
2	73.0	121.0	41.3
3	7.1	725.6	320.2

Peak Analysis by volume

Peak	Area	Mean	Width
1	97.3	20.8	9.5
2	2.3	118.9	66.9

Peak Analysis by number

Peak	Area	Mean	Width
1	100.0	20.8	9.5

TABLE C.4. Particle size analysis of 4 arm PMMA-*b*-PAA having 6 mg/ml concentration in PBS.

Size(nm)	Intensity	Volume	Number
11.1	0.0	0.0	0.0
13.9	0.0	14.3	18.5
17.5	3.6	38.6	43.5
22.1	5.0	34.3	31.5
27.8	0.0	10.0	6.5
35.0	0.0	0.0	0.0
44.1	0.0	0.0	0.0
55.5	0.0	0.0	0.0
69.9	0.0	0.0	0.0
88.0	0.0	0.0	0.0
110.7	0.0	0.3	0.0
139.4	25.0	0.5	0.0
175.5	0.0	0.3	0.0
221.0	0.0	0.1	0.0
278.3	29.0	0.6	0.0
350.3	37.4	0.7	0.0
441.1	0.0	0.3	0.0
555.3	0.0	0.0	0.0
699.2	0.0	0.0	0.0
880.3	0.0	0.0	0.0
1108.3	0.0	0.0	0.0
1395.4	0.0	0.0	0.0
1756.9	0.0	0.0	0.0
2212.0	0.0	0.0	0.0

Peak Analysis by intensity

Peak	Area	Mean	Width
1	8.6	20.2	8.5
2	25.0	139.4	32.4
3	66.4	318.8	137.8

Peak Analysis by volume

Peak	Area	Mean	Width
1	97.1	19.7	10.9
2	1.2	150.0	64.8
3	1.7	333.1	175.0

Peak Analysis by number

Peak	Area	Mean	Width
1	100.0	19.0	9.9

TABLE C.5. Particle size analysis of 4 arm PMMA-*b*-PAA having 1 mg/ml concentration in PBS after three days of degradation.

Size(nm)	Intensity	Volume	Number
5.7	0.0	0.0	0.0
7.2	0.0	0.0	0.0
9.1	0.0	0.0	0.0
11.4	0.0	0.0	0.0
14.4	0.0	0.0	0.0
18.1	0.0	5.7	10.7
22.8	1.7	24.1	33.6
28.7	7.8	35.7	37.1
36.2	5.4	21.8	16.4
45.6	0.0	4.5	0.0
57.4	0.0	0.0	0.0
72.2	0.0	0.2	0.0
91.0	3.5	1.4	0.0
114.5	33.9	3.1	0.0
144.2	43.3	2.6	0.0
181.5	4.4	0.9	0.0
228.5	0.6	0.0	0.0
287.7	0.0	0.0	0.0
362.3	0.0	0.0	0.0
456.1	0.0	0.0	0.0
574.3	0.6	0.0	0.0
723.1	3.5	0.0	0.0
910.4	8.0	0.0	0.0
1146.2	0.0	0.0	0.0

Peak Analysis by intensity

Peak	Area	Mean	Width
1	15.0	30.8	22.0
2	85.0	132.1	55.1

Peak Analysis by volume

Peak	Area	Mean	Width
1	91.8	29.1	17.1
2	8.2	126.4	75.1

Peak Analysis by number

Peak	Area	Mean	Width
1	99.9	27.2	15.7

TABLE C.6. Particle size analysis of 4 arm PMMA-*b*-PAA having 2 mg/ml concentration in PBS after 3 days of degradation.

Size(nm)	Intensity	Volume	Number
4.6	0.0	0.0	0.0
5.8	0.0	0.0	0.0
7.3	0.0	0.0	0.0
9.2	0.0	0.0	0.0
11.6	0.0	15.2	19.5
14.6	6.6	38.6	44.3
18.3	7.1	32.3	30.2
23.1	1.2	9.6	5.7
29.1	0.0	0.7	0.2
36.6	0.0	4.5	0.0
46.1	2.5	0.2	0.0
58.0	6.9	0.6	0.0
73.1	9.4	0.9	0.0
92.0	10.7	0.7	0.0
115.8	14.3	0.5	0.0
145.9	18.6	0.3	0.0
183.6	16.4	0.2	0.0
231.2	6.4	0.1	0.0
291.1	0.0	0.1	0.0
366.5	0.0	0.0	0.0
461.5	0.0	0.0	0.0
581.0	0.0	0.0	0.0
731.5	0.0	0.0	0.0
921.0	0.0	0.0	0.0

Peak Analysis by intensity

Peak	Area	Mean	Width
1	14.9	17.1	8.0
2	85.1	129.6	144.6

Peak Analysis by volume

Peak	Area	Mean	Width
1	96.3	16.4	9.0
2	3.7	80.4	55.2

Peak Analysis by number

Peak	Area	Mean	Width
1	99.9	15.7	8.0

TABLE C.7. Particle size analysis of 4 arm PMMA-*b*-PAA having 4 mg/ml concentration in PBS after 3 days of degradation.

Size(nm)	Intensity	Volume	Number
5.2	0.0	0.0	0.0
6.1	0.0	0.0	0.0
7.3	0.0	0.0	0.0
8.6	0.0	0.0	0.0
10.2	0.0	0.0	0.0
12.1	0.0	0.0	0.0
14.4	0.0	2.7	5.3
17.1	2.5	16.0	23.0
20.2	15.8	32.7	36.2
24.0	22.2	30.9	25.9
28.4	10.7	14.0	8.4
33.7	0.0	2.6	1.1
39.9	0.0	0.0	0.0
47.3	0.0	0.0	0.0
56.1	0.0	0.0	0.0
66.5	0.0	0.0	0.0
78.8	0.7	0.1	0.0
93.4	17.3	0.4	0.0
110.7	22.8	0.4	0.0
131.3	7.9	0.2	0.0
155.6	0.0	0.0	0.0
184.5	0.0	0.0	0.0
218.7	0.0	0.0	0.0
259.2	0.0	0.0	0.0

Peak Analysis by intensity

Peak	Area	Mean	Width
1	51.2	23.4	9.1
2	48.8	107.5	38.2

Peak Analysis by volume

Peak	Area	Mean	Width
1	98.9	22.2	10.7
2	1.1	104.0	46.9

Peak Analysis by number

Peak	Area	Mean	Width
1	100.0	21.0	9.6

TABLE C.8. Particle size analysis of 4 arm PMMA-*b*-PAA having 6 mg/ml concentration in PBS after 3 days of degradation.

Size(nm)	Intensity	Volume	Number
4.3	0.0	0.0	0.0
5.1	0.0	0.0	0.0
6.0	0.0	0.0	0.0
7.1	0.0	0.0	0.0
8.4	0.0	0.0	0.0
10.0	0.0	0.0	0.0
11.8	0.0	0.0	0.0
14.0	0.0	0.0	0.0
16.6	0.0	3.8	5.8
19.7	7.6	28.8	30.8
23.4	70.1	46.1	44.2
27.7	0.0	21.1	19.2
32.9	0.0	0.0	0.0
38.9	0.0	0.0	0.0
46.2	0.0	0.0	0.0
54.7	0.0	0.0	0.0
64.9	0.0	0.0	0.0
76.9	0.0	0.0	0.0
91.2	0.0	0.0	0.0
108.1	0.0	0.0	0.0
128.1	4.8	0.0	0.0
151.9	17.6	0.1	0.0
180.0	0.0	0.0	0.0
213.4	0.0	0.0	0.0

Peak Analysis by intensity

Peak	Area	Mean	Width
1	77.7	23.0	4.2
2	22.3	146.8	30.4

Peak Analysis by volume

Peak	Area	Mean	Width
1	99.8	23.0	8.4

Peak Analysis by number

Peak	Area	Mean	Width
1	100.0	22.7	8.6

TABLE C.9. Particle size analysis of 4 arm PMMA-*b*-PAA having 1 mg/ml concentration in PBS after 7 days of degradation.

Size(nm)	Intensity	Volume	Number
1.1	0.0	0.0	0.0
1.4	0.0	0.0	0.0
1.8	0.0	0.0	0.0
2.2	0.0	5.5	13.8
2.8	1.1	16.3	34.2
3.5	2.1	20.7	30.0
4.4	3.6	18.0	13.5
5.6	5.5	14.2	5.5
7.0	7.9	10.3	2.1
8.8	10.2	6.8	0.7
11.1	12.1	4.1	0.2
14.0	13.0	2.3	0.1
17.6	12.3	1.1	0.0
22.2	10.0	0.5	0.0
27.9	6.6	0.2	0.0
35.2	2.9	0.0	0.0
44.3	0.6	0.0	0.0
55.8	0.0	0.0	0.0
70.2	0.0	0.0	0.0
88.4	0.0	0.0	0.0
111.3	0.6	0.0	0.0
140.2	3.5	0.0	0.0
176.5	8.0	0.0	0.0
222.2	0.0	0.0	0.0

Peak Analysis by intensity

Peak	Area	Mean	Width
1	87.8	14.5	22.0
2	12.2	162.6	55.1

Peak Analysis by volume

Peak	Area	Mean	Width
1	100.0	5.4	4.5

Peak Analysis by number

Peak	Area	Mean	Width
1	100.0	3.5	1.9

TABLE C.10. Particle size analysis of 4 arm PMMA-*b*-PAA having 2 mg/ml concentration in PBS.

Size(nm)	Intensity	Volume	Number
1.2	0.0	0.0	0.0
1.5	0.0	0.0	0.0
1.8	0.0	0.0	0.0
2.3	0.0	0.0	0.0
2.9	0.0	0.0	0.0
3.7	0.0	5.5	12.7
4.6	2.1	17.7	33.0
5.8	5.0	24.3	31.2
7.3	8.3	21.5	15.2
9.2	11.2	15.2	5.7
11.6	12.4	8.9	1.8
14.6	11.4	4.4	0.5
18.3	8.5	1.8	0.1
23.1	4.5	0.6	0.0
29.1	1.4	0.1	0.0
36.6	0.0	0.0	0.0
46.1	0.0	0.0	0.0
58.0	1.2	0.0	0.0
73.0	3.9	0.0	0.0
91.9	7.2	0.0	0.0
115.7	9.2	0.0	0.0
145.7	8.6	0.0	0.0
183.5	5.1	0.0	0.0
231.0	0.0	0.0	0.0

Peak Analysis by intensity

Peak	Area	Mean	Width
1	64.7	12.5	14.7
2	35.3	121.3	111.2

Peak Analysis by volume

Peak	Area	Mean	Width
1	100.0	7.6	6.2

Peak Analysis by number

Peak	Area	Mean	Width
1	100.0	5.7	3.3

TABLE C.11. Particle size analysis of 4 arm PMMA-*b*-PAA having 4 mg/ml concentration in PBS after 7 days of degradation.

Size(nm)	Intensity	Volume	Number
1.2	0.0	0.0	0.0
1.5	0.0	0.0	0.0
1.9	0.0	0.0	0.0
2.4	0.0	0.0	0.0
3.0	0.0	0.0	0.0
3.8	0.0	0.0	0.0
4.8	0.0	0.0	0.0
6.0	0.0	6.3	12.5
7.6	5.5	21.2	33.5
9.5	14.8	29.8	32.7
12.0	21.6	24.2	15.5
15.1	20.7	13.1	4.7
19.1	10.8	4.6	0.9
24.0	0.0	0.8	0.1
30.2	0.0	0.0	0.0
38.0	0.0	0.0	0.0
47.9	0.0	0.0	0.0
60.3	0.0	0.0	0.0
75.9	0.0	0.0	0.0
95.6	6.2	0.0	0.0
120.3	11.5	0.0	0.0
151.5	8.9	0.0	0.0
190.8	0.0	0.0	0.0
240.2	0.0	0.0	0.0

Peak Analysis by intensity

Peak	Area	Mean	Width
1	73.4	13.1	10.3
2	26.6	125.0	71.0

Peak Analysis by volume

Peak	Area	Mean	Width
1	100.0	10.8	7.7

Peak Analysis by number

Peak	Area	Mean	Width
1	100.0	9.2	5.5

TABLE C.12. Particle size analysis of 4 arm PMMA-*b*-PAA having 6 mg/ml concentration in PBS after 7 days of degradation.

Size(nm)	Intensity	Volume	Number
1.9	0.0	0.0	0.0
2.3	0.0	0.0	0.0
2.8	0.0	0.0	0.0
3.4	0.0	0.0	0.0
4.2	0.0	0.0	0.0
5.1	0.0	0.0	0.0
6.2	0.0	0.0	0.0
7.6	0.0	0.0	0.0
9.2	0.0	9.7	14.1
11.3	14.7	30.9	37.5
13.8	32.2	36.6	34.3
16.9	19.0	19.1	12.5
20.6	0.0	3.7	1.6
25.2	0.0	0.0	0.0
30.7	0.0	0.0	0.0
37.6	0.0	0.0	0.0
45.9	0.0	0.0	0.0
56.0	0.0	0.0	0.0
68.5	0.0	0.0	0.0
83.7	0.6	0.0	0.0
102.2	22.5	0.0	0.0
124.9	11.0	0.0	0.0
152.5	0.0	0.0	0.0
186.3	0.0	0.0	0.0

Peak Analysis by intensity

Peak	Area	Mean	Width
1	65.9	14.1	5.9
2	34.1	109.2	31.7

Peak Analysis by volume

Peak	Area	Mean	Width
1	99.9	13.4	7.0

Peak Analysis by number

Peak	Area	Mean	Width
1	100.0	12.7	6.3

TABLE C.13. Particle size analysis of 5-FU loaded (in dimethyl formamide) 4 arm PMMA-*b*-PAA having 2 mg/ml concentration in PBS.

Size(nm)	Intensity	Volume	Number
4.6	0.0	0.0	0.0
5.7	0.0	6.7	14.1
7.2	1.5	20.1	35.1
9.1	2.9	25.2	30.7
11.4	4.5	20.5	13.3
14.4	5.9	13.9	4.8
18.1	6.3	7.9	1.4
22.9	5.4	3.7	0.4
28.8	3.3	1.3	0.1
36.2	1.0	0.3	0.0
45.6	0.0	0.0	0.0
57.4	0.0	0.0	0.0
72.3	0.0	0.0	0.0
91.0	0.9	0.0	0.0
114.6	4.3	0.0	0.0
144.3	9.9	0.0	0.0
181.7	15.2	0.0	0.0
228.7	17.4	0.0	0.0
288.0	14.1	0.0	0.0
362.6	6.7	0.0	0.0
456.5	0.7	0.1	0.0
574.8	0.0	0.0	0.0
723.7	0.0	0.0	0.0
911.2	0.0	0.0	0.0

Peak Analysis by intensity

Peak	Area	Mean	Width
1	30.8	17.7	19.8
2	69.2	224.8	205.1

Peak Analysis by volume

Peak	Area	Mean	Width
1	99.7	11.3	8.9

Peak Analysis by number

Peak	Area	Mean	Width
1	100.0	8.7	4.9

TABLE C.14. Particle size analysis of 5-FU loaded (in 1% acetic acid solution) 4 arm PMMA-*b*-PAA having 2 mg/ml concentration in PBS.

Size(nm)	Intensity	Volume	Number
2.3	0.0	0.0	0.0
2.9	0.0	0.0	0.0
3.6	0.0	0.0	0.0
4.6	0.0	0.0	0.0
5.7	0.0	4.4	11.3
7.2	1.2	14.9	30.5
9.1	3.5	22.6	31.0
11.4	6.7	22.3	17.0
14.4	9.8	17.2	7.1
18.1	11.5	10.6	2.3
22.8	10.4	5.3	0.6
28.8	6.6	2.0	0.1
36.2	2.4	0.5	0.0
45.6	0.0	0.1	0.0
57.4	0.0	0.0	0.0
72.3	0.0	0.0	0.0
91.0	0.8	0.0	0.0
114.6	4.9	0.0	0.0
144.3	11.8	0.0	0.0
181.6	16.2	0.0	0.0
228.7	11.9	0.0	0.0
287.9	2.2	0.0	0.0
362.5	0.0	0.0	0.0
456.4	0.0	0.0	0.0

Peak Analysis by intensity

Peak	Area	Mean	Width
1	52.2	18.8	19.5
2	47.8	180.7	123

Peak Analysis by volume

Peak	Area	Mean	Width
1	99.9	12.3	11.1

Peak Analysis by number

Peak	Area	Mean	Width
1	100.0	9.2	5.8

APPENDIX D

PARTICLE SIZE ANALYSIS BY AFM

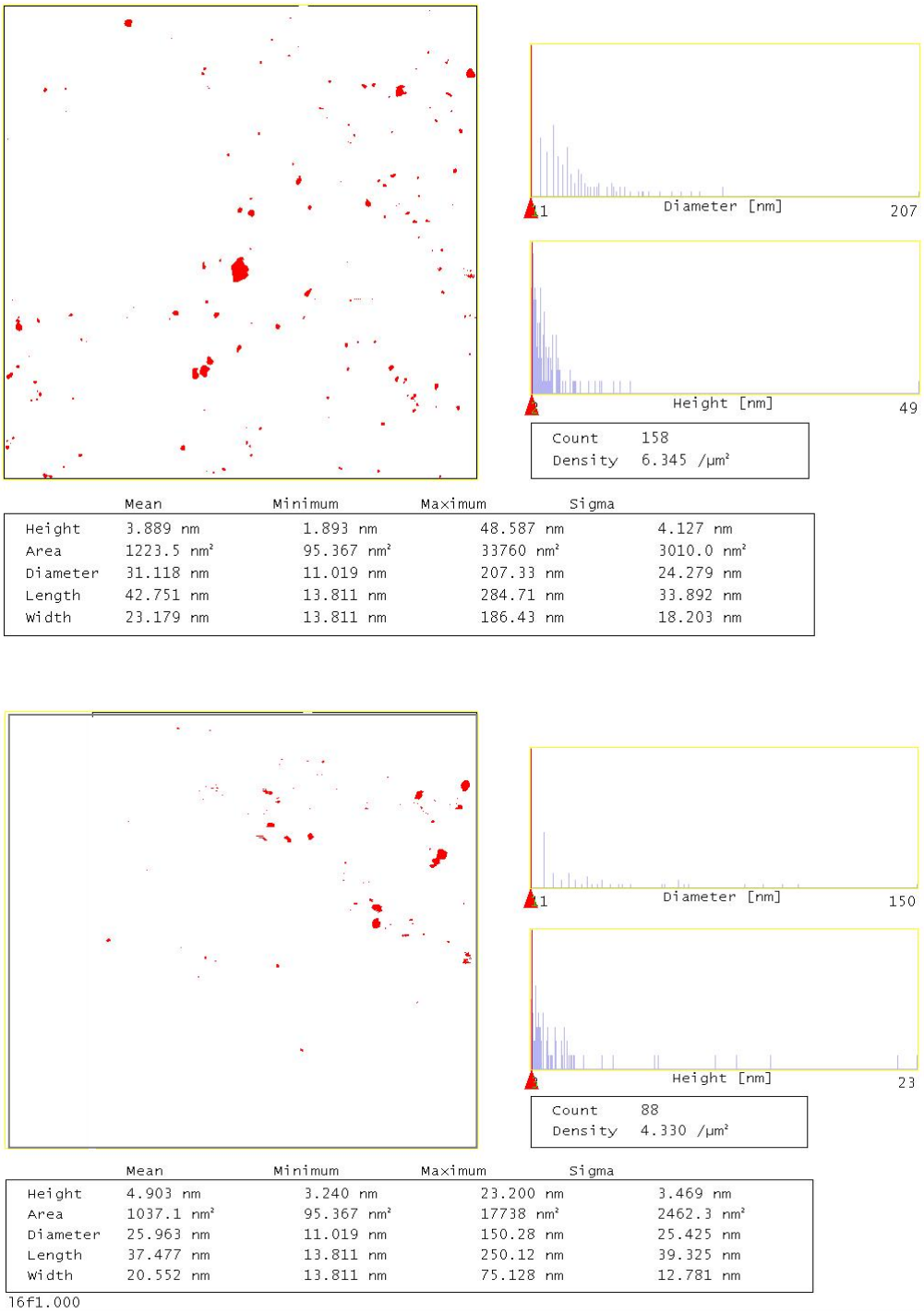

Figure D.1. 4 arm PMMA-b-PAA (MW:4900/18000) dissolved in water at 25°C (n=2).

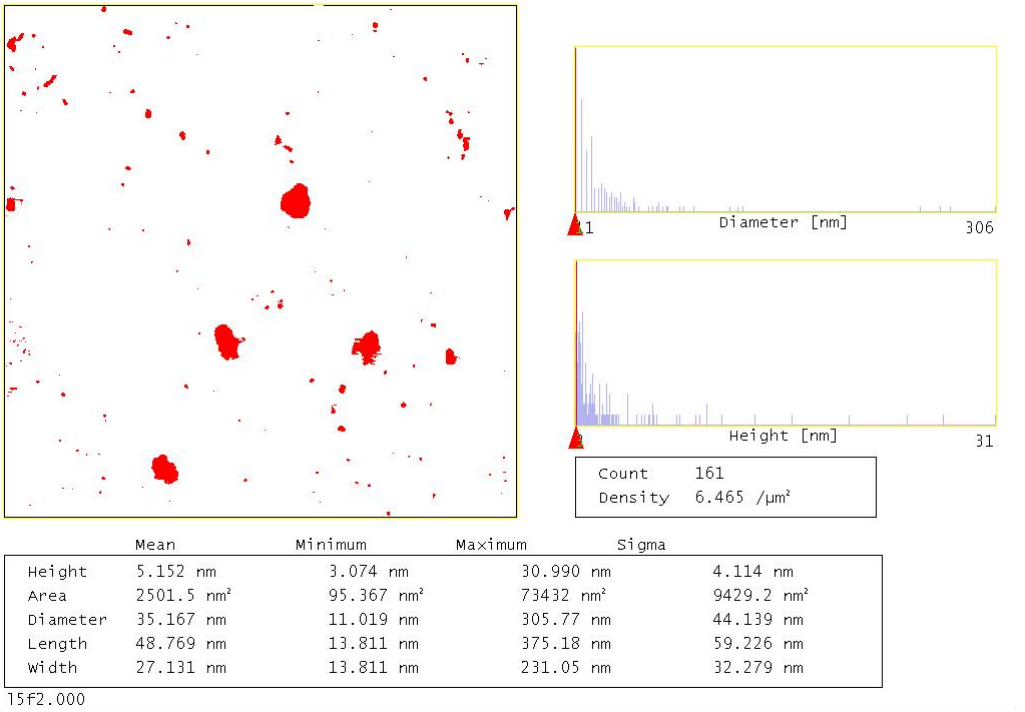

	Mean	Minimum	Maximum	Sigma
Height	5.152 nm	3.074 nm	30.990 nm	4.114 nm
Area	2501.5 nm²	95.367 nm²	73432 nm²	9429.2 nm²
Diameter	35.167 nm	11.019 nm	305.77 nm	44.139 nm
Length	48.769 nm	13.811 nm	375.18 nm	59.226 nm
Width	27.131 nm	13.811 nm	231.05 nm	32.279 nm

15f2.000

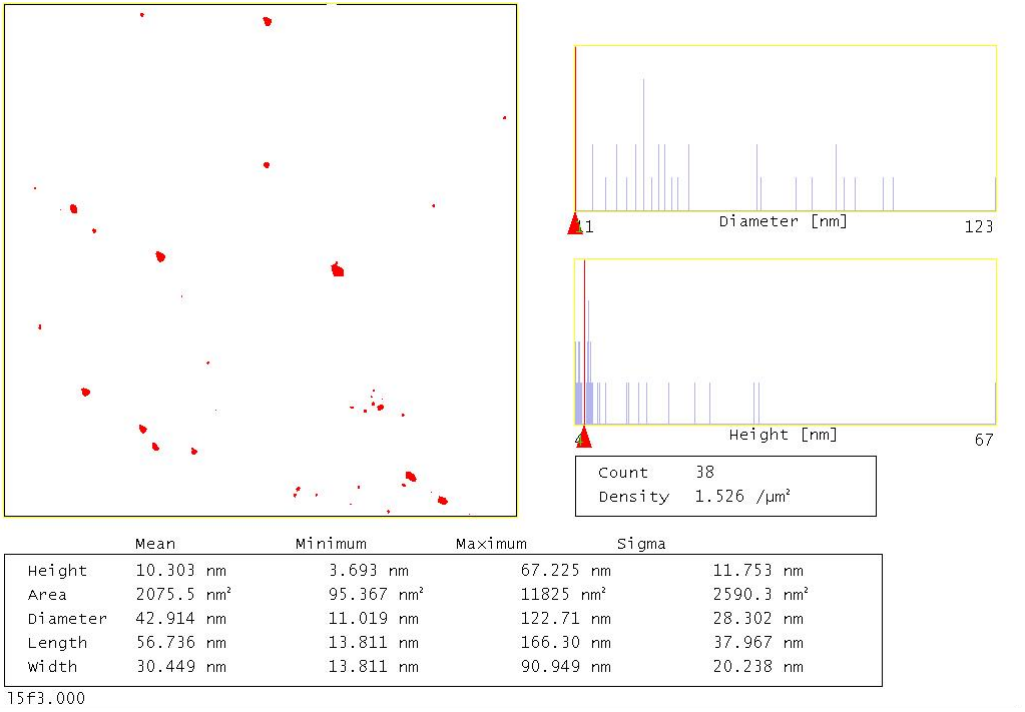

	Mean	Minimum	Maximum	Sigma
Height	10.303 nm	3.693 nm	67.225 nm	11.753 nm
Area	2075.5 nm²	95.367 nm²	11825 nm²	2590.3 nm²
Diameter	42.914 nm	11.019 nm	122.71 nm	28.302 nm
Length	56.736 nm	13.811 nm	166.30 nm	37.967 nm
Width	30.449 nm	13.811 nm	90.949 nm	20.238 nm

15f3.000

Figure D.2. 4 arm PMMA-b-PAA (MW:4900/18000) degraded in water at 37°C for 1 hour (n=2).

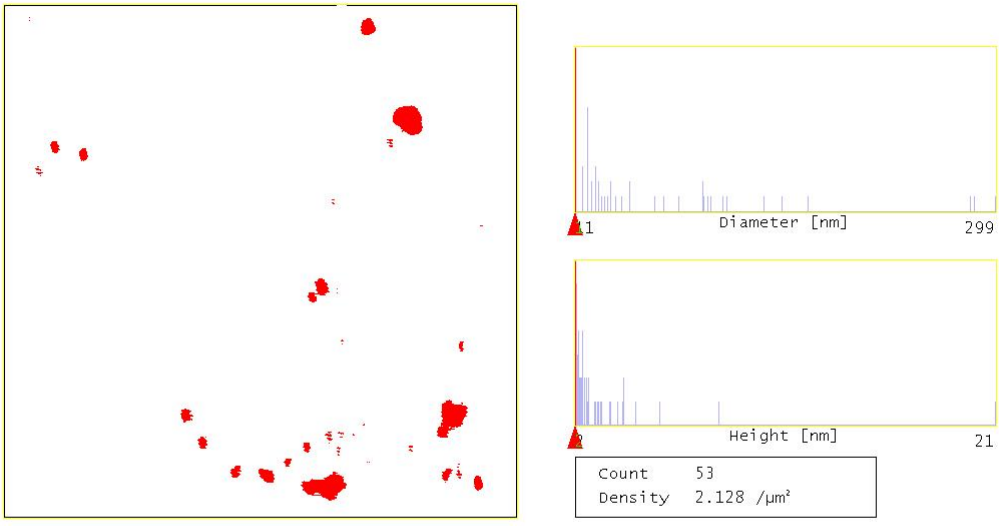

	Mean	Minimum	Maximum	Sigma
Height	3.105 nm	2.026 nm	21.139 nm	2.748 nm
Area	6454.4 nm²	95.367 nm²	70095 nm²	15236 nm²
Diameter	58.264 nm	11.019 nm	298.74 nm	69.450 nm
Length	82.171 nm	13.811 nm	449.64 nm	95.482 nm
Width	43.184 nm	13.811 nm	244.68 nm	51.363 nm

16f2.000

Figure D.3. 4 arm PMMA-b-PAA (MW:4900/18000) degraded in water at 37°C for 1 day.

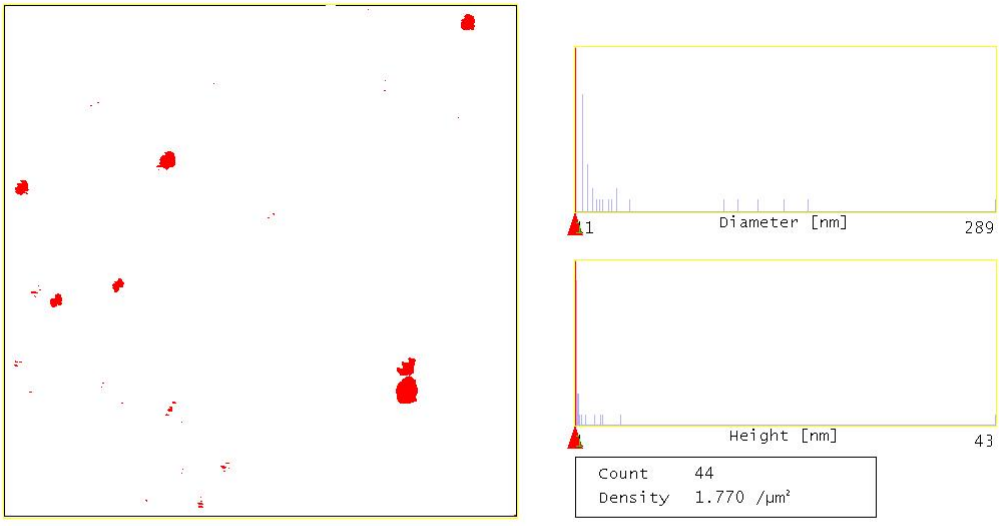

	Mean	Minimum	Maximum	Sigma
Height	2.246 nm	0.902 nm	43.108 nm	6.292 nm
Area	3428.9 nm²	95.367 nm²	65422 nm²	10581 nm²
Diameter	37.817 nm	11.019 nm	288.61 nm	54.182 nm
Length	53.908 nm	13.811 nm	463.22 nm	79.626 nm
Width	29.410 nm	13.811 nm	138.49 nm	34.053 nm

15f5d.000

Figure D.4. 4 arm PMMA-b-PAA (MW:4900/18000) degraded in water at 37°C for 5 days.

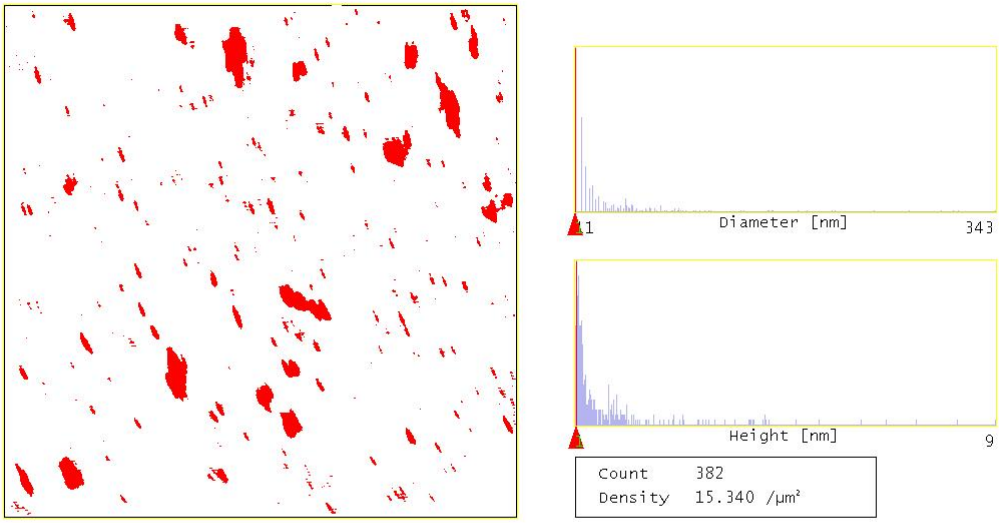

	Mean	Minimum	Maximum	Sigma
Height	1.432 nm	0.865 nm	8.986 nm	1.062 nm
Area	2747.4 nm²	95.367 nm²	92220 nm²	9731.0 nm²
Diameter	36.285 nm	11.019 nm	342.66 nm	46.707 nm
Length	60.379 nm	13.811 nm	689.22 nm	85.400 nm
Width	23.060 nm	13.811 nm	213.59 nm	24.418 nm

15f7d.000

Figure D.5. 4 arm PMMA-b-PAA (MW:4900/18000) degraded in water at 37°C for 7 days.

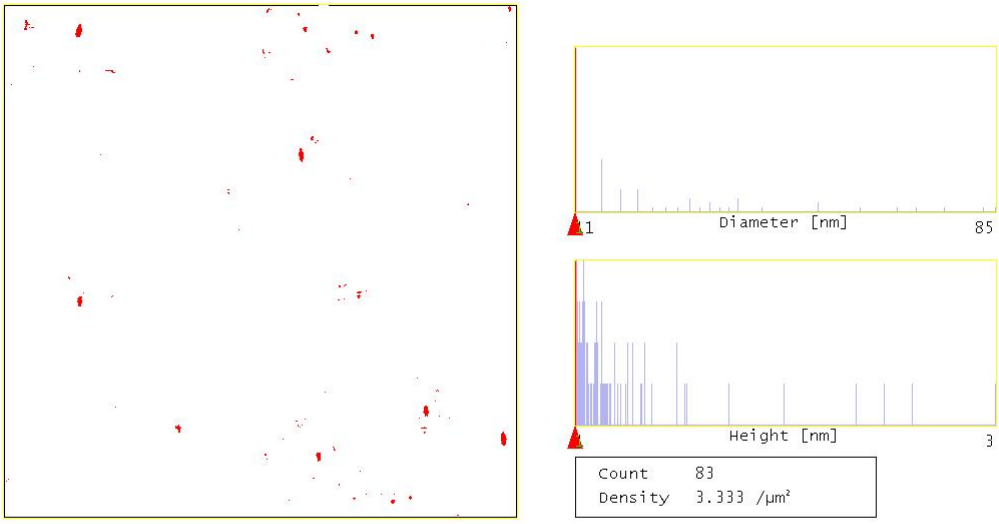

	Mean	Minimum	Maximum	Sigma
Height	1.099 nm	0.882 nm	2.938 nm	0.370 nm
Area	654.93 nm²	95.367 nm²	5722.0 nm²	1164.8 nm²
Diameter	22.650 nm	11.019 nm	85.355 nm	17.913 nm
Length	33.938 nm	13.811 nm	139.82 nm	31.280 nm
Width	17.201 nm	13.811 nm	50.331 nm	7.533 nm

15f10d.001

Figure D.6. 4 arm PMMA-b-PAA (MW:4900/18000) degraded in water at 37°C for 10 days.

VITA

Name: Gözde GENÇ ATİKLER
Birth Date and Place: 1972/İSTANBUL
Marital Satatus: Married

Education:	M.S. in Chemical Engineering Department, IZTECH, 2004 B.S. in Chemical Engineering Department, METU, 1995 İzmir Özel Türk Lisesi, 1990
Work Experiences:	Research Assistant in IZTECH 2001-2010 R&D Engineer in Far-Per Kimya Ltd. Şti. 1997-1999 Quality Control Laboratory Chief in Bağ Yağları A.Ş. 1996-1997
Reserach Subjects:	Nanocrystalline materials, Acrylic polymer synthesis and characterization, Drug loading and controlled drug delivery.
Publications:	Genc G., Altıntaş O., Batıgün A., Bayraktar, O., Tunca, U., Hızal, G. Acrylic Star Block Copolymers as Drug Carriers, Biyomut, 2009. Kocabaş, I., Genç, G., Batıgün, A., Bayraktar, O. Serisin-Poliakrilik asit Graft Polimerlerin Mukozaya Yapışma Özellikleri, 15. Ulusal Biyoteknoloji Kongresi, 2007. Genc G., Alp, B., Balköse, D., Ülkü, S., Cireli, A., Moisture Sorption and Thermal Charcteristics of Polyaramide Blend Fabrics. *J. Appl. Pol. Sci.*, **2006**, *102*, 29-38. Duvarcı, Ö.Ç., Çiftçioğlu, M., Güden, M., Arıkut, G. Preparation and Microstructural Development of Nanocrystalline Titania and Alumina. *Key Engineering Materials.* **2004**, *264-268*, 2355-58.
Certificates:	Total Quality Management, TSE, 1999 Statistical Process Control, TSE, 1999 Documentation, TSE, 1999